THE PREPARATION AND PHYSICAL PROPERTIES OF CERTAIN CHALCOGENIDE SEMICONDUCTORS

A thesis submitted for the Degree of Doctor of Philosophy

by

Timothy George Davey

ABSTRACT

The electrical conductivities of five amorphous chalcogenide semiconducting alloys (Ovshinsky glasses) of potential usefulness in electronic switches and memory devices have been studied at temperatures from ambient to just over 1000°C. The alloys studied in addition to STAG (Si_{12} Te_{48} As_{30} Ge_{10}) were from the S-Ge-As-Te and Se-Ge-As-Te systems. Values of the energy gap for electrical conduction have been determined and found to be similar to those reported in the literature for similar materials. The electrical conductivity of sulphur was determined over the previously uninvestigated temperature range 400°C to 900°C; and the data obtained was found to be consistent with published data for lower temperatures. The phase diagram at the binary system Si-Te has been completed, and the phases produced in the crystallisation of some amorphous chalcogenide alloys have been examined.

TABLE OF CONTENTS PAGE

LIST OF FIGURES PAGE

LIST OF FIGURES PAGE

LIST OF TABLES

PREFACE

The work described in this thesis was carried out over a period of three years at Imperial College, London. The project was supported by the Ministry of Defence, Department of Components, Valves and Devices. The object was to study the synthesis, electrical properties and phase equilibria of amorphous semiconducting chalcogenide materials used in electronic switches and memory components, and to continue the investigation to temperatures well above those previously employed. To prevent decomposition of these materials at high temperatures, it was necessary to work under inert gas at high pressure, and for this reason the project was carried out with the high pressure facilities in the Department of Metallurgy and Materials Science at Imperial College, London.

ACKNOWLEDGEMENTS

The author would like to express his thanks to :

Dr. E.H. Baker of the Department of Metallurgy and Materials Science at Imperial College for his advice and supervision; other members of the department for their practical help and consultations. Acknowledgements are also due to Dr. P.S. Rogers of the Metallurgy Department for his interest and advice; to the Ministry of Defence DCVD for their financial support; and to Cambridge University for the use of their library facilities during the compilation of this thesis.

Note on Units

Although it is now considered normal for all scientific literature to use the S.I. system of units, the two fields that overlap in this thesis remain exceptions to the rule. In dealing with elevated pressures, it is still commonplace to use pounds per square inch and atmospheres, and conductivity and resistivity data are still reported in mho cm^{-1} and ohm cm respectively. For this reason, non-S.I. units may be found in this thesis, with S.I. conversions where appropriate.

1. INTRODUCTION

1:1 High Pressure Research

1:1:1 A brief historical review

Although work at high pressures has a relatively short history as a real science, extending back a hundred years at the most, interest in pressure and its effects goes back much further, to the early 18th century when attempts were made to resolve the question of whether or not water was compressible. The determination of compressibilities remained the object of almost all high pressure research during the 19th century, and although, at first, accurate results were rare due to the lack of the technology necessary to deal with high pressures, the ingenuity of the experimentors and the experience gained paved the way for later work. Between 1869 and 1893, the systematic work of the Frenchman Amagat (1) gave a great boost to the development of the science, and the number of workers increased rapidly. This period coincided with an improvement in the quality of equipment available, and Amagat was followed by Tammann in Germany and Lussana in Italy, whose work, along with others, extended well into the present century.

Just after the turn of the century, advances in the production control and containment of high pressures were made, with techniques borrowed from the developing chemical industry (from which came the idea of "winding" a pressure container from sheet or strip), and from the gun-makers, who developed the process known as autofrettage.

Between 1908 and 1961, the main name in the field was P.W. Bridgeman, who devoted all his efforts to high pressure work, and whose name is associated with many technical innovations, such as "unsupported area" packing (2) and various pressure intensifiers.

Work this century has become more diverse and widespread, with extraordinary pressures being reached, especially in attempts to synthesise diamond. (Even so, this last goal was not attained until 1955). The search for even higher pressures has led to more recent work concerning itself with the transient pressures generated in the shock-waves of an explosion.

1:1:2 Some practical considerations

The pressure vessels used for gases and in the work described here, are the kind used for attaining more modest pressures, below 1000 atmospheres, and are made from sections of Second World War gun barrels, which are more than adequate for the pressures concerned.

The first problem encountered in using a pressure vessel is that of calculating the maximum pressure it can safely withstand. These calculations are comprehensively treated by Comings in his book "High Pressure Technology", (3), but some salient points from his analysis are quoted here as they are relevant to the vessels used in this work.

The simplest way to consider a vessel under stress from an internal pressure is to treat it as a thin-walled cylinder, that is, one whose

wall thickness is small compared to its radius, and in which the same stress is developed throughout the walls of the vessel. This produces a simple equation:

$$\sigma_t = \frac{p\ r}{t} \qquad - 1:1$$

relating the tensile stress σ_t, generated by an internal pressure p in a vessel of internal radius r, and wall thickness t.

Unfortunately, to contain more than a moderate pressure, the vessel requires walls whose thickness is significant compared to its radius. The distribution of stresses in the vessel walls then becomes important, the stress being a maximum at the inside surface, falling off as the wall is traversed. Thus, if the vessel is pressurised to the point at which the inner surface is approaching the yield stress, the material in the rest of the walls is, so to speak, largely wasted, as it is only performing a supporting role and is bearing only a small part of the load. The equations describing this behaviour up to the elastic limit were developed by Lamé and Clapeyron in the 1830's (3).

To make more effective use of the material of the walls, techniques such as autofrettage are used. This involves plastically straining the inner section of the walls and then heat-treating the vessel, which leaves a residual stress distribution going from compressive stresses at the inside face to tensile stress at the outside. An applied pressure modifies this stress distribution, levelling it out, until, at a certain pressure there is an equal stress all the way through the wall. This process ensures that the outer layers "pull their

weight" in restraining the internal pressure. The same effect can also be produced by winding a vessel from sheet or interlocking strip, wound onto a tube under a controlled tension, the so-called "wickel-tape" process. Complex calculations have to be used to find the bursting pressure for such a vessel.

The vessels used in this work, being sections of gun barrels, had been subjected to autofrettage. To calculate the bursting pressure accurately, details of the heat-treatment would be required, but this information was not available for the gun-barrels which were used, so a more simple calculation, ignoring the autofrettaging, is all that is possible in this case. This provides additional safety, as the vessel will be stronger than predicted.

For a vessel whose wall thickness is significant, Comings (3) uses a balance of forces on an element of the cylinder walls to derive the following formula for $(\sigma_t)_{r_1}$, the maximum circumferential tensile stress, which occurs at the inside wall surface:

$$(\sigma_t)_{r_1} = p\left(\frac{K^2 + 1}{K^2 - 1}\right) \qquad - 1:2$$

where p is the internal pressure and K is $\frac{r_2}{r_1}$ (outside radius/inside radius). The vessel used here had $r_2 = 115$ mm and $r_1 = 65$ mm. The yield stress of the steel used was quoted as 50 tons/sq inch (= 770 N/mm^2). Substituting these values in the above formula and adjusting the units shows that the pressure to cause yield is 57,500 p.s.i. or about 4000 atmospheres (= 397 N/mm^2). Since the vessel was not used

here above 120 atmospheres (12 N/mm^2) a considerable safety margin existed.

Before undertaking a piece of work involving pressurised gases, it is as well to consider the choice of materials with which the gas will come into contact. Carbon dioxide will embrittle neoprene 'O' rings and render them useless after one exposure. Hydrogen embrittlement is an obvious problem in certain situations, but it is not the only case where gas dissolution can cause trouble. High pressure oxygen is the most dangerous pressurising medium likely to be encountered, great care being necessary to exclude the slightest films of grease or traces of other combustible material from contact with the gas. Steel vessels are always at risk, as they can burn with oxygen at sufficient pressures if they are overheated. Fortunately, the gas most suitable for the present work was argon, and no problems occurred.

1:1:3 Furnaces for use at high pressures

A difficulty peculiar to high pressure furnaces is convection, which is especially severe in vertical tube furnaces. The heat transported by a given volume of gas is far greater at a hundred atmospheres than at one atmosphere pressure, so convection, which is not much of a problem in an ordinary furnace, becomes a major one at high pressures. It carries away so much heat that it can sometimes make it impossible to reach the desired temperature, or it may generate a steep temperature gradient across the specimen. In any case, the agitation of currents of hot and cold gas makes the sample temperature unsteady. To prevent

these effects, some workers use horizontal pressure vessels, with horizontal furnace tubes, but these have disadvantages if the vessel is used with containers such as conductivity cells, which contain liquid samples. Care has to be taken with the physical arrangement of the sample and insulating materials to try and break up long convection paths.

1:1:4. Plastics and insulators at high pressures

A practical problem in the use of pressure vessels is that of passing electrical leads through the vessel walls either for measurement or for current supply. Perspex is ideal for this application in view of its availability in many shapes and sizes, its high strength and electrical resistivity (4). In the experiments to be reported here, no leakage currents across perspex insulators were ever detected. Against this must be set the fact that perspex is very brittle and difficult to machine accurately; nevertheless, it is widely used where it will not come into contact with heat. Where this is likely, for example in power leads, refractories are preferable. The refractories used for this purpose have a high resistivity and remain unaffected by quite high temperatures. As a result they are used for leads which carry large currents and which are exposed to high temperatures from the windings of furnaces. Their main disadvantage is that they are difficult to fabricate, and it is often easier to use diesel engine igniters, which are made with the same criteria in mind (see experimental section).

Both plastics and ceramics have the disadvantage that although their

strengths are high and therefore they can be used up to high pressures, they are brittle, and are more likely to fail without any warning than a metal part of the vessel. It is therefore usual to design with very large safety factors when using brittle materials.

2. THE PROPOSED FIELD OF RESEARCH : CHALCOGENIDE GLASSES

2.1. Their historical background

The materials known as the chalcogenide glasses have a strange history. The term chalcogenide refers to the elements of Group VIa, namely oxygen, sulphur, selenium and tellurium, and it derives from their association with copper and its ores. Of these elements, the latter two remained mere curiosities until relatively recently. The photosensitive conduction of selenium was noted and exploited in photocells, but otherwise oxygen and sulphur remained the only chalcogenides of practical use. As long ago as 1870 it had been reported (5) that, in conjunction with other elements, the chalcogenides formed strange, amorphous materials, to which the name chalcogenide glasses was given. Over the next 80 years, little interest was shown in them, and knowledge accumulated slowly, mainly to the effect that a vast range of glasses could be produced, especially with arsenic, germanium, silicon and similar elements. In the 1950's came the first hints of a practical use with the discovery that although perfectly opaque to visible light, chalcogenide glasses were transparent to infra-red radiation (6,7,8), and a further spur to research was provided in 1955 when Kolomiets and other Russian workers demonstrated that some glasses had electrical conductivities of the same order as elemental crystalline semiconductors,

(9) and that they possessed similar electrical properties. By this time, the electronics industry was committed to the development of conventional semiconductor devices, in which the properties of ultra-pure germanium and silicon were altered by doping them with selected impurities. As a result of this commitment, they were unwilling to exploit the potential advantages offered by the amorphous chalcogenides, such as their insensitivity to contamination, (10) which would have removed the necessity for expensive purification procedures and would have made their production far cheaper. Phase diagram research, especially in the U.S.S.R., had been pursued and had shown that a large number of glass compositions were possible, (11) and that over a large area of the Ge-As-Te-Si system, for instance, it was not possible to crystallise out either the primary solids or the compounds, such as GeTe. The liquids seemed to generally solidify to a disordered single-phase solid solution which could only be crystallised by extremely lengthy heat treatments, if at all.

The materials thus produced remained unexploited, however, until the late 1950's, when S.R. Ovshinsky, investigating the conductivity of junctions, noticed that some amorphous materials, especially oxides, gave unusual non-Ohmic current-voltage relationships when sandwiched between metal electrodes. (His early work is summarised in reference (12)). In 1960, Ovshinsky started a firm, Energy Conversion Devices, which began to market devices based on this discovery, (13), some of which used the chalcogenide glasses. Theoretical interest increased as a result of this, and grew rapidly from the mid 1960's onwards, with such publications as Ovshinsky's "Reversible Electric Switching

Phenomena in Disordered Structures" in 1968, (14) and for several years the underlying processes were the subject of considerable debate, resulting in a flood of papers to physical journals and the newly formed Journal of Non-Crystalline Solids (15-54). But, by about 1972, it was becoming obvious that a resolution of the mechanisms involved in chalcogenide glass conduction would require long and painstaking research, and the rate of publication of papers has declined considerably since then. This decline was no doubt hastened by the realisation that the electronics market was proving harder to break into than had been imagined, and that widespread usage of the switches and memory devices was, at best, a long way in the future. This lessening of pace has at least meant that it was possible, for the first time, to produce a "state of the art" review which would not be outdated before publication. A number of these have appeared (55,56), including a monograph by Adler (57) and an article in "Nature" by N.F. Mott (58).

2.2. The Switching Phenomenon

To understand the reason for the research reported here, it is necessary to consider the useful properties of the chalcogenide glasses, particularly their electrical conductivities, for, although their transparency to infra-red radiation (59,60,61) has been exploited, it is as electronic components that their greatest applications will be found (62-67). Their random structures make them immune to damage by nuclear radiation, and some amorphous semiconductors have been used in this field (68). For their use in electronics, however,

the property which will be exploited in these devices is the threshold switching phenomenon, sometimes referred to as "Ovshinsky switching". This phenomenon is by no means restricted to the chalcogenide glasses. as it was first noticed in oxides, and has since been seen in many different substances. If a thin layer of one of these materials (say, about 10 μm thick) is sandwiched between two metal contacts and a voltage is applied across the layer, the current/voltage characteristic is, at first, quite normal. The current rises slowly with voltage, and the material exhibits a high resistivity. However, when a threshold voltage level is reached, there is a sudden fall in resistance, which causes a great rise in current. This is illustrated by Figure 1, which shows the current/voltage characteristics of a typical device. The high resistance state is referred to as the "off-state" of the characteristic, and the low resistance state as the "on-state". Once the material is in the "on-state", small voltage changes produce large current changes. Also, the resistance remains low as the voltage is decreased until a value called the "holding voltage" is reached, at which point the resistance returns to its "off-state" value. This holding voltage varies with the material, and may be zero in many cases, in which case the material is a "memory material" as the low-resistance state persists until a specially-shaped current pulse is passed to destroy it. Materials for which the holding voltage is not zero are called switching materials. The voltage/current characteristics of both types are shown in Figure 1. The switching materials are made into a device which has a high resistance until "addressed" by a voltage pulse greater than the threshold voltage, at which point it switches "on", and remains on until the voltage across it falls below

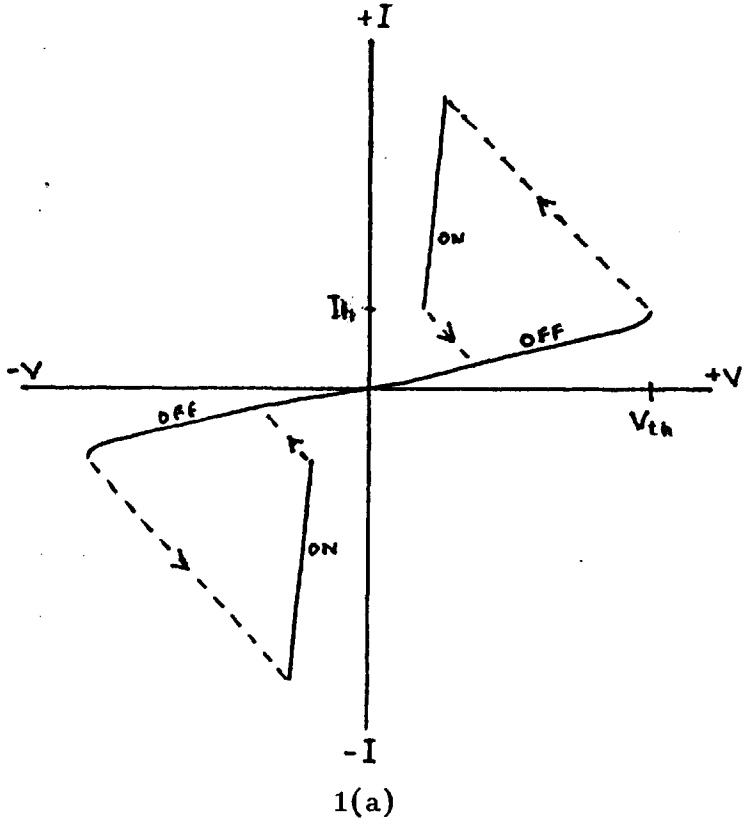

1(a)

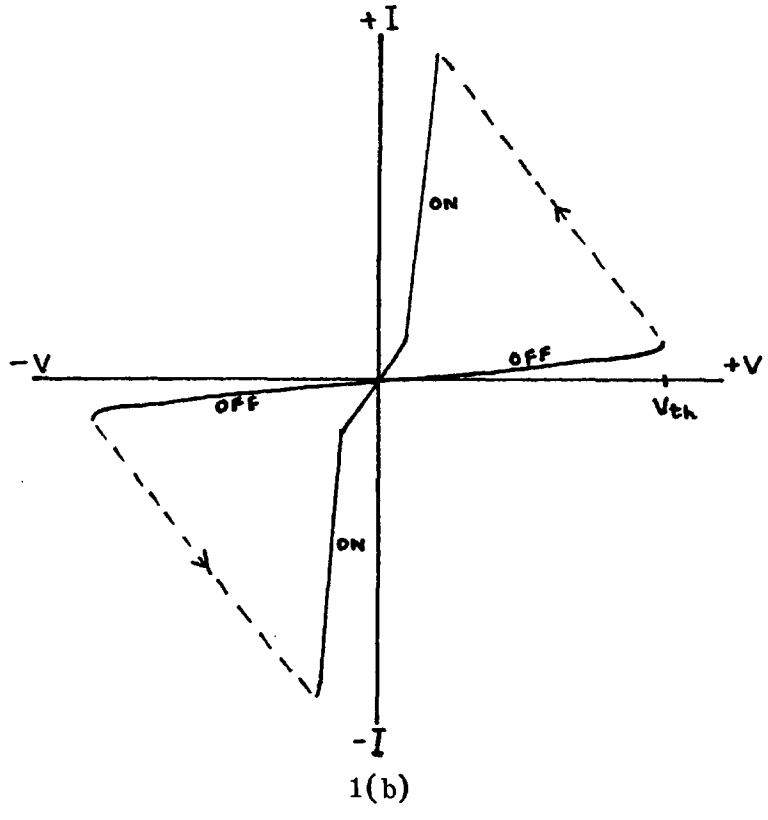

1(b)

Figure 1. Voltage/current characteristics of thin film devices using chalcogenide glasses.

1(a) Switching type. Vth = threshold voltage, Ih = holding current (the corresponding voltage would be the holding voltage, Vh).

1(b) Memory type. Vth = threshold voltage. Once the device reaches the 'on' branch, it can be cycled along it indefinitely unless deliberately turned off.

The solid lines represent stable V/I states. The dotted lines are the unstable process of switching.

the holding voltage, when it automatically switches "off". A memory device, once "addressed", remains "on" until a specially shaped current pulse is sent to it. Such devices can be built up by conventional integrated-circuit technology, and arrays have been produced, both as experiemental computer memories (55), and, in conjunction with light-emitting diodes, as part of a display board.

The behaviour of these materials has still not been satisfactorily explained, and a number of theories have been advanced. The two main contenders are the space-charge theory (16,19,22,34) and the thermal theory (15,17,25,31,32,43,44,46,53,54), the latter being well explained by Male in an article in New Scientist (50).

Although the majority of such material belongs to later chapters, the two theories will be briefly described here, as the differences between them allow the work undertaken in this project to be seen in perspective.

The "space-charge" model states that, at low voltages, the glass behaves as an insulator, as the electrons present in the material are not available for conduction, and those which are injected via the electrodes are immediately trapped, building up a space charge which raises the resistance still higher. The assumption is made that the material, unlike a normal insulator, has an equal number of hole and electron traps, and can thus become "fully compensated",that is, to have all its traps full, and be electrically neutral (no space charge), in which condition it is much more conducting. The theory proposes that, as the applied voltage increase, the space charge barriers penetrate deeper

into the layer of chalcogenide, until they overlap, creating a fully compensated zone, where the conductivity rises, altering the electric field distribution, causing further overlap, and precipitating a runaway situation which gives rise to the rapid switch-on times observed in these materials. When this high-current state is attained, a hot conducting channel is produced, which may vanish when the voltage falls too low, (in a switching glass) or which may be replaced by a crystalline channel at low currents, thus retaining a low resistivity, and keeping the device "on", in which case the material is a memory glass.

The thermal model is somewhat simpler, and is based on the fact that the materials in which this phenomenon occurs have similar conductivity/temperature relationships. The electrical conductivity rises rapidly with temperature up to a certain point, beyond which it becomes relatively temperature-insensitive. This can be seen in the materials investigated here, as well as in the results presented in the literature, (e.g. 69-72). This leads to the conclusion that the current/voltage characteristic is normal at moderate voltages, when the current, and hence the resistance heating, are small. At higher voltages, resistance heating raises the temperature of the device, and thus decreases its resistance. This leads to an increase in current, more heating, even lower resistance, and so on. This could obviously lead to a situation in which the device was vaporized, unless some other effect prevented it. This could either be heat losses to the electrodes, or a levelling-off of the resistivity/temperature graph. One, or both, of these effects causes a stable situation to develop, producing the hot, conducting filament, which has been observed in functioning devices, especially

in As_{55} Te_{35} Ge_{10}, in which switching occurs very slowly (73). The thermal model lends itself to computer modelling, e.g. (32,43), which has, however, so far not produced conclusive evidence either way.

2.3. Investigations into the Properties of Chalcogenide Glasses

While not deciding conclusively in favour of one theory or another, investigations of the electrical conductivity up to very high temperatures can tend to support or weaken the case of the thermal model, depending upon whether the levelling-off which may be required by this model is detected in the curve of conductivity vs temperature. Accordingly, investigations of the conductivity of Si_{12} Te_{48} As_{30} Ge_{10} (known as STAG, and one of the early switching chalcogenide glasses), started by Webb (71), were completed.

In a programme to develop new switching chalcogenides which would have longer service lifetimes, a number of new compositions were devised by the Royal Radar Establishment, containing tellurium, arsenic, germanium and either sulphur or selenium. Four of these materials were manufactured and their conductivities determined up to 1100°C.

Since selenium, tellurium, sulphur, silicon and germanium are basic constituents of many chalcogenide glasses, the temperature/conductivity behaviour of these elements is of interest. For selenium, tellurium, silicon and germanium such data are available over a wide range of temperatures (e.g. 74-80), but in the case of sulphur, only a limited

number of studies have been made, and these only provide data up to about 400°C (79-86). It therefore seemed worthwhile as part of this present study, to extend the conductivity work on liquid sulphur to higher temperatures. Vapour pressure data are available for sulphur (87), and the need for high pressures is evident from this data. It proved possible to measure conductivities up to about 900°C using the apparatus available.

Another parameter which needed to be clarified was the physical behaviour of the components. Although the phase diagrams of most of the important binary systems between the components of chalcogenide glasses are well-known (Ge-Te is given in Smithells "Metals Reference Book", for instance (88)),only sketchy information was available on the interaction between silicon and tellurium in the important series of glasses of which STAG (see above) is a member (89-94). This binary lends itself well to investigation in a high-pressure furnace, consisting as it does, of a volatile element (tellurium) and an involatile one, silicon. At normal pressures, any tellurium present would have evaporated long before the silicon could be melted, so silicon-tellurium alloys can only be made and investigated under pressure. Using argon at relatively modest pressures made it possible to complete the phase diagram using a thermal analysis technique, and to isolate the compound formed, which is Si_2Te_3.

As may be seen by reference to the brief descriptions of the two competing theories of switching which are included above, the memory effect is usually ascribed to the formation of a crystalline filament between the

electrodes. The precise nature of the filaments detected is uncertain, and, if they represent a separate phase, the composition is unknown. Two approaches were tried, to determine the composition of these filaments. First, to simulate the filament on a large scale, a high current was passed through a molten thread of the chalcogenide, which was then analysed to determine whether any migration of the constituents had occurred. Second, as one of the compositions of the series of sulphur-containing glasses proved very easy to crystallise, the phases present were analysed as it is possible that they have some relationship with the material which could crystallise out in the filament.

3. EXPERIMENTAL DETAILS

3.1. Introduction: The Need for High Pressures

The chalcogenide glasses studied here contain elements such as sulphur, selenium and tellurium, which melt at low temperatures, and others, such as silicon and germanium, which melt at very high temperatures. In addition, all of them contain arsenic, which, at 1 atmosphere, has no melting point at all, but sublimes at 613°C, (95). In order to obtain a homogeneous liquid from which a glass can be produced, it is necessary to prevent the boiling of S, Ge, and Te and the sublimation of As, at the same time attaining the temperatures necessary to melt Si and Ge. The traditional technique is to seal the powdered constituents in a strong evacuated silica bulb and heat it to about 800-1000°C, relying on the silica to contain the vapour pressures developed. The bulb is then agitated to try and dissolve the silicon in the liquid mixture thus formed. It is assumed that the vaporised material re-

dissolves as the activity (and thus the partial vapour pressure) falls. An alternative is to apply a high gas pressure, to set up conditions when the equilibrium phase is liquid rather than vapour. Figure 2 shows the vapour-pressure/temperature relationship for arsenic, for which the triple point lies at 816°C and 35.5 atm. (95) (= 3.6 N/mm^2). A pressure of 40 atm (4.0 N/mm^2) was considered sufficient to ensure melting. The activity of the arsenic would fall as it dissolved in the liquid already present, and the full vapour pressure would no longer be exerted. If sulphur were present at unit activity, it would develop a vapour pressure of 150 atm (15.2 N/mm^2) at 1000°C (see Fig. 3) and thus some 200 atmospheres (20.3 N/mm^2) would appear to be necessary to prevent it from boiling. In practice, glasses containing sulphur also contain tellurium, which melts at 451°C and dissolves the sulphur, reducing its thermodynamic activity and thus its vapour pressure. The 40 atmospheres needed to liquefy the arsenic content proved sufficient to prevent loss of sulphur in all the glasses made in connection with this work. Tellurium is much less volatile than arsenic or sulphur, as shown by comparison of Figures 2,3 and 4, and loss of tellurium is not really a problem. Loss of the volatile elements by diffusive evaporation (as opposed to boiling) can also occur, and this was avoided by heating the constituents in a vitreous silica bulb which had a long, vertical tubular outlet. Down this outlet tube passed a silica thermocouple sheath which allowed an annular clearance of about 0.1 mm. Thus, although the silica reaction vessel was not sealed the high pressure argon in the annular space acted as a diffusion barrier and effectively prevented vaporisation loss from the melt. This technique would appear to have had the desired effect, as no signs of

Fig. 2. Vapour pressure/temperature relationship for arsenic, after Baker (95).

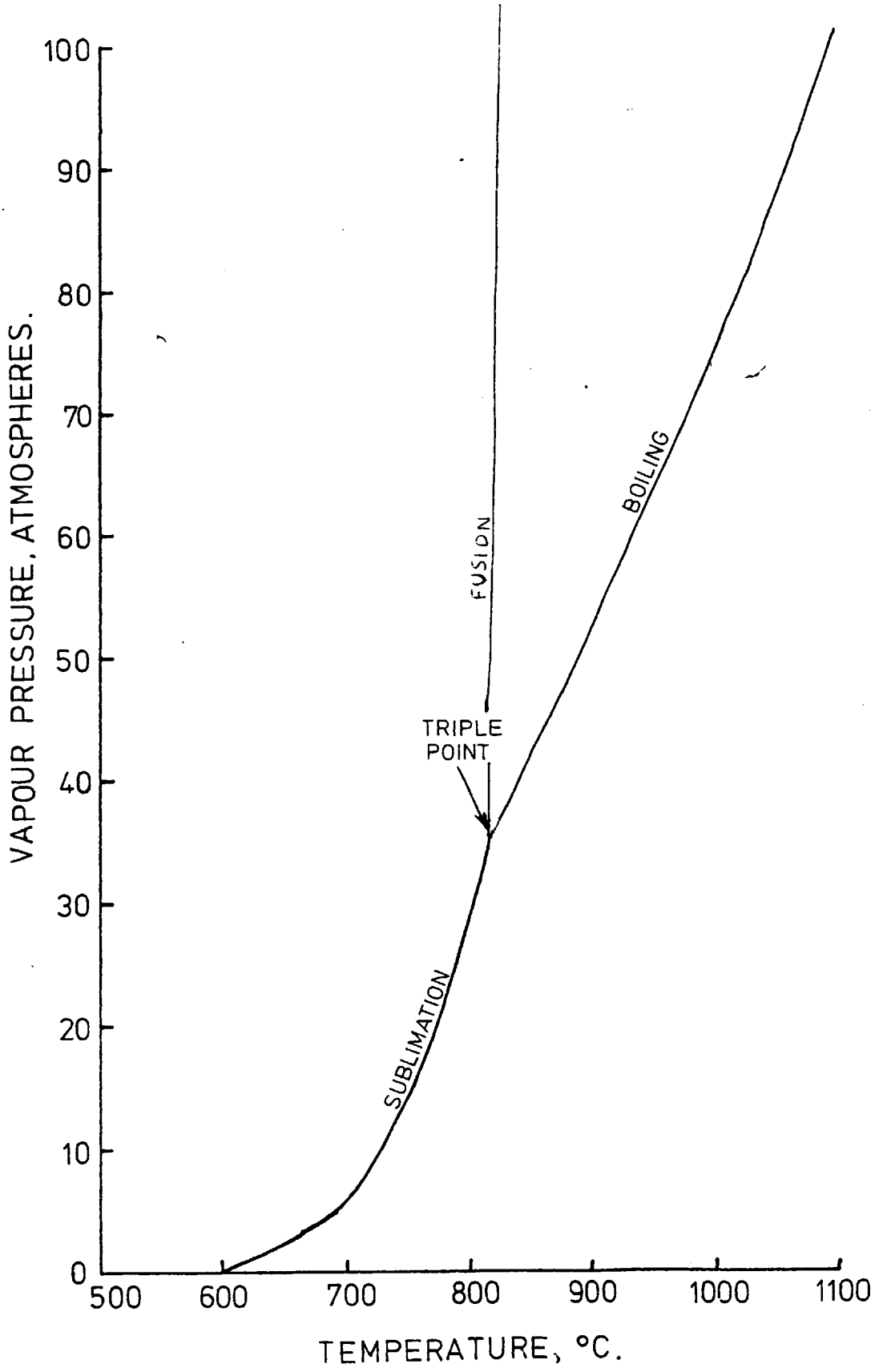

Fig. 3. Vapour pressure/temperature relationship for sulphur according to Baker (87).

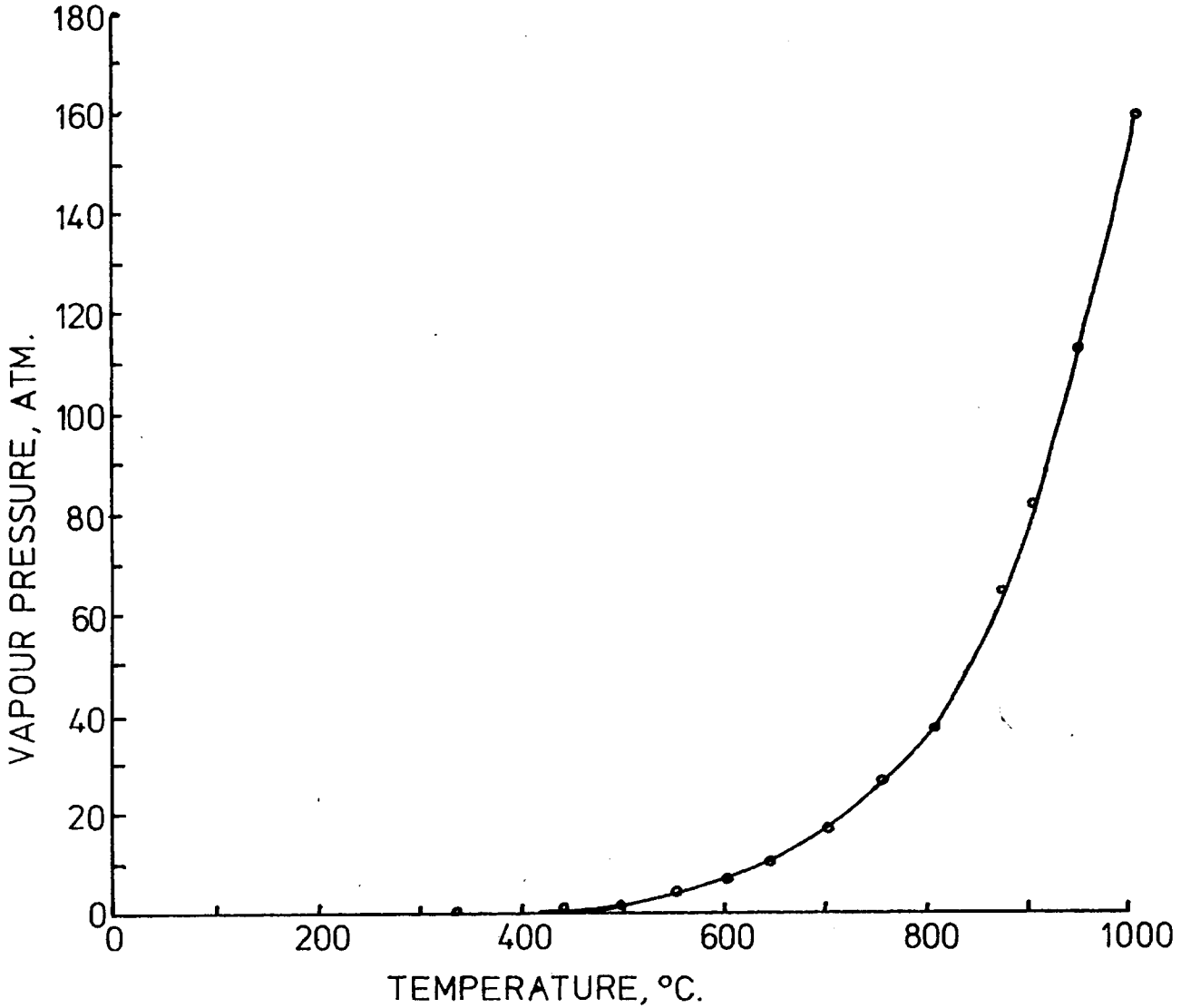

Fig. 4. Vapour pressure/temperature relationship for tellurium after Machol and Westrum (96).

Solid line - Vapour pressure equation given by Machol and Westrum and supported by experimental data.

Dotted line - Present author's extrapolation above normal boiling point, using Machol and Westrum's equation.

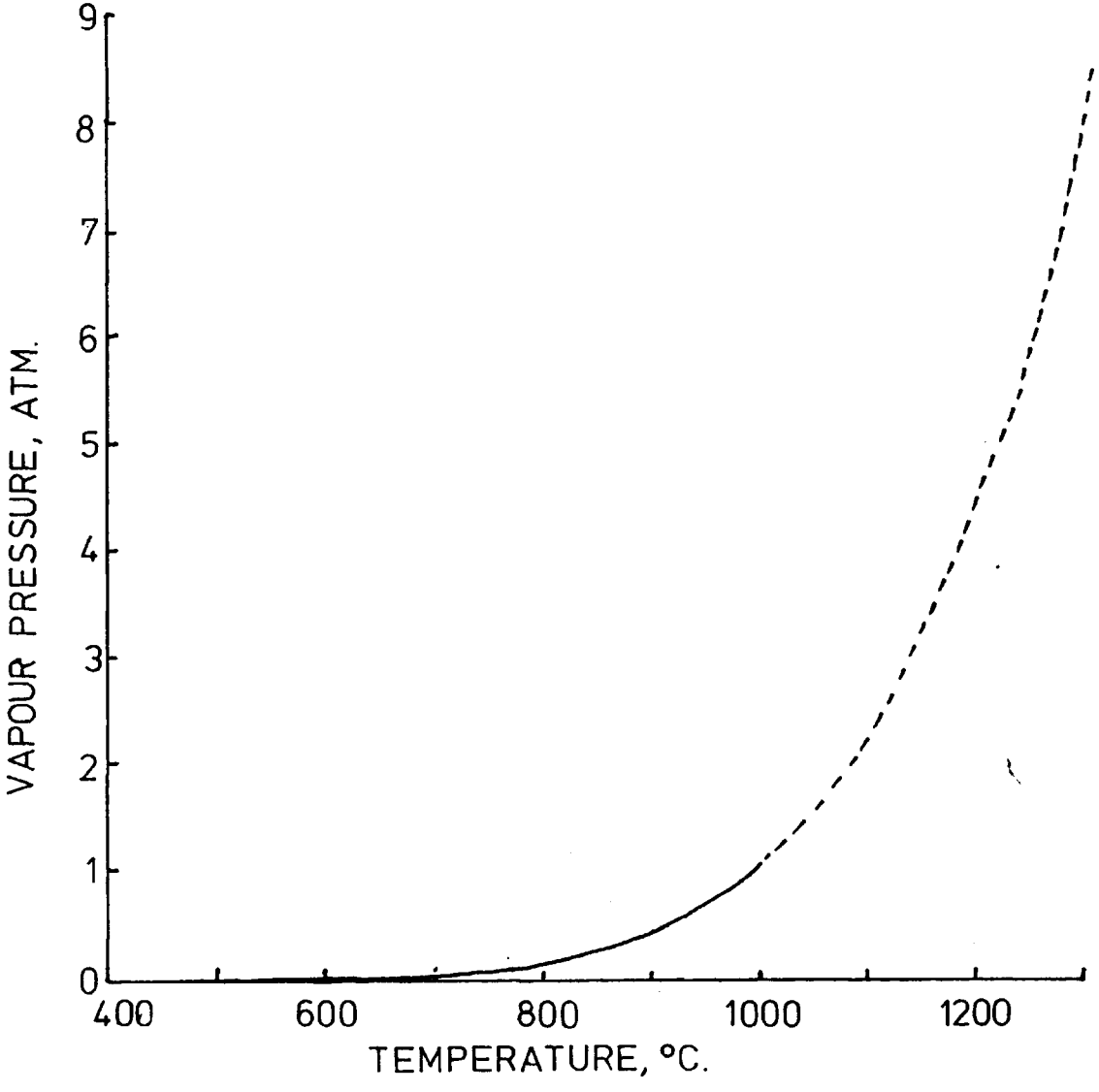

evaporation losses were ever observed.

For the same reasons, high gas pressure and a similar experimental arrangement were used to make the silicon-tellurium alloys.

Once the constituents of the glasses had melted and homogenised, the elements concerned still exerted some fraction of their individual vapour pressures, and so a restraining pressure was still needed to prevent them evaporating off. During conductivity measurements, an argon pressure of about 20-30 atmospheres was judged to be sufficient for this purpose.

In the case of the measurements of the electrical conductivity of sulphur, the sulphur was present at unit activity, and thus exerted its full vapour pressure. The behaviour of sulphur vapour is extremely complex, as it consists of a mixture of molecular species, mainly ranging from S_2 to S_8, in equilibrium with one another. The vapour-pressure/temperature relation is correspondingly abnormal, and has been experimentally investigated by Baker (87), and by Rau et al (97). The vapour pressure/temperature curve steepens markedly at high temperatures, the pressure being only 10 atmospheres at 643°C, but reaching 100 atmospheres at 936°C. The pressures required to prevent the boiling of sulphur were selected on the basis of Baker's results (87) (Fig. 3), in general, an argon pressure about 20% in excess of the equilibrium vapour pressure being employed. A practical limit to the investigations was thus reached at a temperature of 900°C, when an applied pressure of about 100 atmospheres was required, a pressure which was considered to be the safe maximum for the perspex lid of the pressure vessel.

3.2. The Main Pieces of Apparatus Used in the Manufacture and Testing of the Chalcogenide Glasses.

3:2:1. The radio-frequency induction heated furnace, used for manufacture of the glasses.

To manufacture the glasses rapidly, a technique using radio frequency heating inside a pressure vessel was employed. This enabled rapid heating to be achieved, as well as the rapid cooling rates needed to prevent crystallisation, and allowed the temperatures needed to melt the silicon content of the glasses to be reached, temperatures above the range of most conventional resistance-heated furnaces. A diagram of this apparatus is shown in Figure 5. The vessel was water-cooled, and had a bolted-on lid and base, sealed by neoprene 'O' rings in grooves. The thermocouple leads (A) were sealed into a four-bore alumina tube with 'Araldite' resin, the alumina tube being sealed in turn with 'Araldite' into a brass connector, which was screwed into the vessel wall. This is a common technique for passing wires which will carry very little current through the vessel walls, and was satisfactory up to quite high pressures. The radio frequency coil (B) which was in the centre of the vessel, was made from copper tube to allow for water-cooling, and passed through the lid by means of two ceramic insulators. A separate water-cooling circuit was provided for the coil, as a failure of the coil would cause high-pressure gas to escape along the connecting pipe, and would damage the r.f. generator if the latter were connected to the same circuit. The sample (C) was situated in a hollow graphite block (D) which acted as a susceptor. This block was thermally insulated by alumina powder in an alumina outer case (E), which just fitted inside the r.f. coil. No other insulation was necessary,

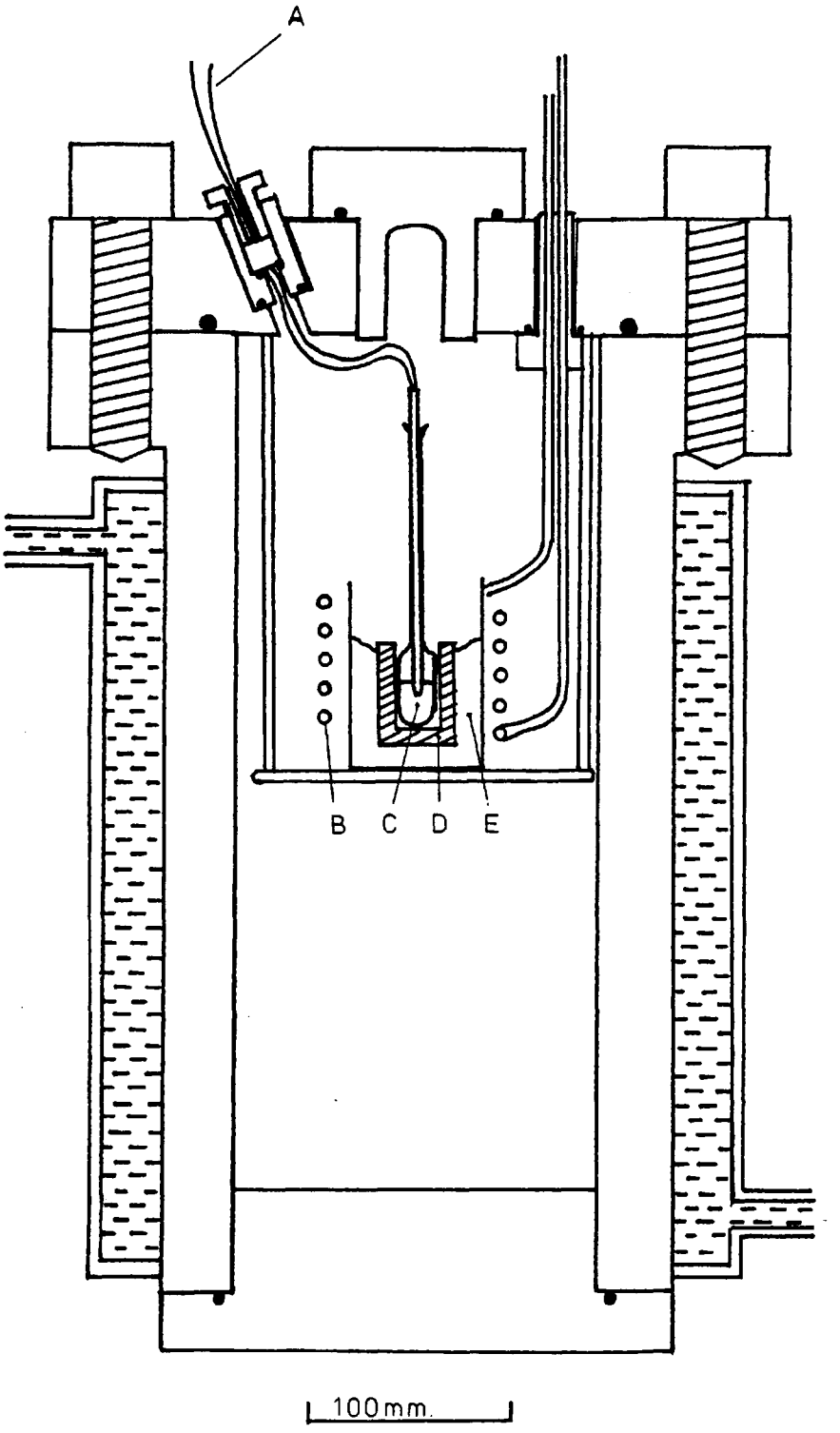

Fig. 5. Water-cooled radio frequency pressure furnace used for manufacture of chalcogenide glasses. Items A - E are described in the text of Section 3.2.1.

the volume between the coil and the vessel walls being empty to assist the rapid cooling of the sample. The gas inlet and outlet (F) were sealed by a conventional type of high pressure joint in which a male conical fitting on the pipe is compressed into a female conical fitting on the vessel by means of a nut. The gas supply was from a proprietary cylinder via a high pressure regulator. The thermocouple output was fed to a "Cambridge" direct reading pyrometer.

3:2:2 The resistance-heated furnace, used for testing of the glasses

Measurements of the electrical conductivity of the chalcogenides required accurate temperature control and an electrically "quiet" environment, which cannot be obtained using radio frequency induction heating, and also involved prolonged experimental runs at temperatures more moderate than those required for the manufacture of the glasses. It was thus considered advisable to use resistance heating for these situations, and the furnace shown in Figure 6 was available from previous work and proved ideal. This consisted of a platinum-wound alumina furnace tube (A). For reasons described in Chapter 1, notably convection, the tube contained a baffle (B) which blocked off the bottom half of its length, and it was fitted with an extra booster winding (C) around its top half to counteract the thermal gradients produced by convection. The vessel was similar in construction to the radio frequency furnace, and bursting pressure calculations regarding it may be found in Chapter 1. The vessel walls and lid were again water-cooled, and gas was supplied direct from a cylinder, flow being regulated by two valves. Unlike the r.f. heated furnace, the vessel containing the resistance-heated furnace was packed with alumina powder as

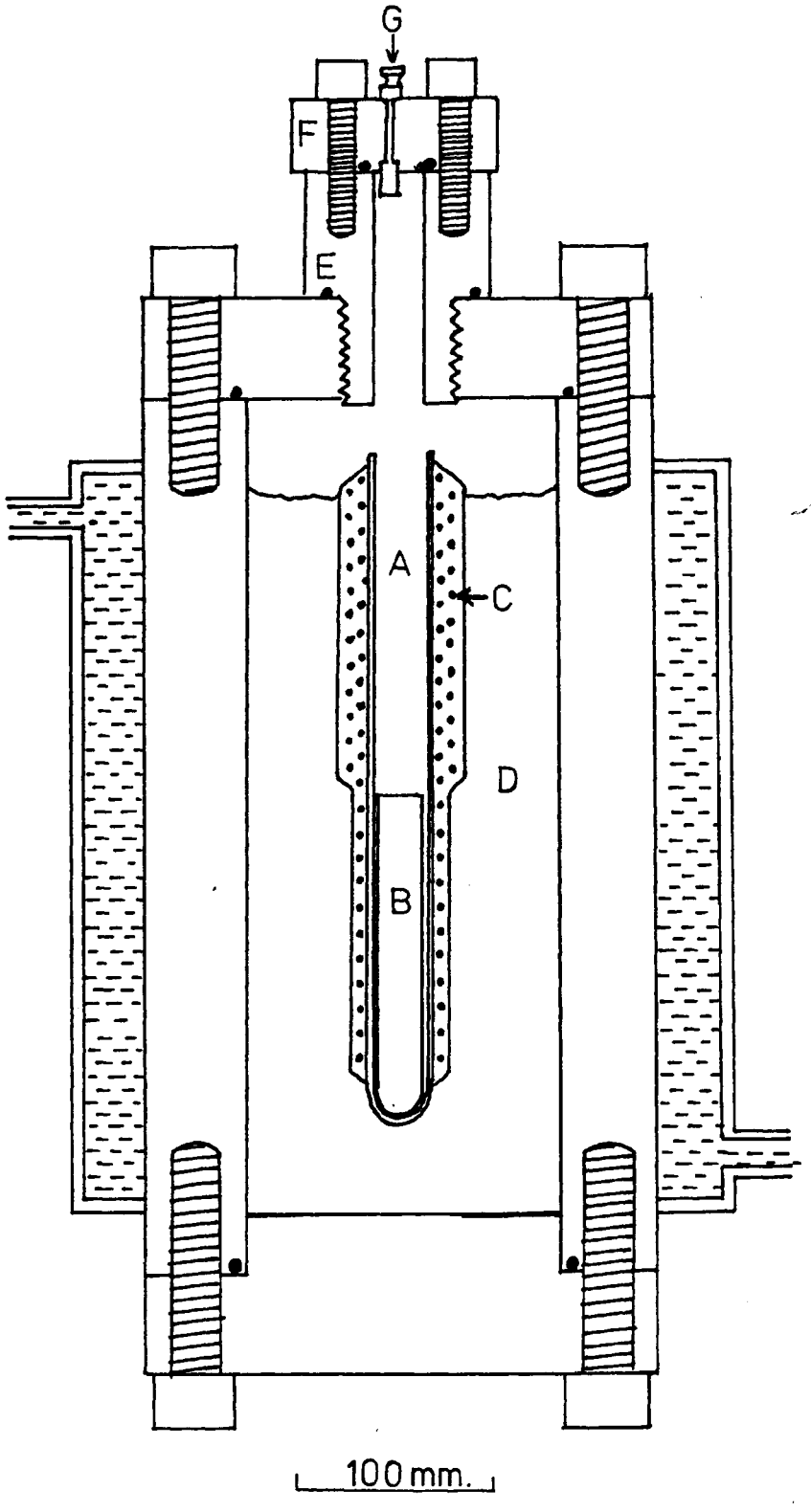

Fig. 6. Resistance heated pressure furnace used for conductivity measurements, etc. Items A - G are described in the text of section 3:2:2.

insulation (D) as temperature stability was more important here than was rapidity of heating and cooling. The vessel lid was fitted with a short cylindrical extension (E) which screwed into the centre and was sealed with an O-ring. This extension had a perspex lid (F) which could be bolted on, and which bore four connectors (G) for use in conductivity measurements (only one connector is shown in Figure 6 for clarity). This lid was intended as the weakest point on the vessel, so its bursting point represented the limit of the resistance heated furnace in its present form. The stress pattern in such a lid will be extremely complex, so any calculation of the safe working pressure will involve considerable simplification, and should be applied with some caution. The formula for the pressure on an unpierced circular plate supported at its edges is $P = \frac{16.f.t^2}{5d^2}$, t being the plate thickness, 25 mm in this case, f being the maximum allowable stress, here set to half the tensile strength of Perspex, 75 N/mm^2 [4]. The value for d, the plate diameter, is more difficult to assign, as the pressure acts only on the area within the O-ring, but the support is at the ring of bolts. If a compromise value of 60 mm is used, a maximum safe pressure of about 21 N/mm^2 (210 atm.) results. The lid in the present case is weakened by the four measurement leads which pass through it, and it was felt prudent to restrict the operating pressure to 100 atmospheres in practice.

Power for the furnace windings was carried into the vessel by the type of connector shown in Figure 7. This was similar to a spark plug, in that it achieved insulation by means of a ceramic insert into which the conductor was bonded. This type of connection is the commonest type where high currents have to be carried, and car spark plugs or marine diesel engine igniters

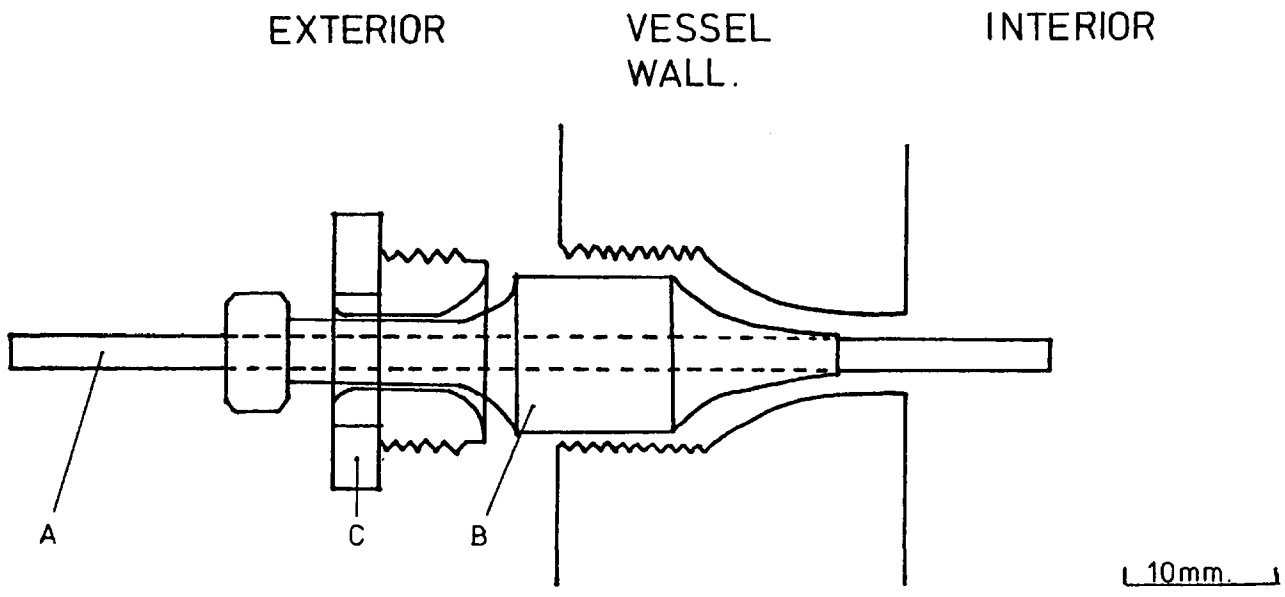

Fig. 7. Type of connector used to take power into the furnace shown in Fig. 6.

Contact is via steel rod 'A', bonded to alumina insert 'B'. This is pressed into the vessel wall by a threaded collar (shown here in Section) 'C'.

are often used as a source of cheap and effective connections which are suitable for moderate pressures. The power could either be supplied from a pair of "Variacs", one for the main and one for the booster winding, or from a Stanton-Redcroft temperature programmer, which provided automatic control of heating and cooling rates.

Temperature display and measurements were performed using a Honeywell two pen chart recorder and a "Cambridge" potentiometer. A "back-off" unit, consisting of two dry cells and a voltage divider circuit, was connected to the chart recorder input so as to oppose the thermocouple e.m.f. This allowed the chart recorder to be used at its maximum sensitivity (1 mV full-scale deflection), even when the true thermocouple e.m.f. would have been sufficient to send the recorder offscale. The potentiometer was connected to the other channel of the chart recorder, and precisely the same backing-off voltage applied to it. The potentiometer was then adjusted to cause the two pen traces to coincide, at which point the potentiometer was supplying precisely the same voltage as the thermocouple. Thus, the potentiometer reading could be used to determine the temperature, by means of the usual cold junction corrections.

The vessel pressure was monitored on a Barnet Instruments bourdon-type gauge, and the gas was fed direct to the vessel from cylinders of high-purity argon supplied by the British Oxygen Company.

The above apparatus was used for the phase diagram work on silicon-tellurium alloys, and for all the determinations of electrical conductivity except those in the range 0 - 200^{o}C.

3:2:3. The apparatus used for the manufacture of chalcogenide glasses by the conventional process.

The conventional method for the manufacture of chalcogenide glasses involves the heating of the constituent elements to about 1000°C in a sealed silica bulb. The bulb is agitated at this temperature for a period varying from 24 hours to several days. The bulb is then quenched into cold water or liquid nitrogen as required. To carry out this process, the apparatus shown in Figure 8 was constructed. The elements were weighed out into a 10 mm diameter vitreous silica tube which was closed at one end. This was then evacuated and sealed off to produce a bulb about 30 mm long containing the constituents of the glass. This was then placed in a 20 mm diameter tube and wedged at an angle across it by wads of silica wool. This outer tube was 700 mm long, and was supported at either end of the furnace by graphite rings which served as "bearings" in which the tube could rotate freely. One end of the tube was attached to a small electric motor which rotated it at approximately 3 revolutions/minute. The furnace was maintained at about 900°C by a Eurotherm temperature controller. The rotation caused the liquid to run from one end of the bulb to the other, providing continuous agitation. After 48 hours, the tube was withdrawn and plunged into cold water to quench the glass, which could then be removed by breaking open the bulb. This technique was used to manufacture several batches of glass, and proved very successful, although much more laborious than the high pressure method, (Section 3:2:1). The material produced proved identical in all respects to that produced at high pressure.

Fig. 8. Apparatus used for conventional method of making chalcogenide glasses.

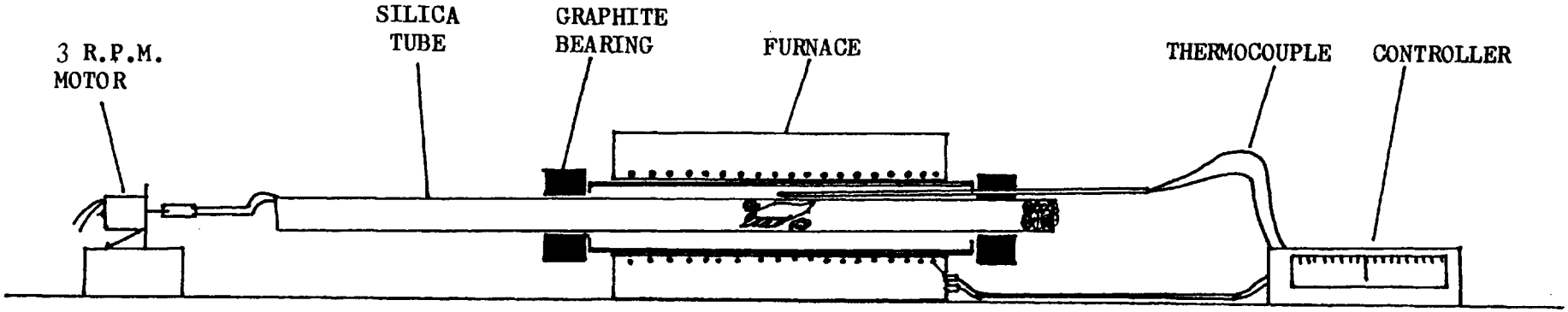

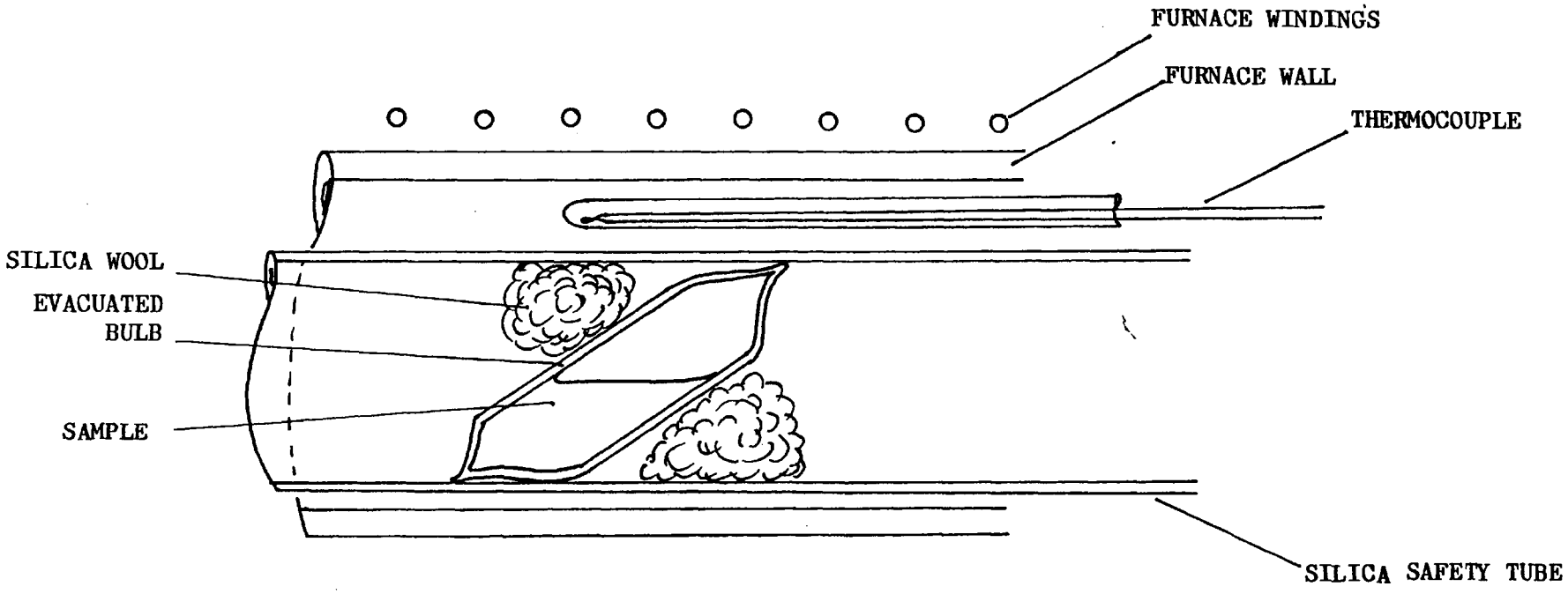

3.3. Experimental Techniques

3:3:1. The technique used to manufacture the glasses

The chalcogenide glasses were normally produced in the radio-frequency induction furnace described in 3:2:1. The starting materials were from the following sources:

Arsenic	:	"Puratronic" grade 1 from Johnson Matthey Chemicals Ltd. Total metallic impurity content less than 5 ppm.
Germanium	:	"Puratronic" grade 1 (Johnson Matthey Chemicals). Total metallic impurities less than 1 ppm.
Selenium	:	Metals Research Ltd. 5N Selenium pellets. 99.999% Se.
Silicon	:	"Puratronic" grade 1 broken ingot (Johnson Matthey Chemicals). Total impurity content 2 ppm.
Sulphur	:	Halewood Chemicals Ltd. "S.1. Sulphur powder". 99.9999% quoted purity.
Tellurium	:	Koch-Light Laboratories. "Tellurium Lumps". 99.999% pure Te.

The required amounts of these elements were weighed out as accurately as

possible, any crushing being carried out in a percussion mortar with a tungsten carbide ball and cup.

The crushed constituents were then placed in a vitreous silica container of the form shown in Figure 9, consisting of a chamber with a long narrow neck, in which a thermocouple sheath was a tight sliding fit. This arrangement allowed gas to enter and leave the bulb freely, but once pressure equilibration between inside and outside had been achieved, the space between the neck and the sheath was filled with static gas, which prevented the vapours of the various constituents from escaping. This assembly was placed in a silica safety tube intended to contain any liquid which would escape were the chamber to crack. This was supported inside the R.F coil of the furnace described in Section 3:2:1, by a graphite susceptor which was mounted in an alumina pot from which it was insulated by alumina powder. The R.F. coil was water-cooled, and was powered by a 450 kHz "Radyne" generator.

When this arrangement was in place inside the furnace, a Platinum/13% Rhodium-Platinum thermocouple was inserted in the sheath and connected to the leads of the pyrometer via the insulators described in 3:2:1.

All the glass constituents oxidise readily when heated, so it was first necessary to remove as much oxygen as possible from the vessel. This was achieved by evacuating the vessel to a pressure of less than 0.1 mm Hg, and then pressurising with argon to 10-15 atmospheres. This gas was then allowed to escape, carrying most of the remaining air with it.

Fig. 9. Bulb used in production of samples.

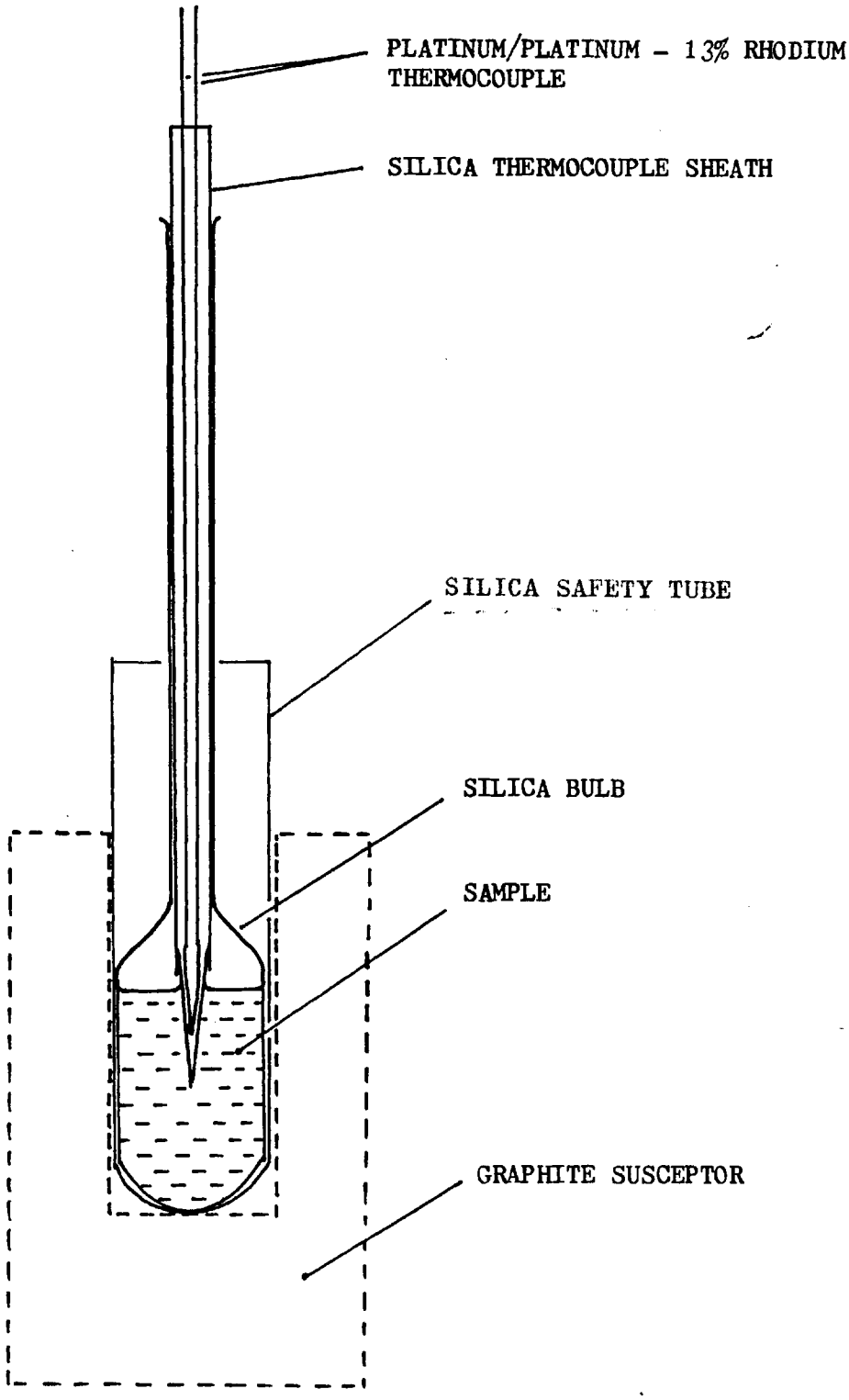

This pressurising and depressurising process was then repeated.

Immediately before heating, the argon pressure in the vessel was raised to 600 p.s.i. (4.14 N/mm^2). In the case of STAG, the material was then heated to 1450°C in about 10 mins, to melt the silicon, and held at 1450 ± 10°C for 20 minutes to allow complete fusion to occur. The mixture was then cooled to 1000°C and held at 1000 ± 20°C for a further hour to allow for homogenisation, after which it was allowed to cool to 600°C for degassing. In the case of the sulphur and selenium-containing glasses, the constituents were heated to 1000°C for 45 mins (as no Si was present) and then cooled to 600°C for degassing. At 600°C, the mixture was far enough above the glass transition temperature to be reasonably fluid, and thus to allow any bubbles of gas to escape, but it was not so hot that the constituents would boil if the pressure were released, so, with the temperature maintained as near to 600°C as possible, the pressure was allowed to fall to 1 atmosphere over a period of about 20 minutes, after which the material was allowed to cool. As the furnace had a low thermal mass and contained very little insulation, cooling was quite rapid, about 10°C/minute at the glass transition point. After cooling, the material was removed by breaking the bulb, and it was then stored in argon-filled desiccators to protect it from long-term atmospheric damage. The material was usually made in 25 gm batches, although larger amounts could have been easily accommodated, up to a maximum of about 100 gm.

3:3:2 Techniques used to determine the electrical conductivities

(a) of the solid chalcogenide glasses

It proved possible to use a very elementary technique to measure

the conductivity of the solid chalcogenide glasses, as these materials showed no signs of decomposition or softening up to temperatures of about 250°C, providing they were protected by argon at 1 atmosphere pressure.

Specimen preparation

The material was cut into small blocks, typically 5 x 5 x 3 mm, using a "Capco" slitting wheel which had a very thin blade, enabling very narrow accurate cuts to be made. Gold was deposited on the two square faces of the blocks, either by means of a manually controlled vacuum evaporator of the kind used for "shadowing" electron microscope specimens, or later by means of a semi-automatic device called a "Hummer" which operated on a glow-discharge principle. The unplated sides of the specimens were then lightly polished on fine emery paper to remove any oxide which might have formed there, and also any gold which had "spilled over" from the top and bottom surfaces. The specimens were then checked to ensure that the corners were all right-angled and that opposite faces were parallel. This check was carried out using a travelling microscope, and the results were always very good, as the "Capco" machine had an accurate traverse and a rotating head calibrated in degrees. The same microscope was used to measure the dimensions of the specimen to enable L/A values to be calculated. Although surface oxidation has been shown to introduce errors into measurements of electrical conductivity only at moderately high temperatures (98,99) the specimens were stored in argon-filled desiccators until they were required.

Experimental arrangement

For this low-temperature range, the experimental arrangement shown in Figure 10 was used, in which two gold plates* (A) served as electrodes, and were held in contact with the gold-coated surfaces of the specimen (B) by an adjustable spring (C). The plunger (D) which acts on the top electrode, and the outer case which supports the lower electrode, were made of Pyrex glass, which has a very high resistivity, ($10^{12}\Omega$-m) and so removes the possibility of short-circuit paths between the electrodes. Since the resistances of the specimens were so large, $\gg 1$ kΩ, the resistances of the leads and contacts were not significant, and variations in spring pressure had no effect on the readings. The arrangement described above was placed in a large pyrex tube which had two leads for conductivity measurements sealed into its walls, and which was provided with inlet and outlet tubes to allow argon to be passed through the cell during the experiment. To eliminate stray capacitance effects, this tube was lined with copper foil which could be earthed to provide an electrical shield. The temperature was adjusted using either a water bath, an oil bath or a small resistance furnace, depending upon the range of temperatures required.

Experimental technique

Argon was first passed through the cell to prevent oxidation. Once air was purged from the container, the argon flow was kept as small as possible to avoid chilling the sample, and the apparatus was heated to the required temperature, which was measured by means of mercury in

---

* Johnson & Matthey "Specpure" gold sheet, $>99.999\%$ purity.

Fig. 10. Apparatus used to measure electrical conductivity of solid chalcogenide glasses (0 - 200°C).

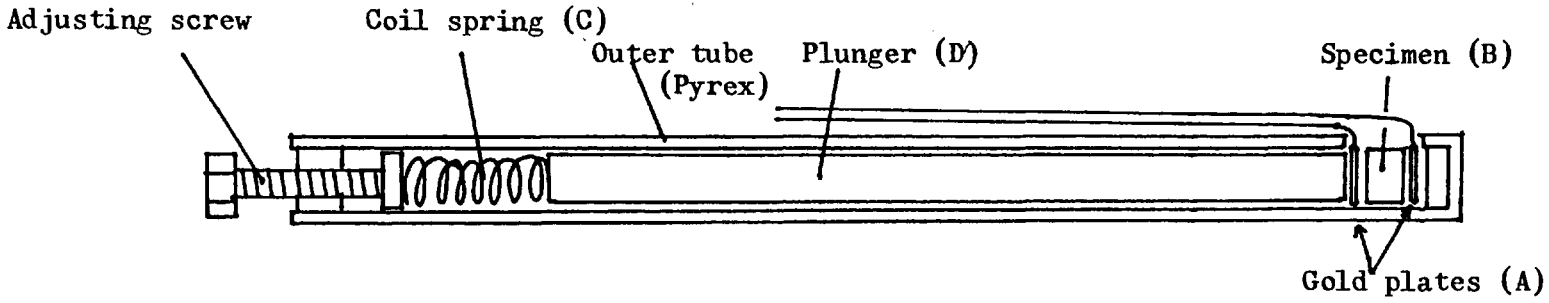

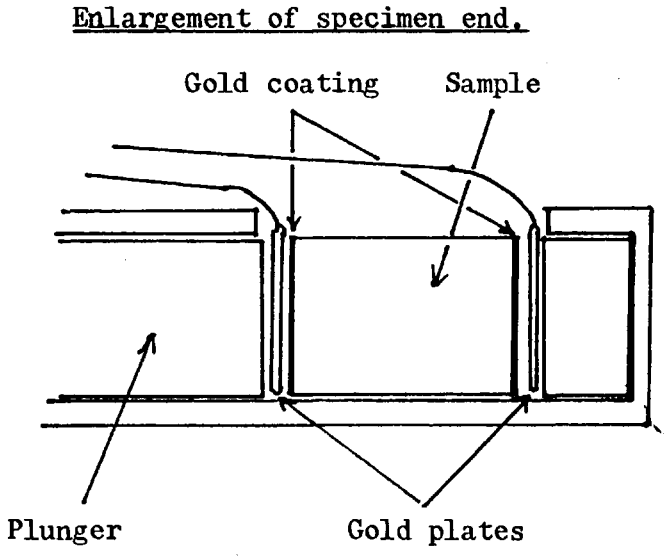

glass thermometers, and allowed to come to equilibrium. The sample resistance was measured with a Wayne-Kerr B221 Universal Bridge, which uses 1592 Hz A.C. and which has a facility for "trimming out" the impedance of the measuring leads. The bridge functions by applying a known voltage to the sample and measuring the resulting current, balance being indicated by a null meter reading on the instrument. The temperature was then raised by 10-20°C and the process repeated.

(b) Measurements on liquid chalcogenide glasses

When chalcogenide glasses of the kind investigated here are heated to about 280°C, theydevitrify rapidly, decomposing into crystalline phases such as GeTe, and, at a slightly higher temperature they begin to melt. A change of technique was therefore required for work at higher temperatures, involving a conductivity cell to contain the liquid and retain the electrodes. The two types of cell used to investigate the conductivity of the chalcogenides above their melting points are shown in Figure 11 (a) and (b), the simpler type (a) being usable up to about 550°C, and the four-armed type being required from 550 to 1150°C.

The cells,which were made of vitreous silica, consisted of a U-shaped capillary section (A) at the bottom, joined to 2 or 4 arms of wider bore silica tube (B) which held graphite electrodes* (C and D). The cell was filled with chalcogenide glass to the level shown, the material in the capillary (bore ~1 mm) providing almost all the resistance between the electrodes, and the liquid in the wider sections (bore ~5 mm)

---

* Johnson & Matthey Specpure graphite rods. Total impurity content <10 ppm.

Fig. 11. Conductivity cells used with liquid chalcogenide glasses.

Fig. 11 (a).

Conductivity cell used up to 550°C

Fig. 11 (b).

Conductivity cell used above 550°C.

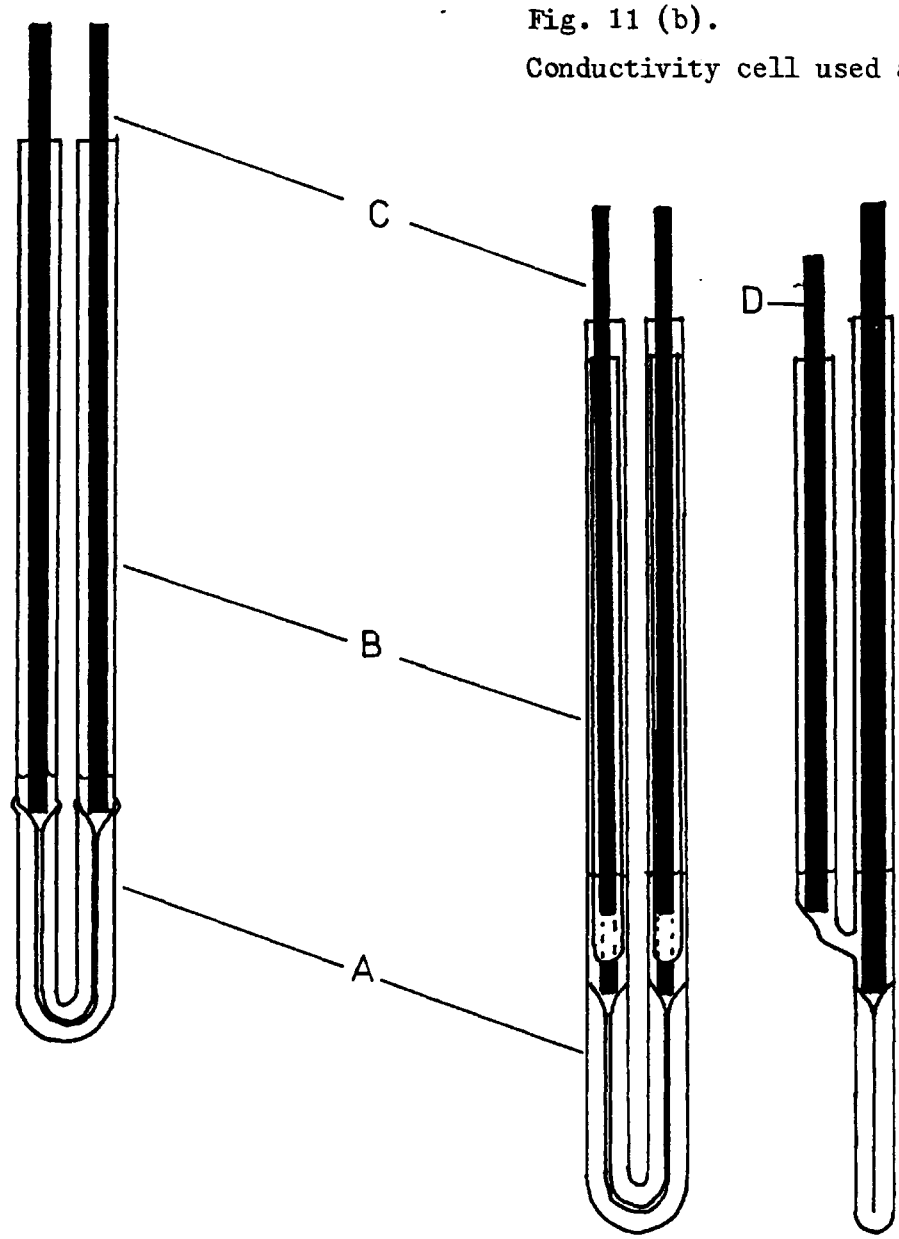

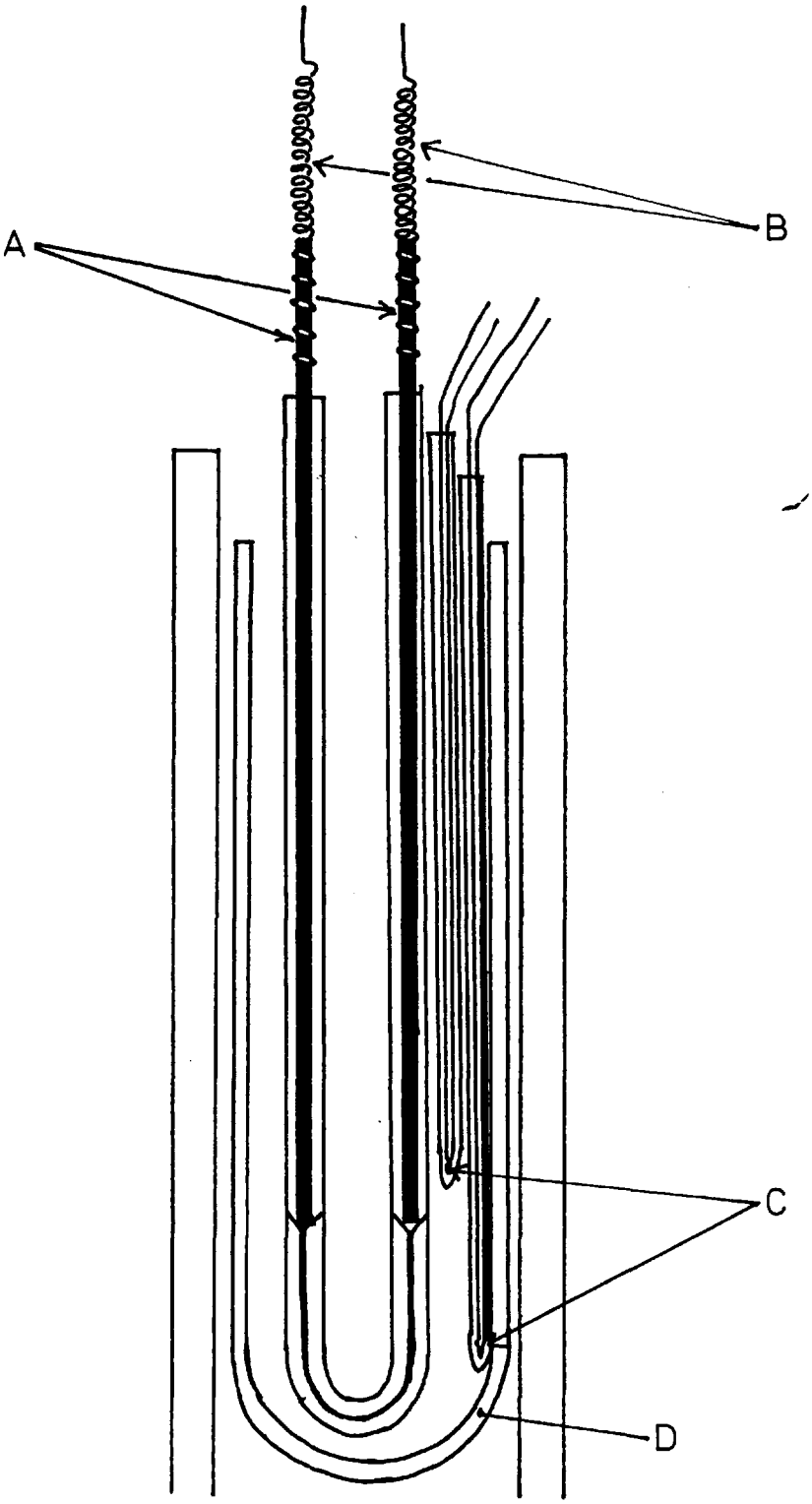

Fig. 11 (c). Conductivity cell in place inside the resistance-heated pressure furnace.

acting simply as contacts between the electrodes and the thread of liquid in the capillary. Between the melting point and 550°C, the resistance of the liquid thread was large in comparison to the resistance of the leads and the junctions between various parts of the measurement leads. Thus, over this temperature range, the simple two-point cell was satisfactory, and the Wayne Kerr Bridge could be used, as in the case of the solid material. To make sure no frequency-related effects were occurring, occasional check readings were made using a Keithly 610 Electrometer, which was a D.C. measurement technique.

As the temperature approached 550°C, the resistance of the thread diminished to the point where lead and contact resistances became significant, and a change of technique was required in order to pursue the measurements any further. The four-probe technique provided an elementary but effective way of avoiding lead resistances, and involved using one pair of electrodes to supply a current to the unknown resistance, and using a second pair of electrodes to measure the voltage drop across a fixed length of it. Using a digital voltmeter (D.V.M.) with a high input resistance (in the case of the Solartron D.V.M. used here, $10^9 \Omega$), the current in the measurement circuit was kept very low (in this case probably 10^{-10} of the specimen current), and the IR drops in the leads and junctions were correspondingly reduced to an insignificant level as the much greater current flowing in the specimen provided a large IR drop to be measured. It would have been possible to determine the resistance by measuring the current and using Ohms law, but it was found to be simpler to measure the voltage drop across a standard

resistor which was in series with the unknown, and thus carried the same current. The specimen resistance could then be found by direct comparison. This could either be achieved with a simple D.C. circuit, or by means of a Q221 adaptor, operating on the same principle which could be used in conjunction with the Wayne Kerr Bridge, and which gave a direct reading of resistance. To accommodate the two current-supply electrodes and the two voltage-measuring electrodes, a four-armed conductivity cell was required as shown in Fig. 11 (b). This type of cell required considerable glass blowing skill and had to be professionally made.

The detailed experimental procedure was as follows:

(1) Determination of cell constant

Although it would still have been feasible to calculate the L/A values for these cells in a similar manner to that used for the solid samples, greater accuracies were obtained by the use of standard solutions, whose specific conductivities are precisely known, as the standardisation process is not subject to the sorts of errors that a calculation would be, (for instance, variations in capillary diameter along the length of the tube which were quite likely to occur as the tube had been deformed during manufacture of the cell).

The specific conductivity of the solution divided by the conductance value obtained when the cell was filled with the solution is a ratio which is called the "cell constant" and can be substituted for L/A.

Thus, in processing the results obtained on liquid chalcogenide materials, the specific conductivity was calculated by simply multiplying the conductance value by the cell constant.

The standard solutions used were 0.1 N and 0.01 N potassium chloride, these being 7.4191 gm/litre and 0.74191 gm/litre solutions respectively. The specific conductivities (K) of these solutions over the range 15-25°C follow equations of the form $K = A + (B \times 10^{-3}T) + (C \times 10^{-6}T^2)$, T being temperature, and A, B, and C being constants, obtained in this case from the International Critical Tables (100).

The cells were first cleaned with distilled water and dried, then rinsed several times with the solution to be used. They were next filled with standard solution to the same level as they would later be filled with the chalcogenide glasses. Two new "Specpure" graphite electrodes were then inserted and checked to ensure that no air bubbles were trapped beneath them. This arrangement was then placed in a water-bath and allowed to come to temperature equilibrium. When equilibrium was reached, the conductance was measured on the Wayne Kerr bridge, and the temperature taken on a mercury thermometer accurate to 0.2°C. The specific conductivity corresponding to this temperature was then read off, and the cell constant calculated as described above. This procedure was then repeated using the second solution, and an average cell constant calculated. This was generally about 300 cm^{-1}, and the values obtained on any one cell using the two different solutions differed by only about 2%.

All the resistance measurements on liquid chalcogenides were performed

in the pressure vessel described in Section 3:2:2, which contained a platinum resistance furnace. The first step of the process was to melt the chalcogenide glass in order to fill the cell. Powdered chalcogenide was placed in one side of the cell, piled high enough to allow for the volume decrease that would occur when the powder liquefied and coalesced. The tops of the arms were lightly plugged with silica wool, and the cell placed in the pressure furnace.

These materials oxidise readily at moderate temperatures, so to exclude oxygen, the vessel was closed and evacuated, then pressurised with argon to 10 atmospheres. After this, the gas was then released, and the pressure allowed to fall to 1 atmosphere to carry out the remaining oxygen. The pressure was then raised to about 10 atmospheres, and the furnace heated to about 500°C and held for $\sim$30 minutes to melt the glass. The liquid flowed into the capillary until an equal column was formed in all the arms of the cell. The practice of only filling one side with powder prevented a bubble being trapped at the bottom of the capillary. The pressure was then increased to 20 atmospheres to compress any bubbles that were present, and the temperature raised to 600°C for 20 minutes to ensure complete fusion. The material was then allowed to cool to room temperature. The cell was then removed, inspected for bubbling and other defects, and set up for use. The experimental arrangement is shown in Figure 11 (c). The electrodes (A) were connected to the lid by copper wires (B) which were coiled like a spring for flexibility, and also to cause them to force the electrodes into position in the cell. The temperatures just above and just below the specimen were measured by the Pt–Pt + 13% Rh thermocouples (C), and the whole arrangement was placed

in a silica safety tube (D) to protect the furnace from any chalcogenide that might escape if the cell fractured. The bottom 150 mm of this safety tube was usually filled with alumina powder to cut down gas turbulence, which otherwise caused temperature fluctuations, and a temperature gradient across the length of the specimen. This arrangement was assembled, all its leads sheathed with braided insulation, and placed in the furnace. The top of the furnace was loosely filled with asbestos wool to provide thermal insulation. The leads were connected to the lid, and the set-up was checked for shorting between leads, thermocouples, and the vessel walls. When assembly and checking were completed, the conductivity bridge was connected to the terminals on the perspex furnace lid, and the door of the protective cabinet around the pressure vessel was closed for the duration of the experiment. Air was flushed out as before, and the apparatus heated under 20 atmospheres argon pressure to begin the experimental run. The furnace temperature was monitored using the Honeywell chart recorder, the potentiometer and the biassing unit (described earlier in Section 3:2:2) in conjunction with the thermocouple located just below the conductivity cell. When the desired temperature was reached, the furnace currents were adjusted to stabilise the furnace at this temperature level. The potentiometer was then disconnected, and the upper thermocouple in the furnace connected to the second recorder pen. The currents in the main and booster windings of the furnace were then re-adjusted so that both upper and lower thermocouple readings were equal and steady. When this was achieved, the potentiometer was re-connected in place of one thermocouple, and a simultaneous temperature and conductivity measurement made.

The temperature was then raised by about 50°C, and the process repeated. When the maximum temperature at which accurate conductivity readings could be taken was reached (i.e. the temperature at which the sample resistance became too low for the bridge to detect), the process was repeated for downward temperature steps of 50°C to check the validity of the readings obtained on heating.

This procedure was adopted for all the conductivity measurements on liquid chalcogenides, except that some of the high-temperature measurements were made under 50 atmospheres of argon to suppress volatilisation which might otherwise have resulted from the higher vapour pressures.

(2) The Electrical Conductivity of Sulphur

The resistivity of sulphur at a given temperature is always much greater than that of the chalcogenide glasses, and to make accurate measurements of the conductivity of sulphur, it was necessary to have a conductivity cell which passed more current than the capillary cells described above at the same voltage, that is, which had a lower cell constant. This can be achieved by enlarging the area of the electrodes or decreasing the distance between them. Eventually, the arrangement shown in Figure 12 was decided upon. The electrodes and their leads were of gold, this being the substance least likely to be attacked by the sulphur. The cell constant determination using standard KCl solutions was identical to that described above for the cells used with the chalcogenide glasses. The filling of the cell, with 99.9999% pure sulphur, was performed in the atmosphere, as the risk of oxidation was far less than that for the chalcogenides. The cell was filled

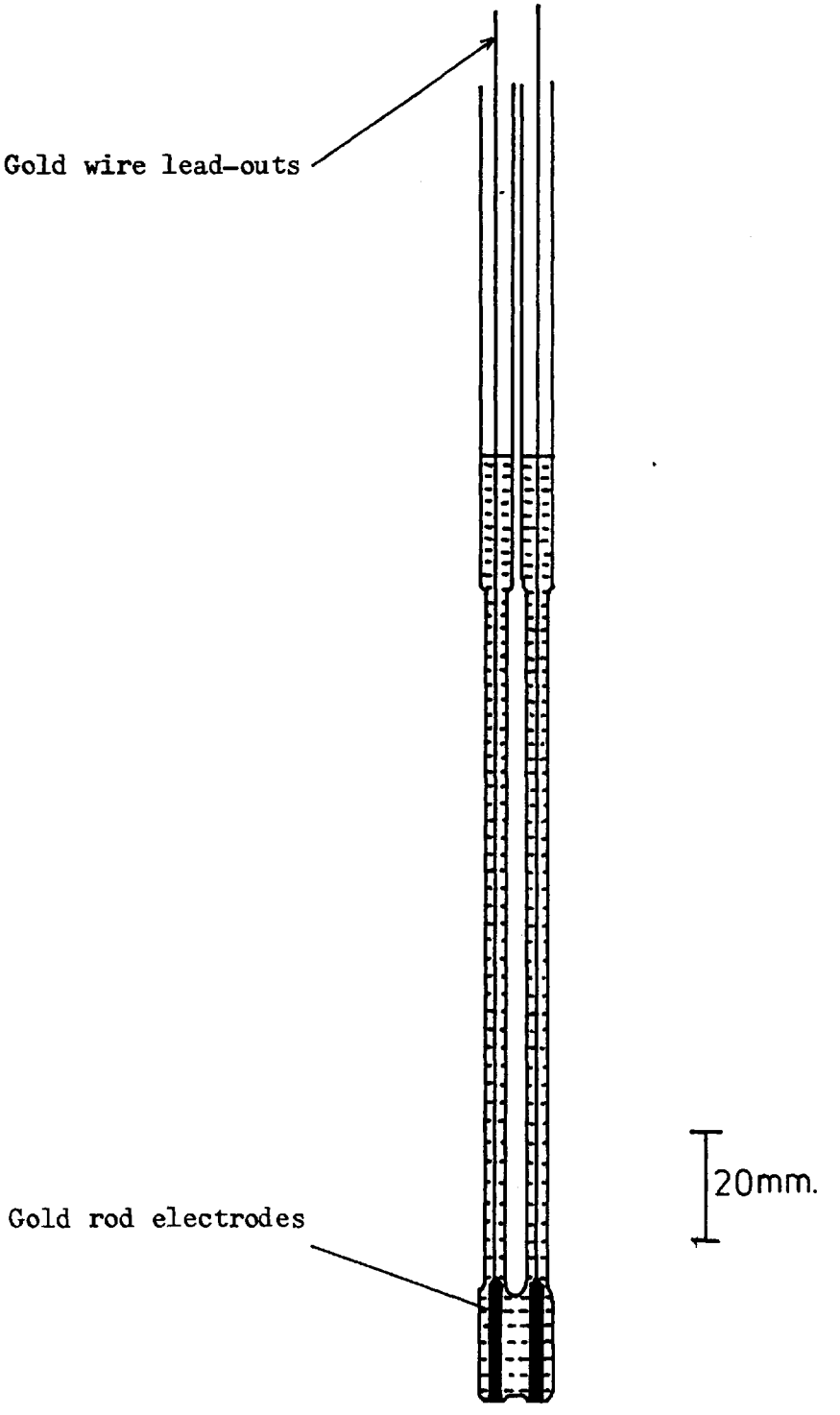

Fig. 12. Conductivity cell used for measurements on liquid sulphur.

with powdered sulphur, and heated over a gas flame until the sulphur melted and all the bubbles were removed. For this it was necessary to keep the temperature within the range over which sulphur is very fluid and pale yellow (120-150^{o}C). (Overheating caused polymerisation and produced an extremely viscous dark red liquid in which the bubbles did not rise).

This cell was set up in the resistance-heated pressure furnace in exactly the same manner as that described for the measurements on chalcogenide glasses, and the same measurement technique was used.

3:3:3. Determination of the Si-Te phase diagram using thermal analysis

Owing to the much greater volatility of Te compared to Si, measurements on the Te-Si system have to be carried out at elevated pressures to prevent loss of tellurium, particularly when working with high-silicon compositions. The various phase boundaries in an alloy system may be detected as a result of the latent heat absorbed or released when the boundary is crossed. This is normally carried out using differential thermal analysis (D.T.A.), in which measurements are made of the temperature difference between the sample in which the phase change is anticipated and a reference sample in which it is not. This is usually done with two thermocouples (one in each sample) connected so that their e.m.f.'s cancel out. The sample and reference are then heated and cooled past the transition point, and any phase changes in the sample are revealed as the thermocouple e.m.f.'s go out of balance. Previous experience (101) had shown that the resistance furnace (described in

Section 3:2:2) was not suitable for D.T.A. techniques as the temperature gradients inside the furnace tube alter as the temperature changes, and the D.T.A. baseline would thus be subject to uncontrollable drifting. No loss in accuracy was involved, with this particular apparatus, in using a simple thermal analysis technique, in which the sample was heated and cooled steadily past the temperature at which a phase change was expected, and the absorption or emission of latent heat detected by the "arrest" which it caused in the smooth curve of specimen temperature.

To ensure that the investigations were being carried out on truly homogeneous materials, 10 gram samples of the alloys to be examined were prepared in scaled-down versions of the long-necked silica bulbs used for manufacture of the chalcogenide glasses, (Fig. 9). The alloys, which generally lay at 10 atom percent intervals across the phase diagram (the exceptions being near the expected compound composition, where more detail was required), were treated, several at a time, in the radio frequency induction furnace, exactly as for STAG glass. The resultant materials consisted of a virtually amorphous mixture of the two elements, those of high silicon content, in particular, showing no detectable crystallinity, and looking very similar to STAG and the other chalcogenide glasses. After processing, the silica vials containing the alloys were stored in argon-filled desiccators until use, to prevent damage by the atmosphere. (The most likely damage being loss of Te).

To determine the thermal arrest points associated with a particular

alloy, the vial containing the material was loaded into the platinum wound resistance furnace described earlier (Section 3:2:2), with similar precautions against gas turbulence, etc. to those used for the chalcogenide glass conductivity determinations; the vial also being buried in alumina powder for the same reason. A thermocouple was inserted into the silica tube passing down the neck of the vial, and was thus located centrally in the sample of alloy to record the sample temperature. A second thermocouple, in its own silica sheath, was placed to monitor the furnace temperature for control purposes. At high temperatures (i.e. on silicon-rich samples), problems were encountered with A.C. pickup from the furnace windings disturbing thermocouple readings, and it was necessary to line the thermocouple sheaths with platinum foil earthed to the pressure vessel body. This provided very effective shielding, and stable readings were then obtained even at temperatures in excess of 1400^{o}C.

When all connections had been checked, the pressure vessel was closed and flushed with argon as described previously, and then pressurised to 3.0 N/mm^{2} (30 atmospheres). The sample was then heated to about 100^{o}C below the temperature at which an arrest was expected, and the heating rate was then adjusted to about 2^{o}C per minute. Heating was continued, and the temperature at which any thermal arrests occurred was noted. Once the last arrest had been recorded, heating was stopped and the sample held at constant temperature for about 10 minutes, to allow for complete mixing of the constituents. The sample was then allowed to cool at about 2^{o}C per minute, and cooling arrests were recorded. When all the cooling arrests had occurred, the entire heating

and cooling cycle was repeated again to check the data obtained. At the high Te end of the diagram, true arrests were only detected on heating. On cooling, the sample would supercool by some tens of degrees even at the slowest practical cooling rate (and even, if as was tried during subsequent runs, foreign bodies, e.g. alumina powder, were added to nucleate solidification), whereupon solidification would occur suddenly with a dramatic rise in temperature. This is entirely consistent with the known behaviour of Te, and, as these measurements were only performed to check those reported at this end of the diagram by Bailey (92), it was not considered of great importance that the heating arrests should be duplicated on cooling. At the high Si end of the phase diagram, no such difficulties were encountered, arrests being duplicated closely on heating and cooling. A determination of the melting point of pure Te was made, again only on heating, but a literature value was used for the melting point of pure Si, to avoid an unnecessary high temperature run, as these were found to seriously shorten the life of the platinum furnace windings, and the furnace was required for the conductivity work.

3:3:4. The technique used to manufacture Si_2Te_3

As part of the investigation of the silicon-tellurium phase diagram, it was decided to prepare some of the system's only known compound, believed to be Si_2Te_3, trying to duplicate the technique used by Bailey (92), who reported that SiTe vapour was formed when powdered silicon and tellurium were heated to 830°C in vacuo, and that the compound Si_2Te_3 was deposited when this vapour came into contact with a surface held at 750°C. A small resistance furnace was obtained and its temperature

profile measured in the upright (i.e. furnace bore vertical) position. When the hottest part of the furnace was at 830°C, a point 70 mm above was at 750°C. Accordingly, a mixture of approximately 5 gm Te and 0.8 gm Si was placed in a silica tube which had been closed at one end, and which had a constriction about 30 mm from the closed end. This was then evacuated and sealed off 70 mm above the base, producing 2 chambers, one to rest in the hottest part of the furnace, in which SiTe would form, and the other to rest in the portion of the furnace at 750°C, in which the Si_2Te_3 would collect, (see Fig. 13). This dumb-bell shaped arrangement was then supported in the furnace at the correct height by an adjustable silica tube, and left for about 4 days for the compound to collect. Any crystals which were dislodged from the walls of the upper chamber were prevented from falling into the lower chamber by the constriction.

This experiment confirmed Bailey's findings, that red, transparent hexagonal crystals are produced, which are instantaneously attacked when exposed to the atmosphere.

3:3:5. High current transport experiment

To determine whether it was possible to observe, on a macroscopic scale, any segregation of the glass constituents as a result of current flow, the single experiment described below was carried out.

A cell was prepared (using vitreous silica) similar to that shown in Figure 11(a), the only difference being that the portion which had

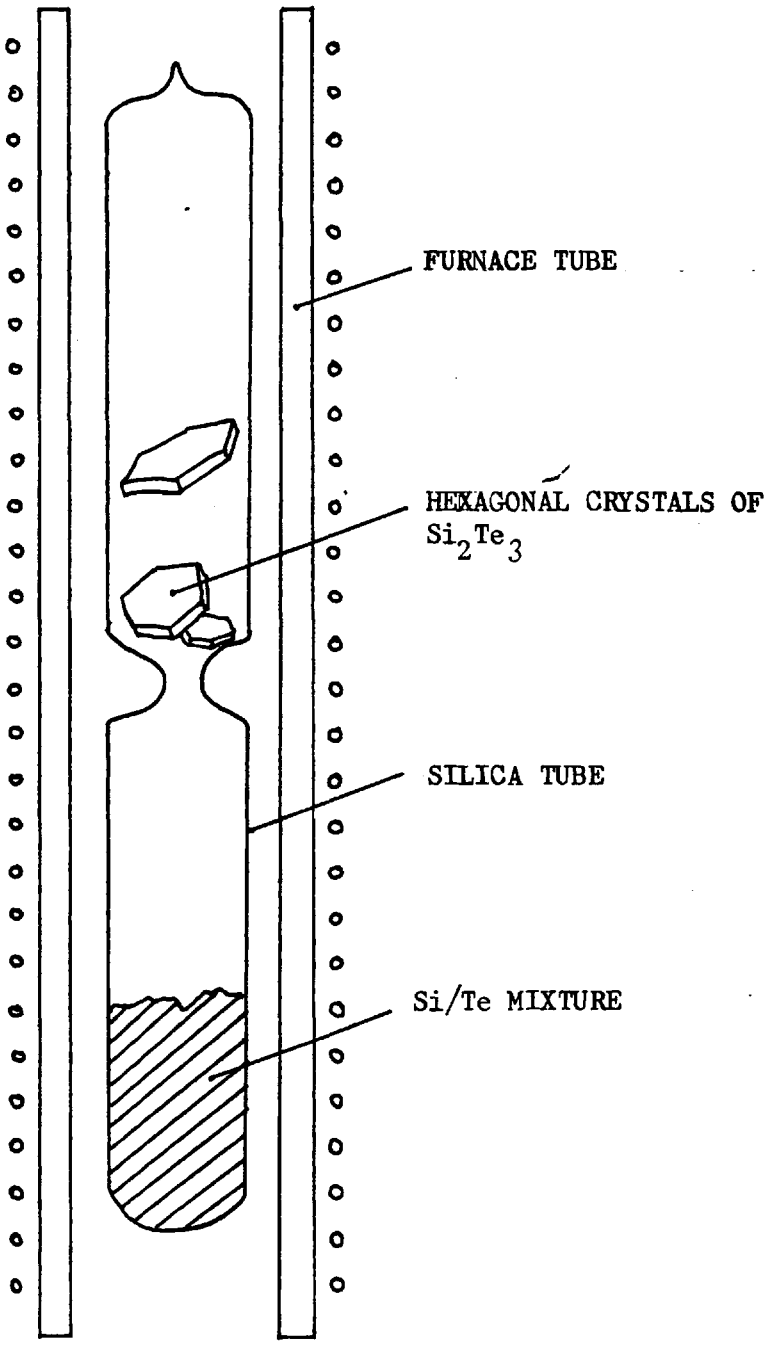

Fig. 13. Arrangement used to duplicate Bailey's vapour phase transport method of producing Si_2Te_3.

previously been made from capillary tubing was in this case made from wider bore tubing, $\sim$ 2.5 mm in diameter, to carry the high current desired. This cell was filled with S_{15} Ge_{33} As_{27} Te_{25}, and graphite electrodes embedded in it, as if for a conductivity run. This arrangement was then placed in the resistance heated furnace, which was flushed, and pressurised to 5.0 N/mm^2 (50 atmospheres) with argon. The sample was then heated to 555°C, and the lead-outs from the two graphite electrodes were connected to a mains-operated D.C. power source. A current of 1.12 amps was passed for 12 hours at 6 volts (overnight). After 12 hours it was observed that the resistance had decreased slightly; so 3.2 amps was passed at 4 volts for the remaining 12 hours of the experiment. At the end of this time, the furnace was switched off, and the sample allowed to cool with the voltage source still connected. When cold, the sample was brought back to atmospheric pressure and sent to the Fulmer Research Institute for analysis using the EDAX (energy dispersive analysis by X-rays) attachment of a scanning electron microscope. Although this technique, which operates on the same principle as electron probe microanalysis (EPMA), is capable of quantitative analyses, only a qualitative estimate of relative concentrations based on relative peak heights could be obtained here. This was attributed to absorption and fluorescence effects due to the other constituents in the glass (102). The sample was broken to give seven approximately equally spaced fragments running from one graphite electrode to the other; and a peak height measurement was made on each of these at a fixed beam current and magnification.

3:3:6. Composition of crystalline phases in $S_{15}Ge_{43}As_{23}Te_{19}$

As mentioned earlier, attempts to manufacture a glass of this composition

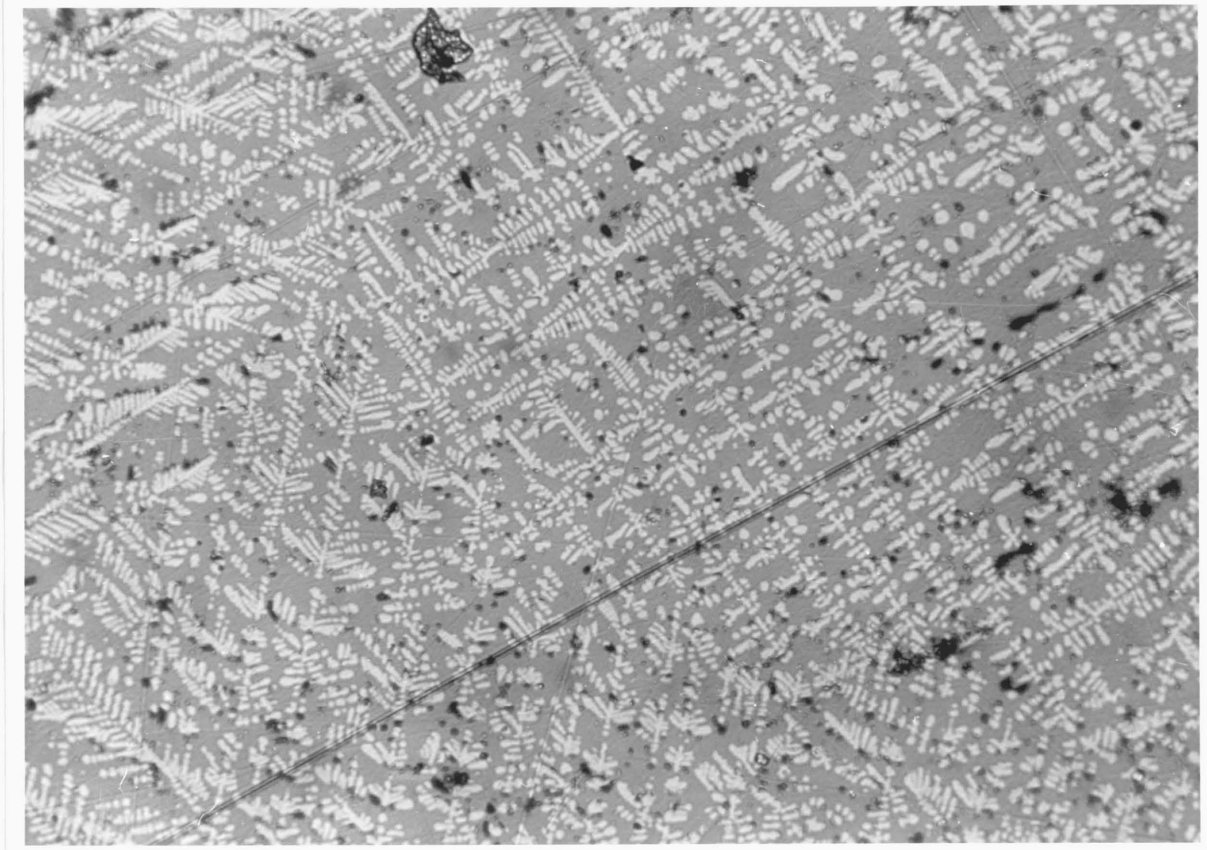

Fig. 14. Micrograph of a polished section of $S_{15}Ge_{43}As_{23}Te_{19}$, showing dendrites.

by the radio-frequency furnace technique were unsuccessful, the liquid crystallising upon cooling to give a dark grey matrix in which both light grey dendrites and light grey crystals were seen (Fig. 14). A polished specimen of this material was submitted to the analytical section of the Department of Metallurgy and Materials Science, and the compositions of the dendrites, the angular crystals and the matrix were determined by electron probe microanalysis.

4. RESULTS

4.1. Electrical Conductivities of the Chalcogenide Glasses

The electrical conductivity data obtained on the five materials $Si_{12}\ Te_{48}\ As_{30}\ Ge_{10}$ (STAG), $S_{15}\ Ge_{23}\ As_{31}\ Te_{31}$, $S_{15}\ Ge_{33}\ As_{27}\ Te_{25}$, and $Se_{15}\ Ge_{23}\ As_{31}\ Te_{31}$ and $Se_{15}\ Ge_{33}\ As_{27}\ Te_{25}$ are given in Tables 1-5 respectively and are shown in Figures 15-19 respectively, plotted as $\log_{10}\sigma$ vs $\frac{1000}{T^{\circ}K}$, which, for ease of interpretation, is the standard form for presenting such data. Figure 15, for STAG, includes some data obtained by Baker and Webb (71), whose work the present author was completing; and also some published data by Male (72), for comparison purposes.

The results show relatively little scatter and best-fit lines can be drawn through them with some confidence. Broadly similar conductivity/temperature relationships were found for all five materials, with a linear portion up to about 250-300°C, followed by gentle upward curvature, possibly leading to another linear region. All five graphs then level off gradually after the temperature exceeds about 900°C.

Table 1. Conductivity/temperature data for STAG ($Si_{12}Te_{48}As_{30}Ge_{10}$)

1(a) Solid material

L/a	Temperature T°C	Conductance (Ω^{-1})	Log_{10} specific conductivity	1000/T°K
0.692	24	60×10^{-9}	-7.382	3.367
"	30	$74 \times$ "	-7.291	3.413
"	42	$189 \times$ "	-6.883	3.176
"	56	$460 \times$ "	-6.497	3.034
"	57	$468 \times$ "	-6.473	3.030
"	77	1.17×10^{-6}	-6.092	2.861
"	95	$3.57 \times$ "	-5.606	2.719
"	82	$2.44 \times$ "	-5.773	2.817
"	74	$1.68 \times$ "	-5.934	2.882
"	62	847×10^{-9}	-6.232	2.985
"	60	$710 \times$ "	-6.309	3.003
"	57	$573 \times$ "	-6.402	3.030
"	19	$43 \times$ "	-7.526	3.425
"	101	4.3×10^{-6}	-5.526	2.672
"	102	$4.7 \times$ "	-5.487	2.668
"	112	$5.77 \times$ "	-5.399	2.597
"	128	$11.7 \times$ "	-5.092	2.494
"	151	$37.4 \times$ "	-4.587	2.358
"	174	$89.1 \times$ "	-4.209	2.237
"	194	$204 \times$ "	-3.850	2.141
"	212	$365 \times$ "	-3.598	2.062
"	194	$230 \times$ "	-3.798	2.141
0.947	18	31.5×10^{-9}	-7.525	3.436
"	52	$449 \times$ "	-6.371	3.077
"	172	45.2×10^{-6}	-4.368	2.247
"	204	$131.4 \times$ "	-3.905	2.096

1(b) Liquid specimens

Cell constant	Temperature $T^{\circ}C$	Conductance Ω^{-1}	Log_{10} (specific conductivity)	$\frac{1000}{T^{\circ}K}$
333 cm^{-1}	448	1.57×10^{-3}	-0.282	1.387
"	427	0.9 x "	-0.523	1.428
"	428	0.93 x "	-0.509	1.427
"	407	0.524 x "	-0.758	1.471
"	374	0.205 x "	-1.166	1.546
"	339	77×10^{-6}	-1.591	1.634
"	311	32 x "	-1.972	1.712
"	304	23 x "	-2.116	1.733
"	287	13.7 x "	-2.341	1.786
"	278	10.6 x "	-2.454	1.815
"	271	8.16 x "	-2.566	1.838
"	260	5.8 x "	-2.714	1.876
"	250	4.1 x "	-2.866	1.912
"	242	2.98 x "	-3.003	1.942
"	228	1.94 x "	-3.191	1.996

Table 2. Conductivity/temperature data for $S_{15}Ge_{23}As_{31}Te_{31}$

2 (a) Results from solid samples

L/a	Temperature T°C	Conductance (Ω^{-1})	Log_{10} (specific conductivity)	$\frac{1000}{T°K}$
1.259 cm^{-1}	24.3	1.68×10^{-9}	-8.675	3.364
	31.3	$3.01 \times$ "	-8.422	3.286
	40.5	$5.96 \times$ "	-8.125	3.189
	49.3	$11.5 \times$ "	-7.841	3.103
	59.5	$23.2 \times$ "	-7.535	3.007
	78.6	$80.9 \times$ "	-6.992	2.844
	51.1	$12.4 \times$ "	-7.806	3.086
	18.0	$0.96 \times$ "	-8.918	3.436
	100.0	$142 \times$ "	-6.748	2.681
0.9962 cm^{-1}	30.1	3.91×10^{-9}	-8.409	3.299
	39.9	$9.38 \times$ "	-8.029	3.196
	48.6	$14.6 \times$ "	-7.837	3.109
	59.0	$27.3 \times$ "	-7.565	3.012
	19.2	$1.42 \times$ "	-8.849	3.422
	69.0	$56.2 \times$ "	-7.252	2.924
	78.5	$108.8 \times$ "	-6.965	2.845
0.6168 cm^{-1}	100	0.37×10^{-6}	-6.642	2.681
	134	$2.41 \times$ "	-5.829	2.457
	145	$4.16 \times$ "	-5.590	2.392
	159	$8.05 \times$ "	-5.304	2.315
	180	$19.23 \times$ "	-4.926	2.207
	202	$45.13 \times$ "	-4.555	2.105
	230	$119 \times$ "	-4.134	1.988
	309	$950 \times$ "	-3.232	1.718
	277	$376 \times$ "	-3.634	1.818

2 (b) Results for liquid samples

Cell constant	Temperature $T^{\circ}C$	Conductance (Ω^{-1})	Log_{10} (specific conductivity)	$\frac{1000}{T^{\circ}K}$
314 cm^{-1}	460	2.84×10^{-3}	-0.0497	1.364
	392	0.378 x "	-0.9255	1.504
	350	97×10^{-6}	-1.516	1.605
	305	21.9 x "	-2.163	1.730
	246	1.2 x "	-3.424	1.927
493.4 cm^{-1}	296	7.79×10^{-6}	-2.415	1.757
	361	68.28 x "	-1.472	1.577
	438	9.54 x "	0.673	1.406
	492	7.27 x "	0.555	1.307
	583	108.5 x "	1.729	1.167
1788 cm^{-1}	416	35.65×10^{-6}	-1.196	1.451
	474.5	312.8 x "	-0.252	1.338
	552.5	3.45×10^{-3}	0.790	1.211
	580.5	11.01 x "	1.294	1.172
	628.5	41.5 x "	1.870	1.109
	669.5	0.1181	2.324	1.061
	708	0.234	2.621	1.019
	802.5	0.588	3.022	0.929
	877	0.833	3.173	0.869
	983	1.087	3.288	0.796
	983	1.064	3.279	0.796
	1056	0.909	3.211	0.752
	1111	1.044	3.271	0.722
	1166	1.087	3.288	0.695
	689	0.25	2.650	1.039
	795	0.556	2.997	0.937
	842	0.667	3.076	0.897
	923	0.794	3.152	0.836

Table 3. Conductivity/temperature data for $S_{15}Ge_{33}As_{27}Te_{25}$

3 (a) Results from solid samples

L/a	Temperature $T^{o}C$	Conductance (Ω^{-1})	Log_{10}(specific conductivity)	$\frac{1000}{T^{o}K}$
1.4501 cm^{-1}	19.6	0.16×10^{-9}	-9.635	3.417
	25.5	0.24 x "	-9.458	3.350
	30.2	0.29 x "	-9.376	3.298
	37.3	0.56 x "	-9.090	3.223
	40.5	0.56 x "	-9.090	3.189
	45.6	1.05 x "	-8.817	3.139
	50.5	1.33 x "	-8.715	3.091
	61.3	2.40 x "	-8.458	2.991
	73.0	5.30 x "	-8.1143	2.890
	82.0	8.70 x "	-7.899	2.817
	110.5	62.0 x "	-7.046	2.608
	155	0.72×10^{-6}	-5.981	2.336
	192	4.14 x "	-5.221	2.150
	214	10.18 x "	-4.831	2.053

3 (b) Results from liquid samples

Cell constant	Temperature T°C	Conductance (Ω^{-1})	Log_{10} (specific conductivity)	$\frac{1000}{T°K}$
315.6 cm^{-1}	475	1.1×10^{-3}	-0.459	1.337
"	429	$0.366 \times$ "	-0.937	1.424
"	380	66.56×10^{-6}	-1.677	1.531
"	313	$5.24 \times$ "	-2.781	1.706
"	263	$0.304 \times$ "	-4.018	1.866
"	338	$12.9 \times$ "	-2.390	1.637
"	321	$5.4 \times$ "	-2.768	1.683
"	339	$12.0 \times$ "	-2.422	1.634
"	407	$169.1 \times$ "	-1.273	1.471
"	446	1.38×10^{-3}	-0.361	1.391
"	450	$2.98 \times$ "	-0.0267	1.383
"	521	$19.93 \times$ "	-0.798	1.259
1010 cm^{-1}	440	79×10^{-6}	-1.098	1.403
"	488	1.03×10^{-3}	0.0644	1.314
"	484	$1.11 \times$ "	0.0502	1.321
"	488	$8.60 \times$ "	0.9389	1.314
"	526	$15.0 \times$ "	1.1805	1.252
"	606	$88.2 \times$ "	1.949	1.137
"	603	$90.7 \times$ "	1.962	1.142
"	666	0.463	2.669	1.065
"	670	0.476	2.682	1.060
"	712	0.781	2.897	1.015
"	770	1.171	3.073	0.959
"	849	1.538	3.192	0.891
"	844	1.538	3.192	0.895
"	896	1.724	3.241	0.855
"	961	1.912	3.286	0.810
"	963	1.912	3.286	0.809
"	1056	2.092	3.325	0.752

Table 4. Conductivity/temperature data for $Se_{15}Ge_{23}As_{31}Te_{31}$

4(a) Solid samples

L/a	Temperature T^oC	Conductance (Ω^{-1})	Log_{10} (specific conductivity)	$\frac{1000}{T^oK}$
2.183 cm^{-1}	19	1.1×10^{-9}	-8.619	3.425
"	43.4	8.7 x "	-7.722	3.161
"	57	22.9 x "	-7.301	3.030
"	71	56.8 x "	-6.907	2.907
"	83.5	137 x "	-6.524	2.805
"	91	217.5 x "	-6.323	2.747
"	156	5.22×10^{-6}	-4.943	2.331
"	165	7.08 x "	-4.811	2.283
"	182	12.3 x "	-4.572	2.198
"	195	26.2 x "	-4.242	2.137
"	215	59.1 x "	-3.889	2.049
"	235	135.3 x "	-3.529	1.968
"	265	316.6 x "	-3.160	1.859
"	315	2.66×10^{-3}	-2.236	1.701

4 (b) Liquid samples

Cell constant	Temperature °C	Conductance (Ω^{-1})	Log_{10}(specific conductivity)	$\frac{1000}{T°K}$
457.6 cm^{-1}	494	6.89×10^{-3}	0.499	1.304
"	453	$1.01 \times$ "	0.336	1.377
"	400	2.05×10^{-6}	-1.027	1.486
"	549	49.7×10^{-3}	1.357	1.216
"	562	77.2×10^{-3}	1.548	1.198
"	519	18.9×10^{-3}	0.936	1.263
"	423	411.2×10^{-6}	-0.725	1.437
"	361	51.9×10^{-6}	-1.624	1.577
"	302	5.965×10^{-6}	-2.564	1.739
339.4 cm^{-1}	473	4.588×10^{-3}	0.192	1.341
"	568	$105.2 \times$ "	1.553	1.189
"	653	1.395	2.675	1.079
"	741	3.625	3.090	0.986
"	804	4.826	3.214	0.928
"	838	5.63	3.281	0.900
"	909	6.472	3.342	0.846
"	591	0.344	2.068	1.157

Table 5. Conductivity/temperature data for $Se_{15}Ge_{33}As_{27}Te_{25}$

5 (a) Solid samples

L/a	Temperature T°C	Conductance Ω-1	Log_{10} (specific conductivity)	$\frac{1000}{T°K}$
1.079 cm^{-1}	45.2	4.65×10^{-9}	-8.299	3.143
	60	14.7×10^{-9}	-7.799	3.003
	70.5	31.3×10^{-9}	-7.472	2.911
	77.5	51.0×10^{-9}	-7.259	2.853
	98	195×10^{-9}	-6.677	2.695
	158	5.11×10^{-6}	-5.258	2.320
	203	38.4×10^{-6}	-4.382	2.101
	139	1.97×10^{-6}	-5.672	2.427
	229	124 x "	-3.873	1.992
	245	192.2 x "	-3.683	1.931
	278	548 x "	-3.228	1.815
	301	690.3 x "	-3.128	1.742

5 (b) Liquid samples

Cell constant	Temperature T°C	Conductance Ω^{-1}	$\log_{10}$ (specific conductivity)	$\frac{1000}{T°K}$
353.4 cm^{-1}	395	171×10^{-6}	-1.219	1.497
	481	6.72×10^{-3}	+0.376	1.326
	531	80.62 x "	1.455	1.244
	559	0.201	1.852	1.202
	644	1.459	2.713	1.091
	661	1.866	2.819	1.071
	703	2.871	3.006	1.025
	754	3.788	3.127	0.974
	755	4.047	3.156	0.973
	837	5.000	3.247	0.901
	855	5.181	3.263	0.887
	888	5.556	3.293	0.861
	917	5.747	3.308	0.840
	984	6.329	3.349	0.795
	1049	6.711	3.375	0.756
	1144	7.042	3.396	0.706
	571	0.311	2.041	1.185

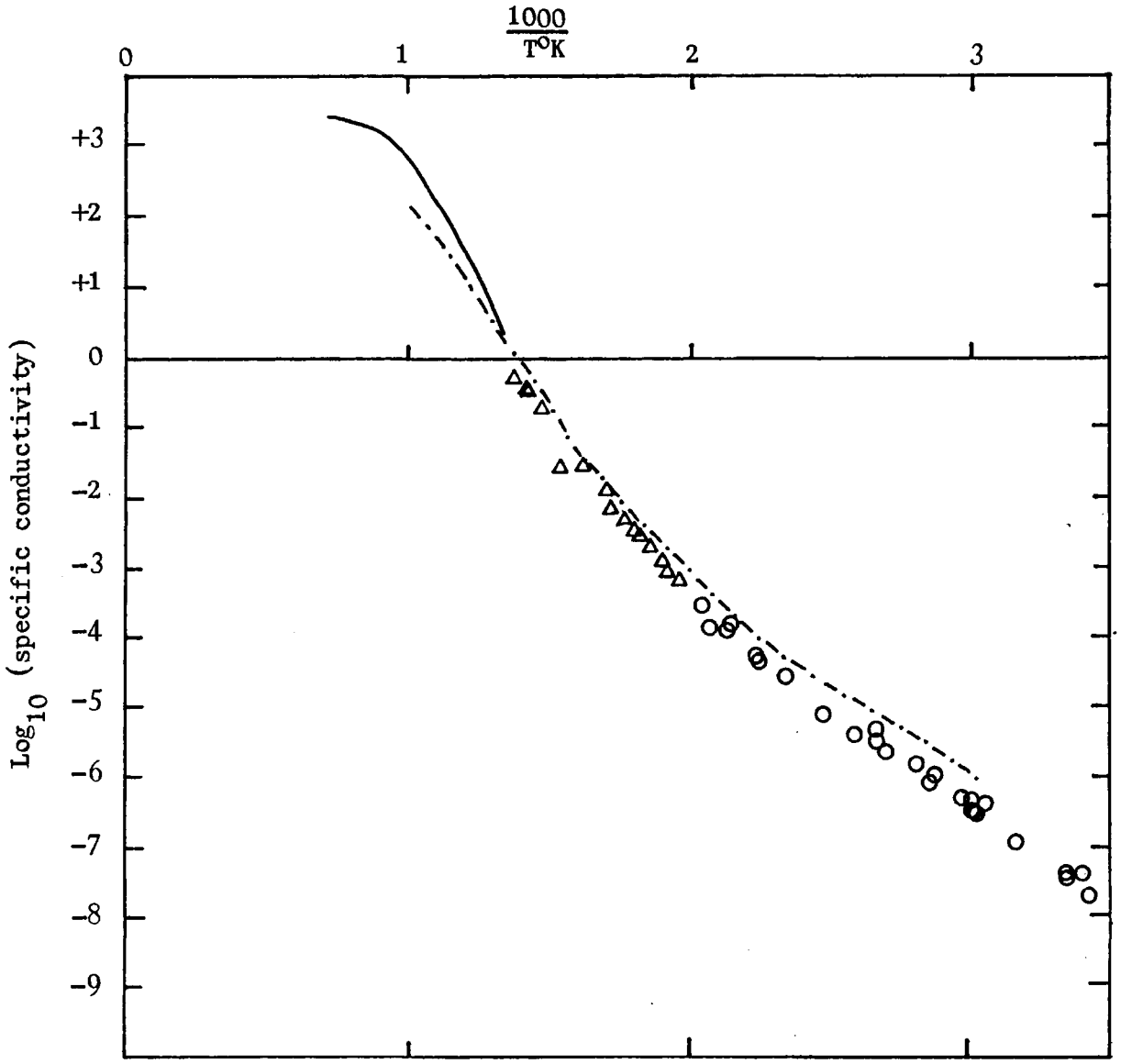

Fig. 15. Conductivity/temperature relationship for STAG Si_{12} Te_{48} As_{30} Ge_{10} shown as log (conductivity) vs $\frac{1000}{T^{\circ}K}$.

Present work) O = results using solid specimens
) Δ = results using liquid specimens

—— = results of Baker and Webb (71), using similar experimental techniques.

-.-.- = results of Male (72), using different experimental techniques.

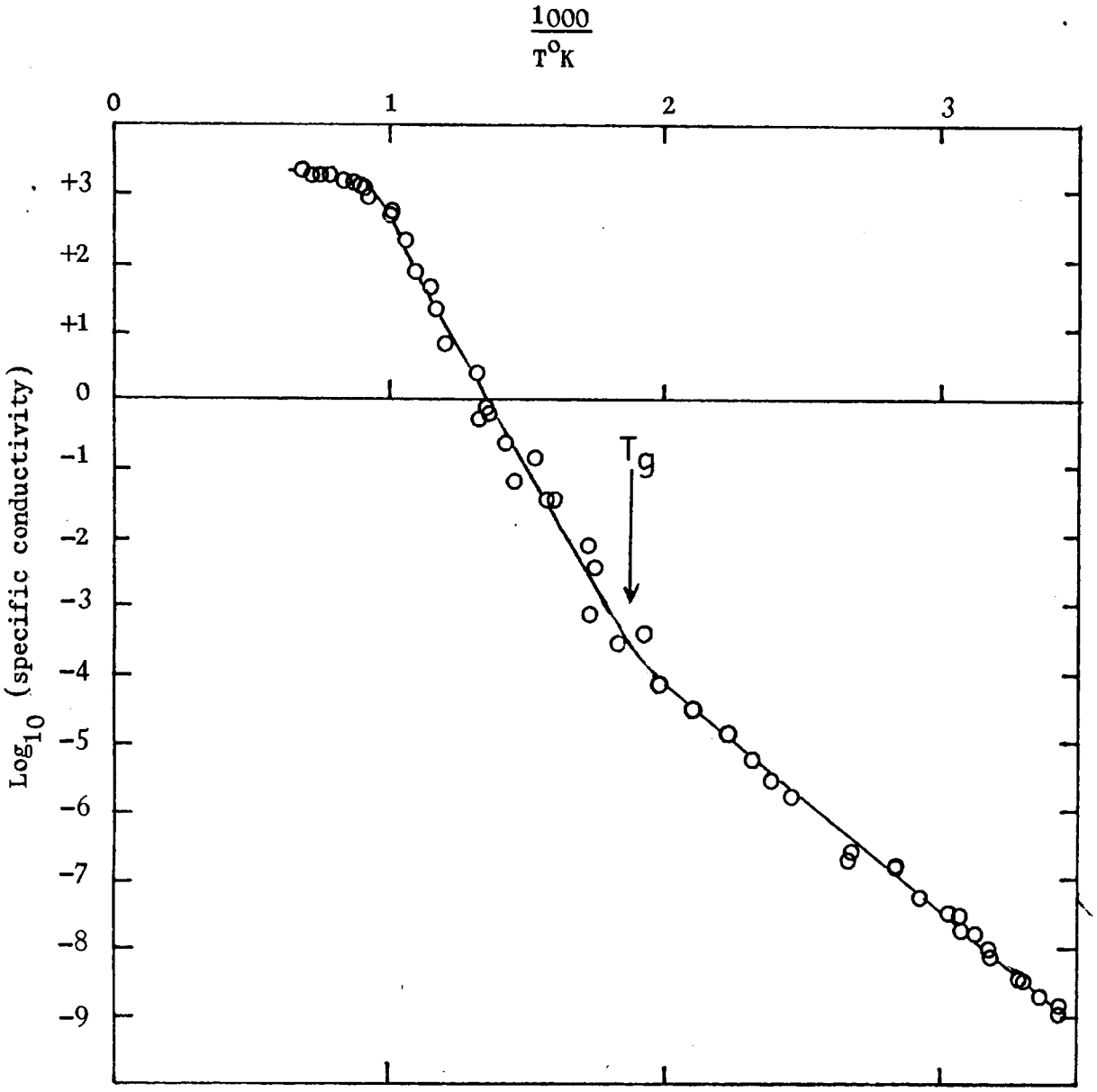

Fig. 16. Conductivity/ temperature relationship for $S_{15}\ Ge_{23}\ As_{31}\ Te_{31}$.

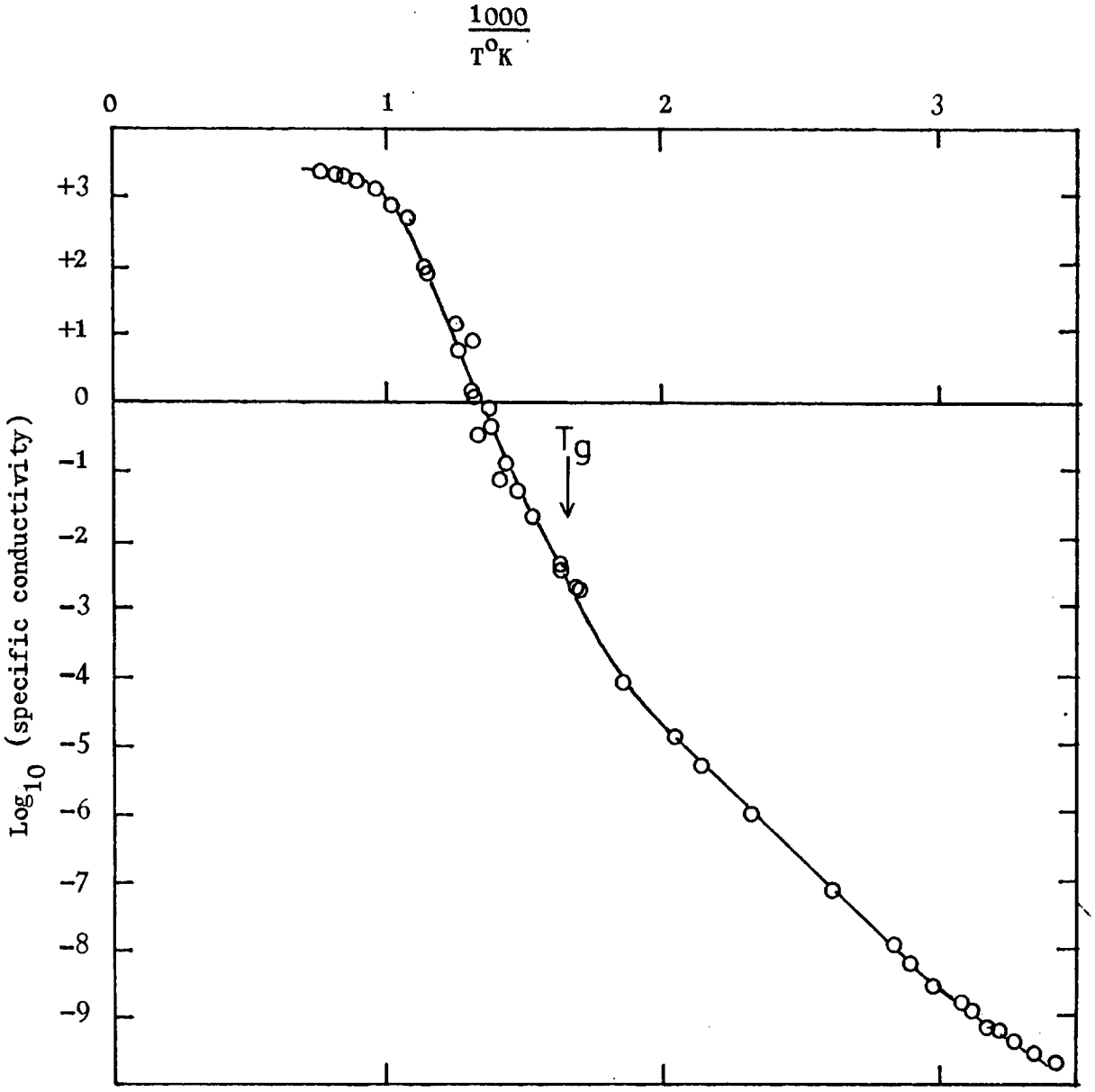

Fig. 17. Conductivity/temperature relationship for S_{15} Ge_{33} As_{27} Te_{25}.

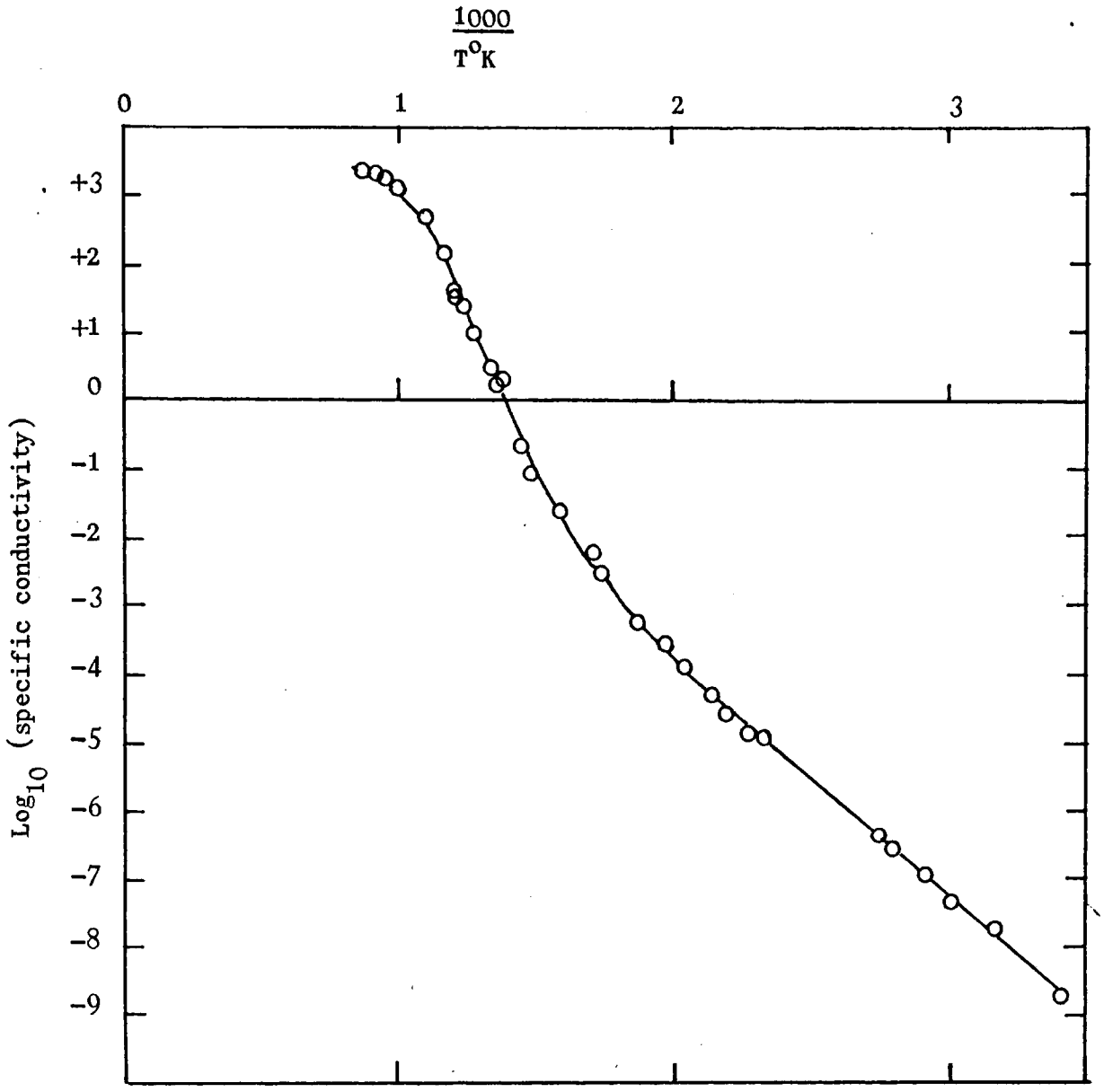

Fig. 18. Conductivity/temperature relationship for $Se_{15}\ Ge_{23}\ As_{31}\ Te_{31}$.

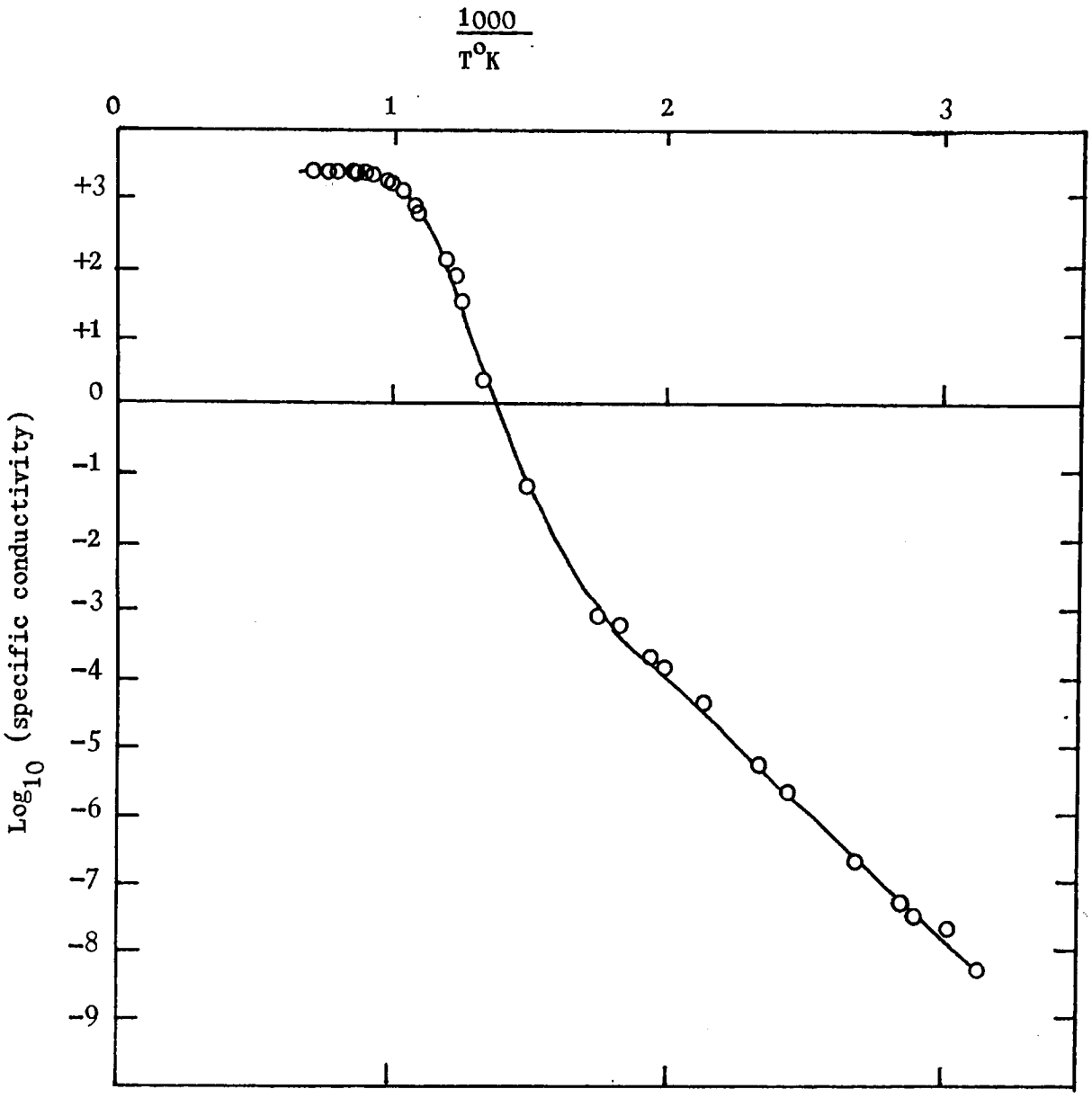

Fig. 19. Conductivity/ temperature relationship for Se_{15} Ge_{33} As_{27} Te_{25}.

The results obtained for STAG (Fig. 15) provide a useful check on the manufacturing and testing techniques used in the present work, as they may be compared with those obtained by Male (72) using a different experimental technique. Male's results, also given in Figure 15, show good agreement with those obtained in the present work and with those of Baker and Webb (71), using the same experimental technique, and this indicates that the present techniques are capable of giving valid results of as great an accuracy as those presented elsewhere in the literature.

4.2. Electrical Conductivity of Sulphur

These results are given in Table 6, and plotted in Figure 20, together with some data obtained by Baker using similar techniques at lower temperatures (103).

In the present author's work, both A.C. and D.C. measurement techniques gave similar values for the electrical conductivity of sulphur over the temperature range under consideration, approximately 300-900°C, and the $\log_{10}\sigma$ vs $1000(T^{\circ}K)^{-1}$ plot was essentially linear over the range 500-900°C. Below about 500°C, the present data curve slightly, giving a gentler slope, and join up with the values obtained by Baker, using graphite electrodes and distilled sulphur, but an otherwise similar experimental technique. Baker found these results to be less reliable than his other set of results (also in the figure) obtained using platinum electrodes, and attributed this to contamination of the sulphur by impurities extracted from the graphite. It is known that electrophoretic conduction due to impurities was responsible for high

Table 6. Electrical conductivity results for liquid sulphur.
Cell constant determined using KCl solutions = 0.3897 cm^{-1}.

Temperature ^{o}C	Conductance Ω^{-1}	$\frac{1000}{T^{o}K}$	Log_{10} specific conductivity	A.C. or D.C.
666	9.38×10^{-6}	1.0644	-5.437	A.C.
825	40.28 x "	0.9112	-4.8042	"
868	69.64 x "	0.8764	-4.5664	"
698	6.74 x "	1.0293	-5.5806	"
693	6.17 x "	1.0352	-5.6192	"
892	86.8 x "	0.8580	-4.4707	"
896	87.7 x "	0.8558	-4.4663	"
762	13.7 x "	0.9666	-5.2728	D.C.
850	48.3 x "	0.8905	-4.725	"
819	31.3 x "	0.9162	-4.9144	"
750	17.6 x "	0.9779	-5.1636	"
706	5.49 x "	1.0219	-5.6694	"
572	0.833 x "	1.1834	-6.4884	"
536	0.152 x "	1.2353	-7.2257	"
603	1.126 x "	1.1409	-6.3576	"
297	2.381×10^{-9}	1.7543	-9.0325	"
361	10.20 x "	1.5773	-8.4005	"
437	56.2 x "	1.4085	-7.6597	"
635	2.34×10^{-6}	1.1019	-6.0408	"
714	7.46×10^{-6}	1.0137	-5.5364	"
517	84.0×10^{-9}	1.2658	-7.4848	"
554	0.99×10^{-6}	1.2092	-6.4136	A.C.
548	0.50×10^{-6}	1.2180	-6.7102	"
432	41.2×10^{-9}	1.4194	-7.7943	"
438	37.0×10^{-9}	1.4075	-7.8406	"
379	21.2×10^{-9}	1.5326	-8.0829	"
318	6.135×10^{-9}	1.692	-8.6214	D.C.

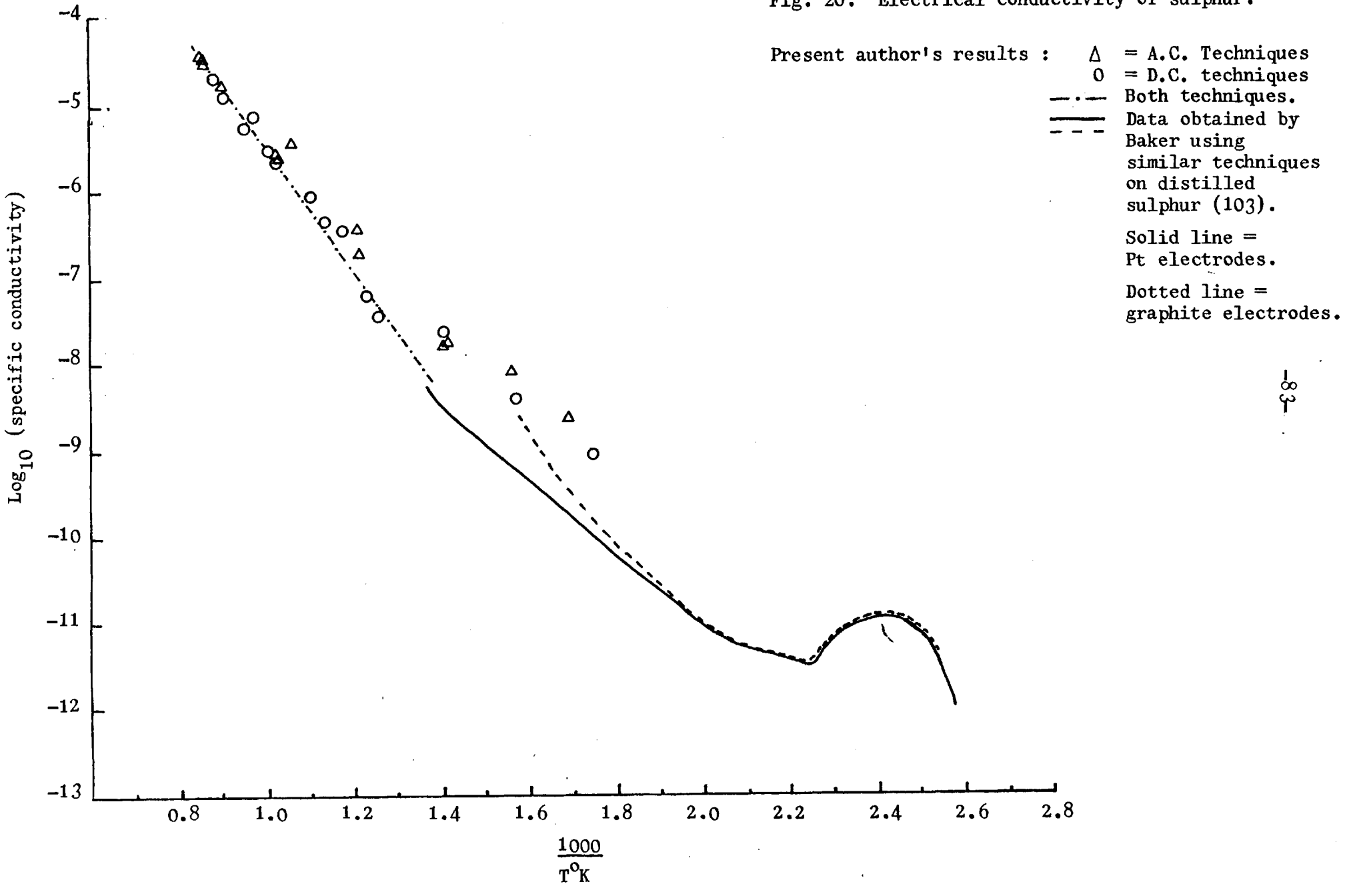

Fig. 20. Electrical conductivity of sulphur.

Present author's results : Δ = A.C. Techniques
O = D.C. techniques
—·— Both techniques.
——— Data obtained by Baker using similar techniques on distilled sulphur (103).

Solid line = Pt electrodes.

Dotted line = graphite electrodes.

values of conductivity in many of the early determinations of the conductivity of sulphur, and this may be why the present author's data show a lessening of slope below about 500°C, as, although the sulphur used was extremely pure, and did not attack the gold electrodes, it may nevertheless have contained enough impurities to give artificially high conductivity values between 300 and 500°C. Above 500°C, the true conductivity of the sulphur had probably become sufficiently high to swamp any effects due to impurities, and the graph thus resumed its true linear form. If the above reasoning is correct, the true graph of the conductivity of sulphur may be drawn by joining the present results with those of Baker for platinum electrodes, the solid line in Figure 20.

4.3. Silicon-Tellurium Phase Diagram

The thermal arrests obtained for the series of alloys investigated are shown in Table 7, and the phase diagram which may be constructed from the data is shown in Figure 21, which also shows the phase boundaries noted by Bailey (92).

4.4. High Current Transport Experiment

The results of the EDAX analysis carried out at the Fulmer Institute are reported in Table 8 in the form of peak heights for each of the four elements comprising the glass. The conclusion of the analyst was that these results suggested some increase in tellurium content near the positive electrode, but that the trend was too small to be taken as conclusive evidence of a real concentration gradient.

Table 7. Temperatures at which thermal arrests were found in the investigation of the Si-Te system.

Alloy composition, atom. %	Arrest Temperature °C
Si 10 : Te 90	402, 405
Si 20 : Te 80	402, 407
Si 25 : Te 75	402, 408
Si 33 : Te 66	403
Si 40 : Te 60	No arrests detected
Si 50 : Te 50	878, 1296
Si 60 : Te 40	888, 1352
Si 70 : Te 30	1370
Si 80 : Te 20	884, 1380
Si 90 : Te 10	1380

Fig. 21. The Si-Te phase diagram.

——— = phase boundaries given by Bailey (92).

Δ = present author's experimental results (Table 7).

- - - - = phase boundaries indicated by present results.

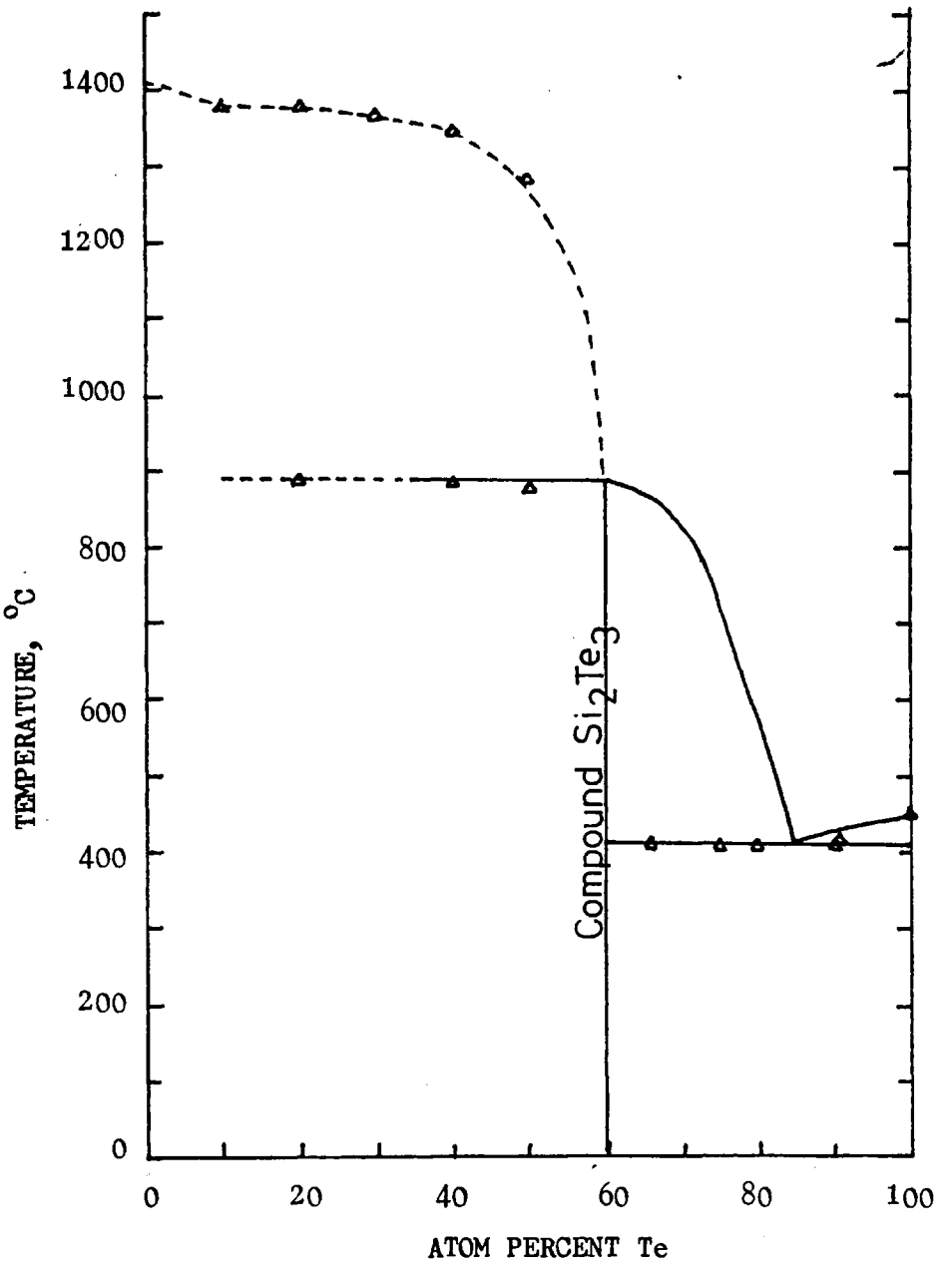

Table 8. Results of EDAX analysis of sample from high-current transport experiment. (Carried out by Fulmer Research Institute).

Specimen code *	Peak Heights (counts x 10^{-3}) **			
	Te Lα (3.8 KeV)	Ge Kα (9.9 KeV)	As Kα (10.6 KeV)	S Kα (2.3 KeV)
0+	13.2	7.3	4.0	3.0
1+	14.7	7.7	5.1	2.8
2+	14.9	8.4	5.4	2.9
3+	13.9	8.1	5.1	2.9
3-	12.9	9.8	5.3	2.4
2-	12.8	8.9	4.7	2.6
1-	13.3	9.6	5.5	3.0

* See below.

** Count time 100 sec. All samples counted using constant beam current and magnification.

Specimen location

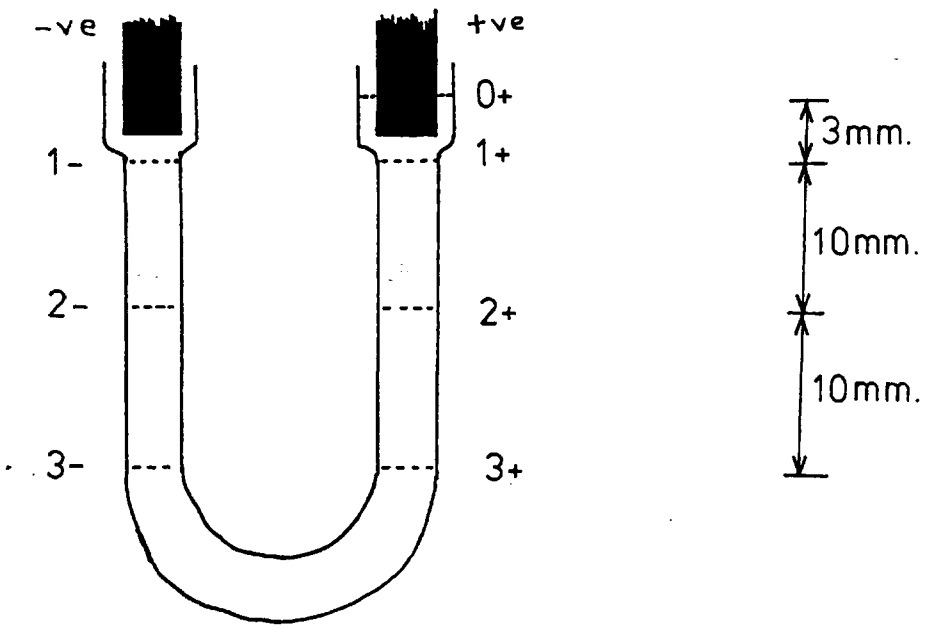

4.5. Composition of Crystalline Phases in $S_{15}Ge_{43}As_{23}Te_{19}$

The results of spot counts carried out on the polished sample of $Si_{15}Ge_{43}As_{23}Te_{19}$, when corrected by the NPL–IC–BM Mk.5 computer programme, indicated a matrix composition of $S_{30}Ge_{42}As_{11}Te_{16}$, differing considerably from the target composition. The dendrites shown in Figure 14 were found to be $Ge_{50}Te_{48}$, which, within the accuracy of the technique, can probably be said to approximate to GeTe. Radiation corresponding to about 1.0 atom percent of sulphur and arsenic was also detected from these dendrites, but this was thought to have been picked up from the matrix. The rectangular crystals which were also present in some parts of the sample were found to be $Ge_{66}As_{33}$ i.e. Ge_2As, again with small amounts of the other two constituents being detected, about 1 atom percent sulphur and 0.5 atom percent tellurium, and these were almost certainly being picked up from the surrounding material. All these counts were taken using a reduced beam current (25–30 nA rather than the usual 100 nA) to prevent damage to the sample; and the beam voltage was set to 25 kV.

Traces taken across the rectangular crystals showed that the matrix immediately surrounding the Ge_2As crystals was depleted in Ge and As and enriched in Te and S compared to the bulk matrix remote from the crystals.

5. DISCUSSION OF RESULTS

The different groups of results will be discussed in the order in which they were presented in Chapter 4.

5.1. Electrical Conductivities of the Chalcogenide Glasses

5.1.1. Semiconducting materials: General considerations

The electrical conductivity of a material depends upon the ability of the electrons in that material to leave the atoms or ions to which they are attached, and move through the material in the applied electric field. This ability depends upon the location of the valence and conduction bands, and the ease with which electrons can pass from one to the other. An electron in the valence band is tied to a particular atom and cannot participate in conduction, but once in the conduction band, it is free to move through the material. In an insulator, the gap between the two bands is too large for electrons to cross, so no current will flow and in a metal, the two bands overlap, and there is no forbidden gap. However, in a semiconductor, the gap is such that electrons can cross it by thermal promotion, and thus the conductivity will be one which increases with increasing temperature. Such a material is known as an intrinsic semiconductor, as it will show semiconducting properties in its pure, crystalline form. In the case of crystalline materials, it is possible to make semiconducting a material which would normally be an insulator. This is achieved by adding selected impurity atoms of a different valency to the host material. These impurity atoms then set up localised states within the band gap, which are capable of donating electrons to the conduction band, thus allowing current flow to occur. This type of semiconductor is known as extrinsic, and, as well as the conventional type of conduction described above, in which the current is carried by electrons (n-type), it is possible to arrange for the states generated by the impurity atoms

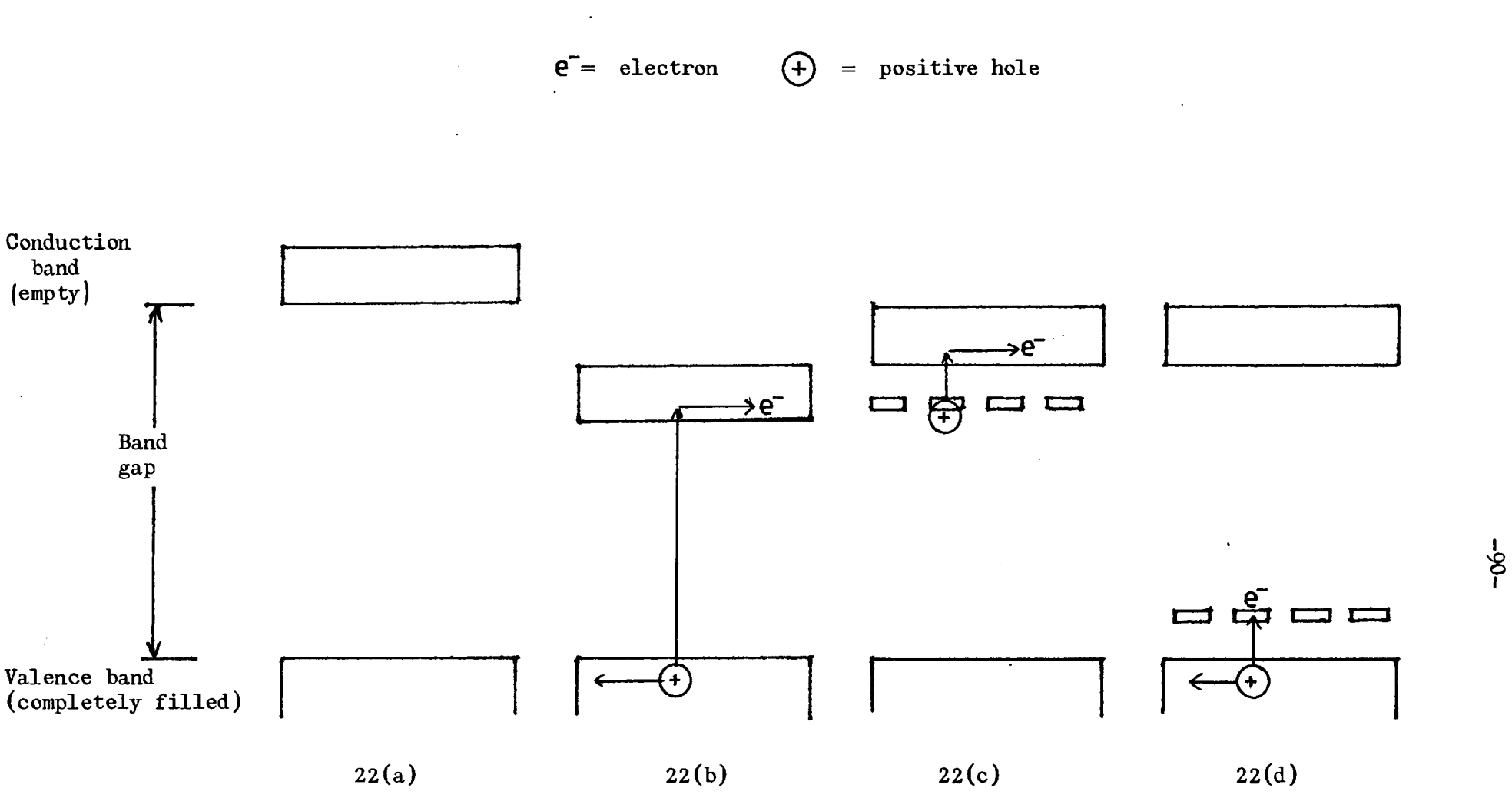

Fig. 22. Band gap picture of

(a) an insulator, (band gap too large, no electrons can cross it).
(b) intrinsic semiconductor. (Thermally promoted electrons travel in the conduction band, resulting holes move in valence band),
(c) extrinsic n-type semiconductor, (donor levels give thermally promoted electrons to conduction band),
(d) extrinsic p-type semiconductor (acceptor levels give rise to mobile positive holes in the valence band).

to be capable of receiving electrons rather than of donating them. Passage of an electron from the conduction band to one of these acceptor states leaves behind it a positively charged centre, a hole, which can also travel through the material, giving the appearance of conduction by positive charge carriers. This type of semiconductor is known as p-type. The simple band picture for all 3 types of semiconductor (and for an insulator) is shown in Figure 22.

To determine which type of extrinsic conduction is operating, i.e. which sign of carrier is responsible for the flow of current, two methods are commonly used. The first is to determine the polarity of the e.m.f. which arises when a temperature gradient is maintained along a sample of the semiconductor. The sign of this thermopower indicates the majority charge carrier. The second technique involves passing a current along the axis of a bar of the material to be investigated, whilst applying a magnetic field perpendicular to the current flow. The effect of the field on the charge carriers will be to deflect them in the direction which is perpendicular to both current flow and magnetic field. This is known as the Hall effect, and the sense of the deflection will depend on the sign of the carrier involved. From Hall effect measurements it is also possible to calculate the carrier mobility.

As was noted above, all these types of semiconducting behaviour are controlled by the existence of an energy gap, which the charge carriers have to cross before conduction can take place. The energy required comes from thermal motions, and processes of this type show an exponential dependence upon temperature. In the case of semiconductivity,

the specific conductivity σ (usual units $\Omega^{-1}cm^{-1}$) at a temperature $T^{o}K$ is given by

$$\sigma = \sigma_0 \exp\left(\frac{-\Delta E}{kT}\right) \qquad - 5:1$$

where σ_0 is a constant, ΔE is the energy gap, and k is Boltzmann's constant (8.6169×10^{-5} eV/^{o}K). This equation describes the behaviour when only one charge carrier is acting, as in an extrinsic, (doped) semiconductor. If both electrons and holes are present in equal numbers, the equation becomes

$$\sigma = \sigma_0 \exp\left(\frac{-\Delta E}{2kT}\right) \qquad - 5:2$$

Behaviour described by equations 5:1 and 5:2 is encountered at normal temperatures (i.e. ambient and above), and gives rise to the negative temperature coefficient of resistivity which is characteristic of semiconductors.

All the above reasoning applies to crystalline semiconductors, in which, as a result of the processes by which semiconductivity arises, the magnitude of the conductivity and the maintenance of semiconducting behaviour are strongly influenced by minute additions of impurity atoms. It was thus thought that such behaviour required the maintenance of a high degree of order and purity in the crystal structure. This being the case, it was considered puzzling that similar properties should be shown by a vast range of amorphous materials, in which all except the shortest range crystal order was absent, and in which the behaviour was

relatively insensitive to impurity additions and to changes in the composition of alloy semiconductors. It is to this group of materials that the five glasses investigated here belong.

5.1.2. Amorphous semiconducting materials, general considerations

The range of amorphous materials in which semiconducting behaviour has been detected is, as has been indicated above, very large, and includes elements (e.g. Te, Ge, Si), stoichiometric compounds (e.g. GeTe, As_2Se_3) and nonstoichiometric mixtures, one of the most well-known of the latter class being "STAG", $Si_{12}\ Te_{48}\ As_{30}\ Ge_{10}$. In the first two classes, comparisons can be made with the crystalline counterparts, and it has been found that the first co-ordination number of the crystal is preserved in the glass.

As the conductivity of crystalline semiconductors is determined by the density of states within the material, and the same is presumably true of amorphous semiconductors, it is generally assumed that the density of states in the amorphous case is controlled by the first co-ordination number, (carried over from the crystalline state), and by the interatomic distance, which may be slightly different from the crystalline one.

Considering the band picture developed for crystalline semiconductors, Figure 22, the change on going to an amorphous state will be to the band picture shown in Figure 23(a). The band edges can no longer be sharp, as the structural order necessary for sharp edges is no longer present. There is now a gradual fall off in the density of states with

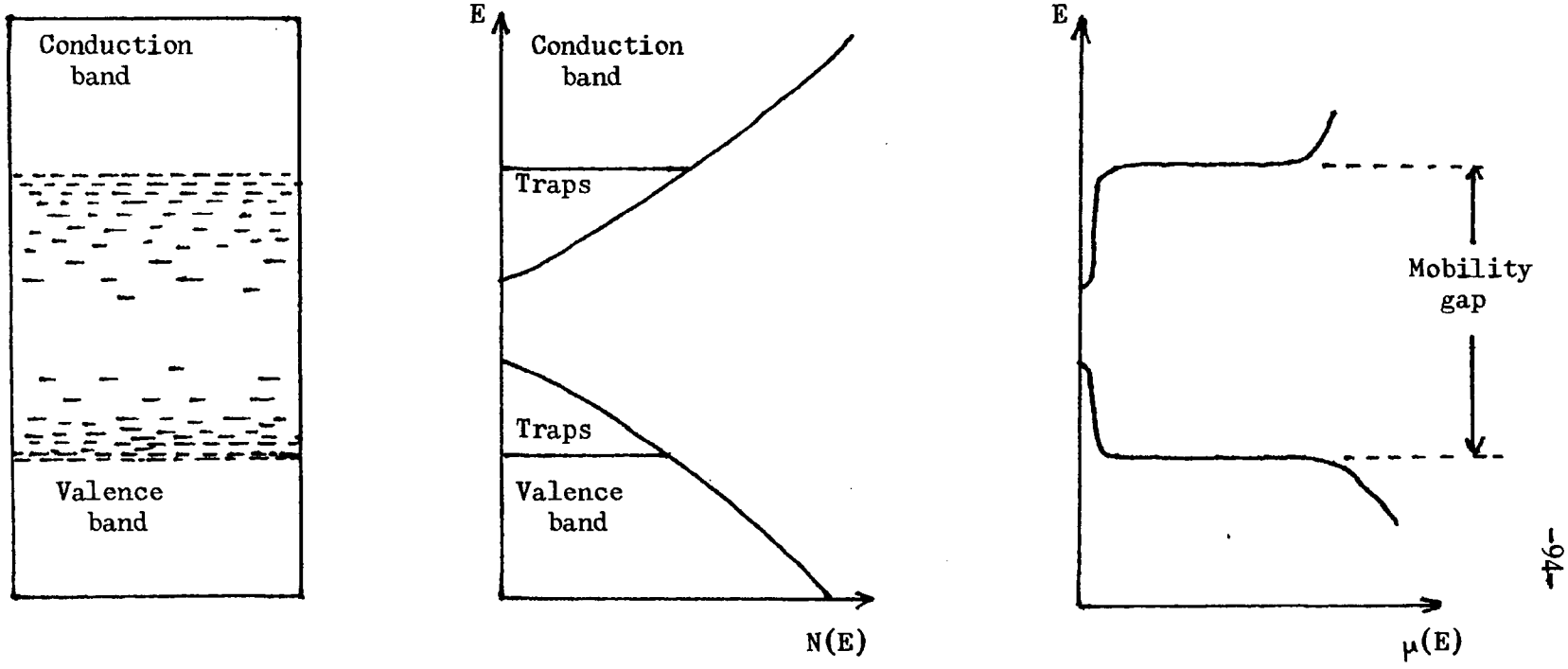

23(a) 23(b) 23(c)

Fig. 23. (a) Band-gap picture of amorphous semiconductor.
(b) Corresponding density of states N(E) vs E (electron energy) graph.
(c) Corresponding mobility $\mu(E)$ vs E (electron energy) graph, showing mobility gap.

an ill-defined gap opening up between valence and conduction bands. There is nevertheless no real forbidden region on the density of states graph and thus no true gap as defined in the case of crystalline semiconductors. The implications of this are described by the Mott-C-F-O theory, so called because it combines contributions from N.F. Mott in the U.K. and Cohen, Fritzsche and Ovshinsky in the U.S.A. (see for example ref. 104). To explain why the density of states graph of Figure 23 (a) does not result in metallic conductivity, the theory uses the fact that Anderson had shown (105) that the density of states could not be reduced indefinitely with the states still remaining continuous. Any fall below a certain critical level would result in those states becoming localised. Mott realised that this could describe what happened when the density of states was as depicted in Figure 23 (a). A region of localised states would appear between conduction and valence bands, as shown in Figure 23 (b), and this would become a region in which trapping could occur. The carrier mobility would be greatly reduced in that region, as Figure 23 (c) shows, separating the valence and conduction bands by a set of states with very low mobilities, the so-called "mobility gap". Mott and Davis (106) use the facts that the amorphous semiconductors cannot be doped, and that the gap estimated from electrical measurements is about half that estimated from optical measurements to show that the Fermi level (the boundary of filled states) lies somewhere near the centre of the mobility gap. Suggestions that it is pinned there by an overlap of the band tails or by a narrow band of allowed states at the centre of the gap, (Fig. 24), have been made, but no evidence has been obtained to confirm any of these suggestions. In any event, all three hypotheses are similar in their effect, and

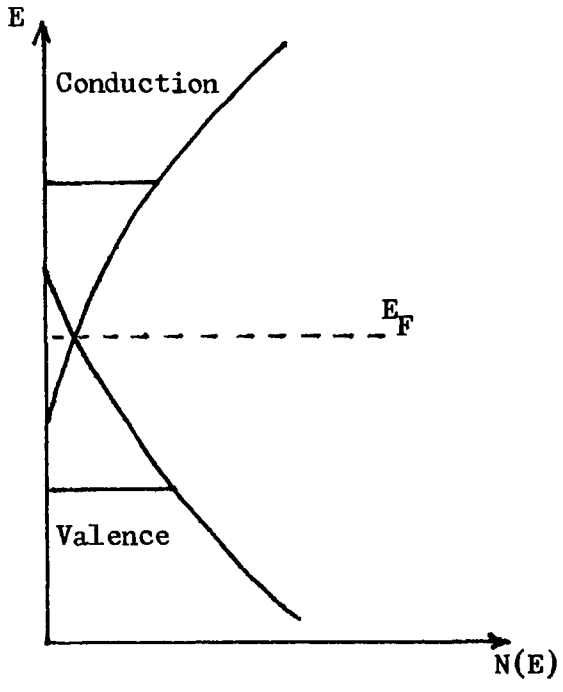

24(a)

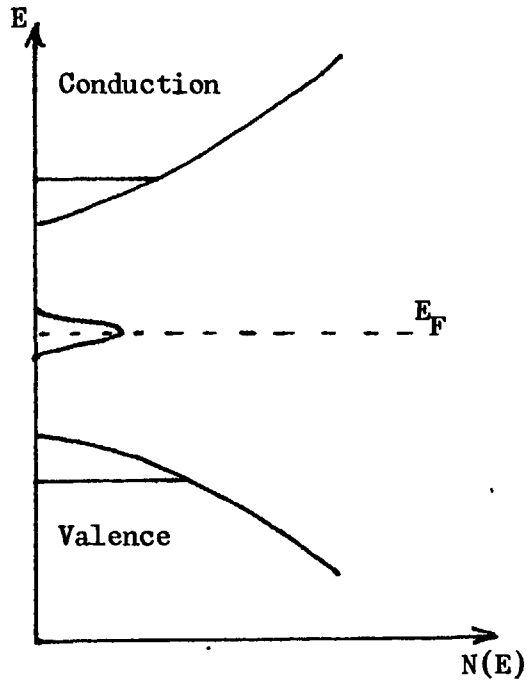

24(b)

Fig. 24. The two main theoretical density of states arrangements causing the Fermi energy (E_F) to be pinned at the centre of the mobility gap.

(a) Pinning by an overlap of the band "tails".

(b) Pinning by narrow band of allowed states.

three types of conduction can be postulated in amorphous semiconductors, all of which obey equations of the type $\sigma = \sigma_0 \exp$ (constant/kT), where σ_0 is a constant.

The first type involves thermal excitation of charge carriers through the mobility gap and into the non-localised states in the conduction band. Such conduction (called Type 1 by Mott and Davis) is similar to that observed in conventional semiconductors, and since it is an activated process, will obey equation 5:1 ($\sigma = \sigma_0 \exp\left(-\frac{\Delta E}{kT}\right)$). In this case, ΔE represents the mobility gap, and for hole conduction the relevant gap is $E_F - E_V$ (= Fermi energy - Valence band energy). Taking logarithms of equation 5:1, it can be seen that a plot of $\ln \sigma$ vs $1/T$ will be linear if ΔE is a linear function of T. This has been found to be the case experimentally, and $E_F - E_V$ can be represented as $E_0 - \gamma T$, where E_0 and γ are constants. Substituting this expression into equation 5:1, it can be seen (by analogy with $y = mx + c$) that the slope of a $\ln \sigma$ vs $1/T$ graph will be E_0/k, and the intercept on the $\ln \sigma$ axis will be $\ln (\sigma_0 \exp \frac{\gamma}{k})$. This type 1 conduction is probably the most common one at normal temperatures ($> 273^{\circ}K$). The other two are: hopping conduction of holes excited into the region of localised states near the band edges (type 2 conduction) and tunnelling conduction between localised states near the Fermi energy (type 3 conduction). The last-named will only give a linear plot of $\ln \sigma$ vs $1/T$ if the tunnelling is between nearest neighbour sites. At low temperatures, a variation of type 3 with long-range tunnelling is thought to occur, giving rise to a $\ln \sigma$ proportional to $T^{-\frac{1}{4}}$ relation. According to Mott and Davis, values of the pre-exponential constant $\sigma_0 \exp(\frac{\gamma}{k})$ should indicate the dominant

mechanism, as follows: type 1, 10^2 - 10^4 $\Omega^{-1}cm^{-1}$, type 2, $\sim 10\,\Omega^{-1}cm^{-1}$, type 3 $< 10\ \Omega^{-1}cm^{-1}$. It has been observed experimentally that most of the multicomponent chalcogenide glasses have σ_0 between 10^2 and 10^4 above room temperature, this being known as Stuke's rule.

As described above, in crystalline semiconductors, the sign of the majority charge carriers can be determined by examining the signs of the Hall effect and the thermopower (Seebeck effect). In the case of amorphous semiconductors, the situation is not so clear, as the Hall and Seebeck coefficients are opposite in sign (107, 108, 109, 110). A further problem occurs if the Hall effect is used to assess carrier mobilities, as the mean free path is found to be less than the interatomic distance. This problem was recognised as early as 1960 (78). Both these anomalies have proved difficult to resolve, and have hampered the development of an overall theory for amorphous semiconductors. Even at the present time (1980) the position is still not clear, although it is widely assumed that it is hole conduction which is occurring in the amorphous chalcogenides.

This uncertainty does mean that some workers following Edmond (108), have disagreed with Mott and Davis' use of equation 5:1 which covers the case where there is only one charge carrier present. The other authors prefer the equation given as 5:2, which assumes both types of carrier are involved in conduction, and has the advantage of giving equal ΔE values for both optical and electrical measurements. Apart from this feature, the second approach has little to commend it, and in the author's opinion, the approach using equation 5:1 is likely to be correct. For

that reason, this equation has been used in discussing the present set of data.

5.1.3. Consideration of the present set of experimental data

Before considering the differences in conductivity/temperature behaviour caused by the differences in glass composition, it is worth noting the striking similarity in behaviour shown in Figure 25 where all the results are plotted on one graph. All five curves (including here that obtained for STAG, which makes use of some results of Webb and Baker) show very similar shapes. From room temperature up to 250–300°C there is a reasonably linear portion, followed by a gentle curving of the graphs to steeper slopes, as the temperature increases further. This curvature persists up to about 500°C. Beyond this point the graphs appear to straighten slightly, and there is a second approximately linear portion up to about 700–800°C, followed at even higher temperatures by a gradual levelling off, suggesting temperature independent behaviour by about 1200–1300°C.

To the author's knowledge, all truly amorphous chalcogenides for which data have been published show much the same form of temperature conductivity relationship, even in quite diverse materials such as InSb (111), AsTeI, AsTeGe, and AsTe (112), GeAsSe(113) and GeSbSe(114) to name but a few examples. There is usually a slope change at the glass transition temperature (Tg), and this is also true for the present set of glasses. Values of Tg for the sulphur-containing materials have been determined at the Royal Radar Establishment (102) and found to be 259°C for

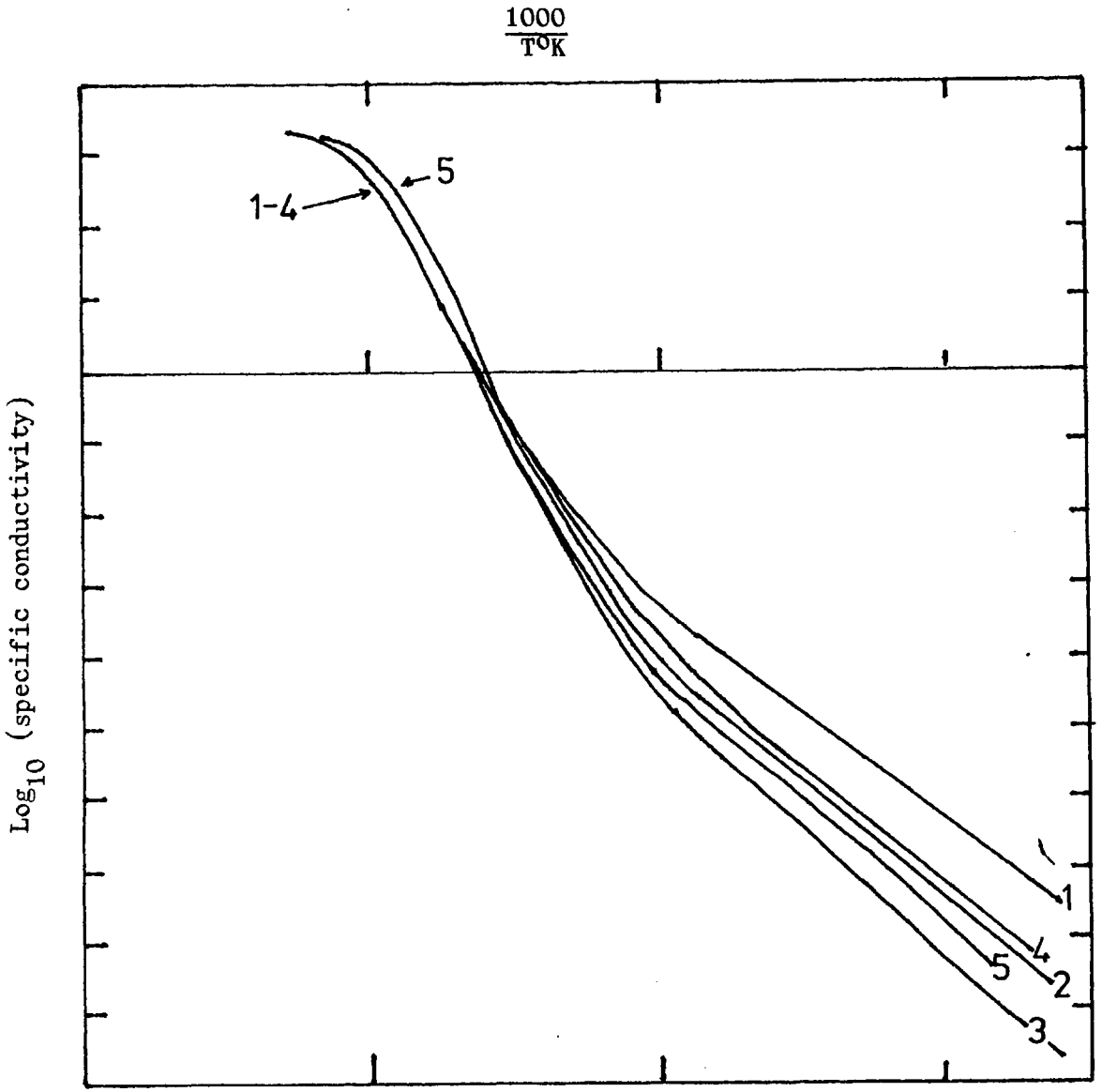

Fig. 25. Conductivity/temperature relationship for STAG, and for the sulphur and selenium-bearing glasses.

(1) = Si_{12} Te_{48} As_{30} Ge_{10} (STAG)

(2) = S_{15} Ge_{23} As_{31} Te_{31}

(3) = S_{15} Ge_{33} As_{27} Te_{25}

(4) = Se_{15} Ge_{23} As_{31} Te_{31}

(5) = Se_{15} Ge_{33} As_{27} Te_{25}

S_{15} Ge_{23} As_{31} Te_{31}, and 324°C for S_{15} Ge_{33} As_{27} Te_{25}. These values are plotted in Figures 16 and 17, and support the generally held view that the slope change in the $\log_{10}\sigma$ vs 1000/T graphs is associated with the structural changes occurring on melting. Tg for the selenium-bearing glasses was not determined, so the hypothesis could not be tested for these materials. If it is true, the slopes of the conductivity/temperature graph suggest that Tg for the selenium glasses will not be very different from that of their sulphur-bearing analogues.

Some materials show a sharp upward kink at the glass transition temperature (Tg), whereas others are continuously curving in the temperature range around Tg. It is unlikely that this is an effect caused by different degrees of experimental error of differing experimental techniques, but the factors controlling the type of behaviour near Tg are not clear. It has been suggested (115) that the simpler compound semiconductors like As_2Se_3 show the sharp transition in slope whereas the complex alloy type show a gentle curvature; and the present results, which are best described by curved lines, are consistent with this.

The more stable a glass is, the less distinction there is between the liquid and the solid states and the more likely it is to show a smooth transition in properties, including conductivity behaviour between the two states. Although experimental difficulties mean that data near Tg are rather sketchy for the present set of materials, the sulphur-bearing glasses do not seem consistent with the above hypothesis, as work at Sheffield University (116) showed that S_{15} Ge_{23} As_{31} Te_{31} lies further into the glass forming region of the S-Ge-As-Te system than S_{15} Ge_{33} As_{27} Te_{25}. However, Figs. 16 and 17 show the latter to have more of a gentle curve than the former.

A similar trend holds for the selenium-containing analogues, but unfortunately, the phase diagrams in this system have not been determined. In view of the uncertainty of the graphs in the region of Tg, the hypothesis can only be considered to be weakly supported by the present set of results.

Considering the data obtained in detail, the linear nature of the $\log_{10}$ σ vs 1000/T graphs for the materials in the solid state (below Tg) suggests that the Mott-CFO theory adequately describes the behaviour of the solid glasses, and that conduction is controlled by a "mobility gap" which replaces the ΔE of the extrinsic semiconductor equation. Thus it is possible to find ΔE from the slopes of the graphs, and the values obtained are shown in Table 9. Values of ΔE reported in the literature for related materials generally range between 0.5 and 1.0 eV, and the present data also fall in that range.

Values of the pre-exponential constant in the general form of the equation $\sigma = \sigma_0 \exp\left(-\frac{\Delta E}{kT}\right)$, can also be found for the linear portion of the graphs, and are given in Table 10. For the sulphur-containing glasses, it is around 160 $\Omega^{-1}cm^{-1}$, and for the selenium-containing ones about 1000 and 3100 $\Omega^{-1}cm^{-1}$. These are in the "normal" range of the Stukes law, but the value for STAG is not; being about 30 $\Omega^{-1}cm^{-1}$. The data of Male for STAG (72), also shown in Figure 15, extrapolate to a similar value. If Mott and Davis are correct, this suggests a possible difference in conduction mechanism between STAG and the other four glasses. The latter are all showing conduction in extended states, whereas the value for STAG lies between that for hopping between localised states

Table 9. Slopes of $\log_{10} \sigma$ vs $1000/T^{\circ}K$ graphs and resulting ΔE values for five glasses investigated.

Material	Slope	ΔE eV
$S_{15} Ge_{23} As_{31} Te_{31}$	-3.22	0.64
$S_{15} Ge_{33} As_{27} Te_{25}$	-3.89	0.77
$Se_{15} Ge_{23} As_{31} Te_{31}$	-3.36	0.67
$Se_{15} Ge_{33} As_{27} Te_{25}$	-3.82	0.76
$Si_{12} Te_{48} As_{30} Ge_{10}$	-2.60	0.52

Notes: These values apply over the range $0^{\circ}C$ to approximately $250^{\circ}C$ ($\sim$ Tg) and were calculated assuming

$$\sigma = \sigma_0 \exp\left(-\frac{\Delta E}{kT}\right)$$

Table 10. Intercept values on the $\log_{10}\sigma$ vs $1000/T^{\circ}K$ graphs, and the resulting σ_0 values (see text).

Material	Intercept (log σ axis)	$\sigma_0 \exp\left(\frac{\gamma}{k}\right)$	σ_0 $(\Omega^{-1}cm^{-1})$	
			If $\gamma = 4 \times 10^{-4}$ eV/$^{\circ}K$	If $\gamma = 2 \times 10^{-4}$ eV/$^{\circ}K$
$S_{15} Ge_{23} As_{31} Te_{31}$	2.2	159	1.53	15.58
$S_{15} Ge_{33} As_{31} Te_{25}$	2.2	159	1.53	15.58
$Se_{15} Ge_{23} As_{31} Te_{31}$	3.0	1001	9.64	98.17
$Se_{15} Ge_{33} As_{31} Te_{25}$	3.5	3167	30.47	310.4
$Se_{12} Te_{48} As_{30} Ge_{10}$	1.5	31.6	0.30	3.104

along the band edges; (around 10 $\Omega^{-1}cm^{-1}$) and the range (100-10,000 $\Omega^{-1}cm^{-1}$) associated with extended state conduction. The present set of results are insufficient to clarify the nature of conduction in STAG.

In addition to the analysis using the pre-exponential constant given above, Mott and Davis argue, as quoted earlier, that a linear ln σ vs. 1/T graph also results from a gap with a linear dependence on temperature. Representing such a gap by the equation $\Delta E = E_0 - \gamma T$, where γ is the temperature coefficient of the gap, and substituting this into equation 5.1, they argue that this treatment gives a ln σ vs. 1/T line offset from that due to the simple treatment by an amount (γ/k), where k is Boltzmann's constant. They give limiting values of σ_0 for different conduction mechanisms, calculated using this second treatment. However to make use of these limits, it is necessary to calculate σ_0 from the experimental results, which requires a knowledge of γ. Mott and Davis suggest that γ is usually about half of β, the temperature coefficient of the optical gap. For a large number of amorphous chalcogenides, β is $4\text{-}8 \times 10^{-4}$ eV/^oK. The resulting range of γ gives rather alarge range of σ_0 values, as Table 10 shows. The most reasonable values are produced by assuming $\gamma = 2 \times 10^{-4}$ eV/^oK, as Mott and Davis suggest σ_0 is usually between 100 and 500 Ω^{-1} cm^{-1} for extended state conduction. STAG is again shown to be different to the other four glasses, possibly suggesting a difference in conduction mechanism. In view of the somewhat arbitrary values for γ, and the large influence this has on the value of σ_0, it is probable that less significance should be attached to the discrepancies in σ_0 than to the anomalously low value of the pre-exponential constant, which is closer to the direct experimental observations.

The above comments only apply to the glasses in the solid state, in

which the structures of the glasses will almost certainly consist of long chains of atoms of a largely random composition, arranged in a random manner. This assumption can be justified on the grounds that pure Se, Te and S have chain-like structures. Bonding along the chain length will be chiefly covalent in nature, with inter-chain bonds being weaker, probably of the Van der Waal's type. Once melting occurs, the interpretation of the data becomes less certain, although most workers conclude that semiconduction is still occurring in the liquid, with an ever-narrowing energy gap. This seems logical, as the glassy nature of these materials means that little structural change occurs on melting, apart perhaps from a small rise in density resulting from the fact that the chains of atoms are free to re-arrange themselves in the liquid state. The $\log_{10} \sigma$ vs $1000/T$ graphs all show an upward curvature just above Tg, indicating that the energy gap begins to narrow quite rapidly, especially in the range up to $1000/T^{\circ}K = 1.5$ ($\sim 480^{\circ}C$). Over this range, the long chains of atoms of which the glass is composed just above Tg will begin to break up, and this probably accounts for the narrowing of the gap. At still higher temperatures, the graphs appear to straighten, and it is tempting to view this as a stabilisation of the gap which can be treated similarly to that in the solid. It is unlikely that this is realistic, however, as the slope of this high-temperature portion suggests an energy gap about 1-2 eV wide for the different glasses. It is difficult to reconcile this with the fact that the gap has previously been narrowing, with the high actual conductivity values measured, and with subsequent behaviour as the temperature is raised still further. At very high temperatures, the graphs curve over as though they are going to become temperature independent, or possibly

even fall. This is a characteristic of metallic conduction, and suggests that the gap has closed altogether at these temperatures. This would be expected to occur at some point as the gap narrows, and as the average chain length in the melt approaches one or two atoms, at which point it resembles a liquid metal. This seems to be the only explanation for the behaviour above about 700°C, and for it to be true, the "linear" portion from 500–700°C cannot be due to an activated process with an activation energy as large as 1–2 eV. The apparently linear portion must represent a transition between the upward curvature generated by an energy gap narrowing from the values found for the solid, and the downward curvature produced by the metallic behaviour occurring at higher temperatures.

Few investigations of chalcogenide glasses have been pursued to the high temperatures necessary to show whether metallic conduction is going to occur. This is partly because of the high vapour pressures which have to be contained, and partly because many results of theoretical interest are obtained at temperatures below ambient rather than above. Nevertheless, in all cases where conductivity measurements have been pursued to a sufficiently high temperature, this type of levelling off has been observed (e.g. Edmond (110) on As_2Se_3 and STAG).

The effect of temperature on the conductivity and structure of the sulphur and selenium-containing materials may thus be summarised from the above reasoning as follows: Room temperature up to Tg ($\sim$ 250–300°C): thermally activated conduction across an energy gap between 0.5 eV (STAG) and 0.77 eV (S -containing glass with 33% Ge). Structure, long

randomly arranged chains of covalently bonded atoms.

From Tg up to around 500°C: thermally activated conduction across an ever-narrowing energy gap, structure breaking down into a melt of shorter chains.

From 500°C upwards: metallic conduction becoming important as gap closes up, eventually becoming fully established at ~ 1100°C. Melt structure breaking down, approaching liquid metal structure at highest temperatures.

It is quite probable that the conductivity/temperature behaviour of STAG may be described by the same processes. The only doubt is over the "room-temperature up to Tg" range, where the value of C suggests a hopping mechanism.

5.1.4. Effects of glass composition

The above discussion has treated the four S and Se containing glasses as essentially identical, and for the purposes of that discussion, the assumption holds true. However, it is also worth examining the data for evidence of the effect of glass composition. Inspection of Figure 25, on which all four glasses are shown together, shows that four approximately parallel sets of log σ vs 10^3T^{-1} data are produced at the lower temperature range, but that, above ~250°C, the lines begin to converge, becoming to all intents and purposes identical in the higher temperature range up to 700°C. This effect has been observed in other systems (117). Similarly, the curving over of all four graphs

at the highest temperatures is the same, as they all level out to a plateau value around $\log_{10}\sigma = 3.4$. In general terms, this can be understood as resulting from the effect of composition being greatest in the solid, where such factors as chain length and average interatomic distance will be heavily influenced by the composition, less in the liquid, where smaller structural units are present, and essentially zero when the liquid is reduced to single atoms.

The effects of the elements concerned here on the structure of the glass can be broadly subdivided into chain-forming and chain-cross-linking. Chain-formers are those elements which, when crystallising on their own, form long chains of atoms. These will be sulphur, selenium and tellurium. Cross-linking elements, which have a more conventional structure when pure, and which have a different valency to the chain-formers, tend to cause an extensive three-dimensional network structure. Ge and As would be examples of this latter type of element, and their effect is to increase the tendency of the melt to form a glass. Since the compositions investigated here were not chosen with the intention of examining compositional effects, but were practical examples of chalcogenide glasses, it is difficult to draw any firm conclusions by comparing one sulphur-glass with the other. The same applies to comparison of the selenium-glasses. At a fixed sulphur or selenium content, an increase in Ge and a decrease in As and Te can be observed to cause a fall in the conductivity of the solid at any given temperature, and a rise in ΔE. This is in conflict with the notion that Ge and As are cross-linking elements and Te a chain former. The changes described would be expected to

result in a more heavily cross-linked structure, the most likely result of which would be a higher conductivity. The significance of these results must be to indicate that the effect of composition on structure is more complex than the simple picture would suggest. However, the present set of results do not allow any different model to be developed.

The other comparison which can be made with these results is that between each sulphur-glass and its selenium-bearing analogue. A change from S to Se caused a small increase in conductivity, as might be expected from the fact that selenium is a much better conductor than sulphur, the latter being virtually an insulator at the temperatures considered here (see results obtained in Section 4.2). Since sulphur and selenium are covalently bonded, whereas the other elements involved, Ge, As, Te, have a more metallic nature, it is likely that S and Se reduce the conductivity by interrupting the passage of charge carriers along the chains of atoms of which the solid and low-temperature liquid are composed. As the temperature is increased, these chains will disintegrate, and the effect of S and Se will not be so marked. The curves remain together at the upper end of the temperature range studied here, at which point the liquid must have degenerated mainly to single atoms, and compositional differences can have little detectable effect.

The relative insensitivity to compositional effects, and the unusual direction of the small effects which have been detected are doubtless due to the nature of the mobility gap which controls the conduction in these materials. Relatively large compositional changes would be required (in view of the unstructured state of the material) to cause

any major change in the conduction and valence band edges which might then be reflected in a conductivity difference; and this will doubtless be more true in the liquid state than in the solid. (As noted much earlier, this insensitivity to composition and to contamination was one of the chief attractions of chalcogenide glasses to the electronics industry).

According to the thermal model for the switching phenomenon in these materials, it is the shape of the conductivity temperature curve which allows a stable "on-state" to develop (118). The curve must have a portion in which the conductivity rises rapidly with temperature, followed by a portion in which it is relatively temperature-independent. It is the fact that this form of curve is exhibited by all materials which show switching and memory behaviour that has led to the widespread acceptance of the thermal theory. The four materials examined here have thus been shown to fit the established pattern. One of the main objections to the theory is that it requires a complex physical and chemical process to take place with great rapidity. In the measurements carried out here, the equilibration of conductivity was rapid compared to the rates of change of temperature involved. However, as these were slow in comparison to the switching reaction, (the temperature change involved in these measurements was only a few tens of degrees a minute whereas switching, in which some portion of the device is thought to be raised to 1000^{o}C or more, occupies a few hundred picoseconds (118)) this scarcely constituted a test of the time required for the conductivity to come to equilibrium. A totally different design of apparatus would be required to test this. Such experiments would present

many practical difficulties, as the apparatus would have to be capable of detecting events which occurred on a picosecond time-scale. To the author's knowledge, the critical experiments have not been performed to date.

The present results indicate that the (admittedly very small) volume of material in the hot conducting channel would have to be heated to values of $10^3/T^{\circ}K$ of about 0.85 or less before the flattening of the curve would allow a stable situation to develop (see Figs. 16-19). This corresponds to a temperature of $900^{\circ}C$ or more. However, proponents of the thermal model have hypothesised temperatures several hundred degrees above this on the basis of computer simulations (118).

Thus, the contribution provided by the present results to the debate as to which of the two competing models represents the switching process must be considered small. They provide one more example of the type of conductivity/temperature relationship required for the thermal model. Apart from this, the results are consistent with either model.

5.2. The Electrical Conductivity of Sulphur

The conductivity/temperature relationship produced in Figure 20 by combining the present author's results with those of Baker does not agree particularly well with others published in the literature; Watanabe and Tamaki (79), for instance, reporting conductivities over an order of magnitude higher than the present data, although their measurements stop at $500^{\circ}C$. Such a disagreement is scarcely surprising,

however, as the various sets of data presented in the literature do not agree with one another as to the actual value of the conductivity at a given temperature, although there is some consensus as to the slope of the conductivity/temperature curve, as shown in Figure 26, where various published curves are shown (79,80,82) together with the present author's and Baker's results. Vezzoli's data is only published in the form of resistance values, rather than resistivity, so the vertical location of the dotted line in the Figure is, of necessity, quite arbitrary. At low temperatures, good agreement as to the shape of the curve is shown by Baker (103) and Feher and Lutz (82), and these also agree with the early results of Wigand (81); who also found a maximum conductivity at 150°C ($1000/T^{\circ}K = 2.36$) and a minimum at around 170°C, ($1000/T^{\circ}K = 2.26$). At low temperatures, it is hard to reconcile the curves produced by Vezzoli (79) and Watanabe and Tamaki (82) with one another, or with the consensus of Baker, Feher and Lutz, and Wigand. In particular, the several "spikes" in Vezzoli's curve are not reproduced elsewhere. At higher temperatures, where the experimental difficulties caused by the very low conductivity of sulphur are lessened, there is a measure of agreement between Watanabe and Tamaki and the present author as to the slope of the graph. Vezzoli found a similar slope between about 250°C and 350°C, but other data in the relevant temperature range does not reproduce the sharp upturn which he reports at 350°C. Most of the conductivities measured by the present author are at such a high temperature that no published work exists with which they might be compared. However, the agreement with the slope found by Watanabe and Tamaki up to about 500°C is encouraging, and there is no reason to doubt the experimental finding that this slope persists

$\log_{10}$ for molten sulphur.

- - - data of Vezzoli (80), but see text.

-.-.- data of Watanabe and Tamaki (79).

..... data of Feher and Lutz (82).

——— data of present author at T >500°C + data of Baker (103) at T < 500°C.

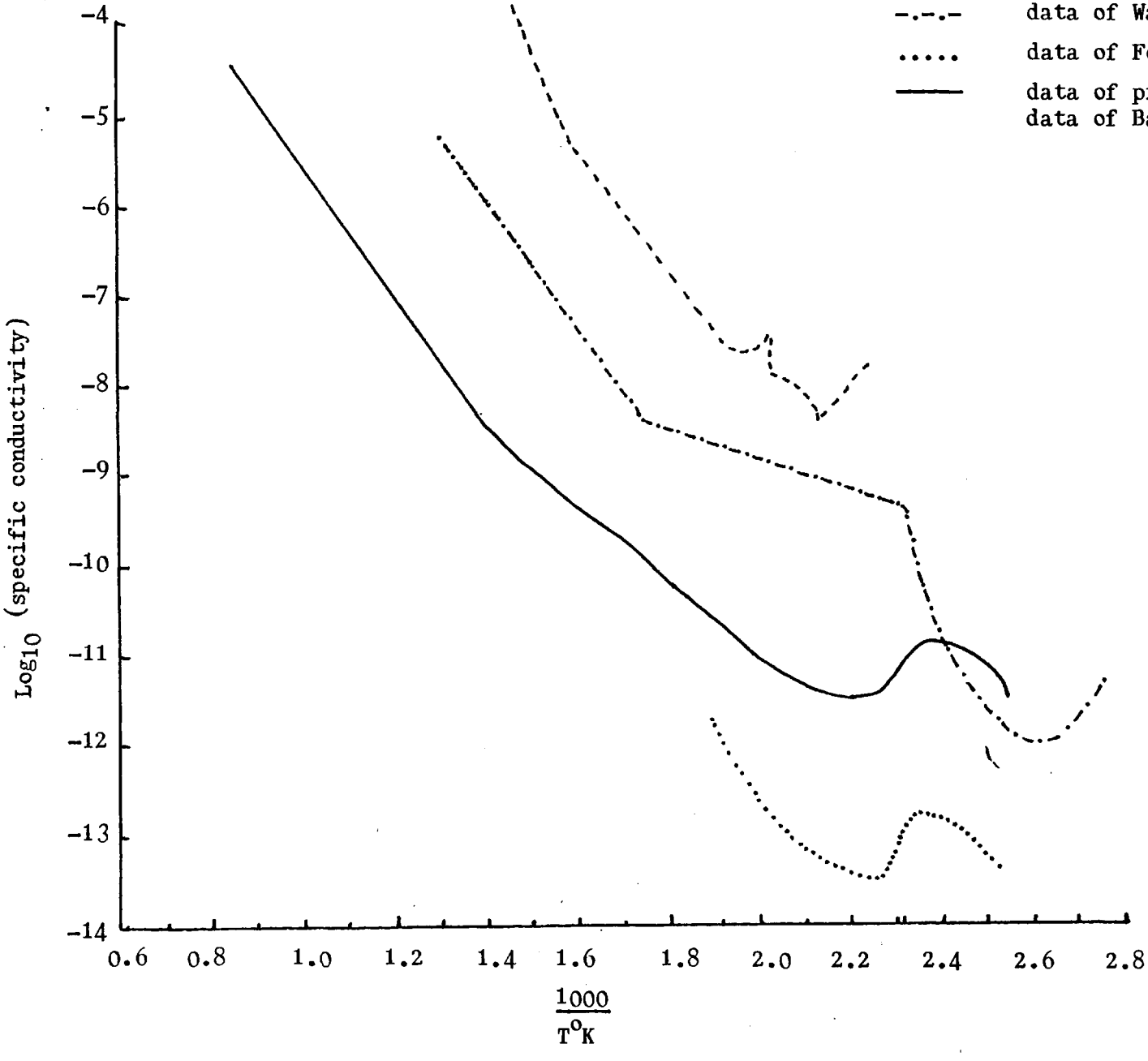

to 900°C.

The unusual viscosity changes which occur in liquid sulphur just above the melting point have been the subject of many investigations and have led to considerable understanding of the polymeric nature of liquid sulphur. It was noted at the beginning of the century that the viscosity/temperature relationship showed some parallels to the conductivity/temperature one. The viscosity behaves quite normally from the melting point (113°C) up to 160°C. At this point, the eight-membered rings of which the liquid was composed begin to break open and form long chains, causing a rise in viscosity (119) from 8 poise at 160°C to nearly 1000 poise at just over 190°C. Above this temperature, the viscosity falls steadily again, reaching 10 poise at about 330°C. The sudden rise above 160°C corresponds to the gentle maximum found by Baker, Feher and Lutz, and Wigand near $1000/T^{\circ}K = 2.35$, and the viscosity maximum to the conductivity minimum they report near $1000/T^{\circ}K = 2.25$. The correspondence was noted to be inexact, however, but did lead to a realisation of the need for pure sulphur, as the viscosity-related conductivity was for a time attributed to the movement of charged impurities.

When the reason for the viscosity behaviour became clear, investigations of chain length were made which showed how polymerisation, once initiated at 160°C, caused the development of very long chains, which only became fragmented by thermal motion at relatively high temperatures. Since the breaking of chains might be expected to release charge carriers into the melt, it was hoped that the mean chain length, usually called

"P",* might be more directly related to conductivity. The relationships of $\log_{10}$ P and $\log_{10}$ C with temperature are given in Figure 27. Log C is used here for convenience as both curves then slope in the same direction. With the exception of the point at 1040°C, the chain length data is taken from Poulis and Massen (120), and is based on magnetic susceptibility and electron spin resonance measurements, both of which agree well with theoretical estimates of chain length from the polymerisation equations. No experimental data is available above 600°C, except at the critical point (1040°C), where vapour phase measurements can be used, as liquid and vapour have identical compositions. Baker (121) and Rau, Kutty and de Carvalho (96) found values of 3.4 and 2.78 respectively, for the mean chain length at the critical point. It has also been assumed that at the start of the viscosity anomaly, i.e. at 160°C, the liquid is composed of S_8 rings, with P = 8. As shown in the figure, the parallel between these two plots is quite good, the falling conductivity up to 160°C being due to processes in the 8-membered ring liquid, the rise up to about 190°C being due to the polymerisation reaction, and the continuous fall thereafter, up to 1000°C, being due to a falling chain length. The relationship is obviously still far from simple though, as the slopes of the curves differ markedly, and the behaviour of the chain length at low temperatures (<200°C) is much more dramatic than that of Baker's resistivity data.

Considering only the present author's results, however, a plot of $\log_{10}$ P vs $\log_{10} \rho$ is quite instructive, as shown in Figure 28. The plot is only slightly curved, becoming more linear as the temperature rises (smaller P and ρ values). This graph has a slope of approximately

*) expressed in terms of single atoms, not S_8 units.

Fig. 27. Comparison of resistivity behaviour and mean chain length for sulphur.

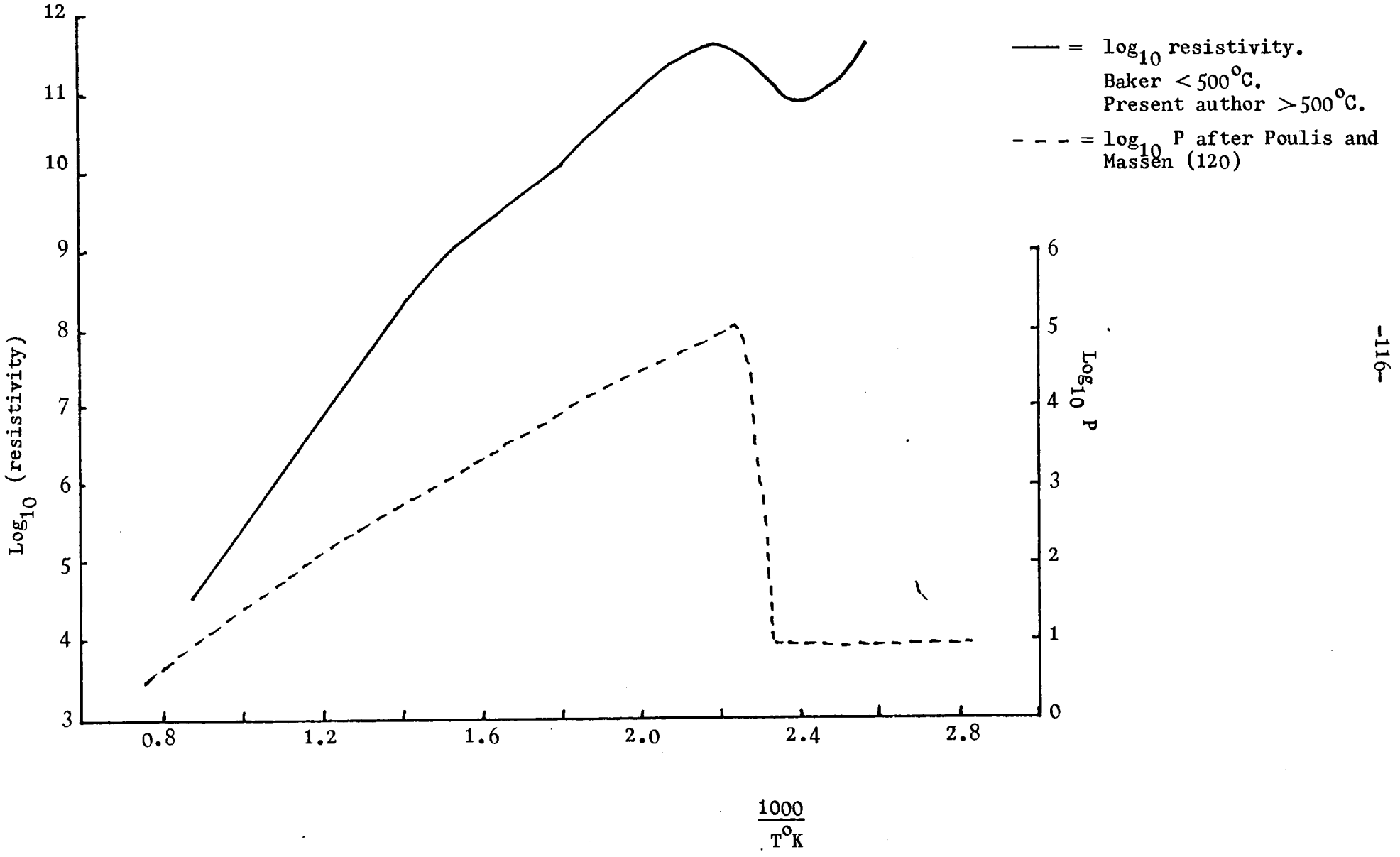

Fig. 28. Relationship between mean chain length P and resistivity ρ for liquid sulphur.

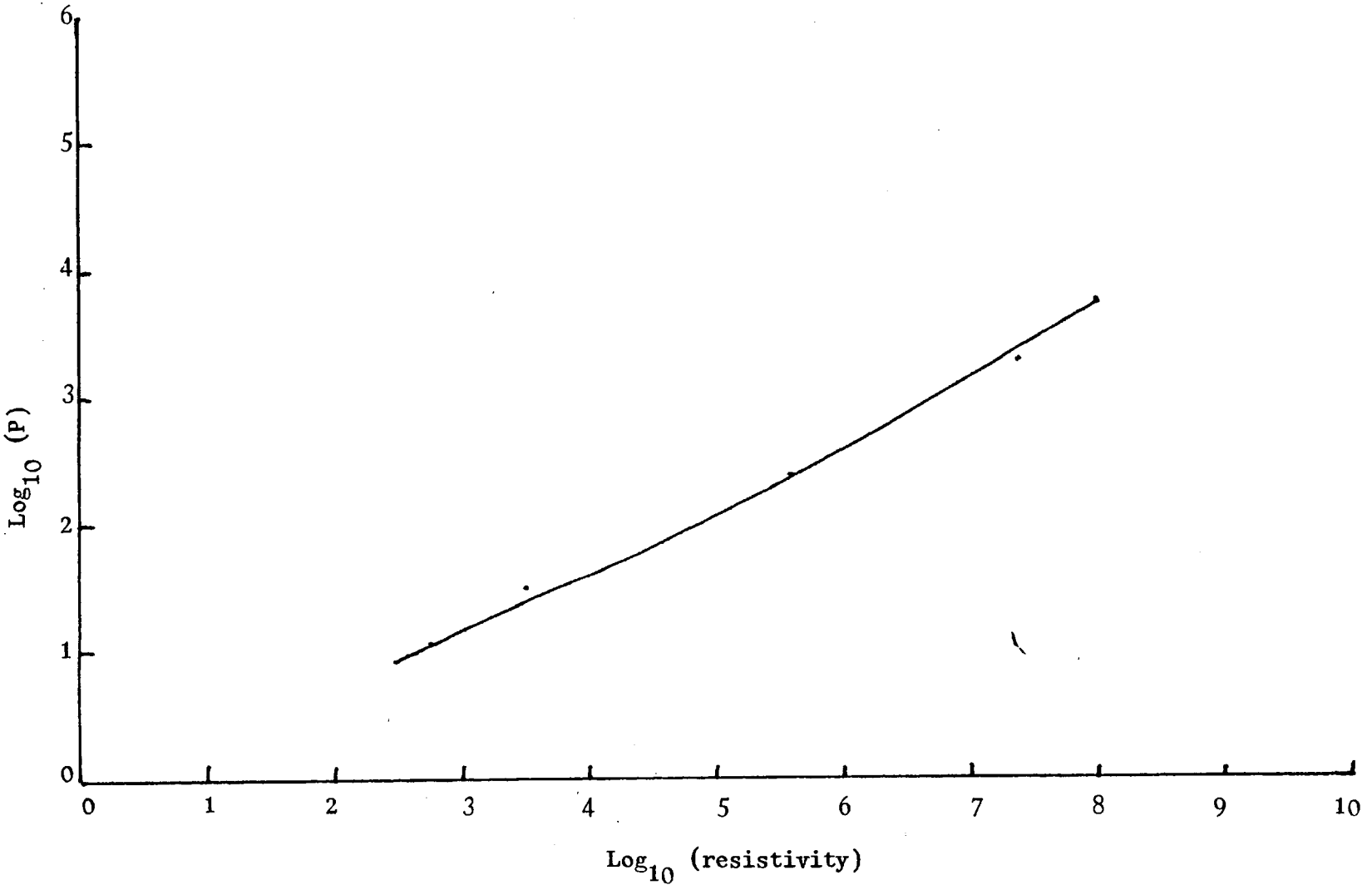

0.5, i.e. $\log_{10}\rho = 2.0 \log P$. The resistivity is thus seen to be roughly related to the square of the mean chain length. This relationship vanishes abruptly when the chain length maximum is passed (going towards the melting point). The effect of chain length on resistivity has been attributed to new charge carriers being released or to changes in the amount of charge carrier scattering produced by chain break-up (122). To judge from the experimental evidence presented here, it is likely that this simple view needs some qualification, the most likely of which is that chains of different lengths have different effects on the conductivity. It may thus be that short chains are particularly effective charge carriers (or ineffective carrier scattering centres), as this could account for the way the sulphur conductivity graph, Fig. 26, tends to curve upwards over the middle temperature range around 500°C, and for the way the $\log_{10} P$ vs $\log_{10}\rho$ plot shows a continuous slight deviation from linearity. To the author's knowledge, no investigation has been carried out to determine how the chain length is distributed about its mean value, and it may be a shift in this distribution which causes the curvature in log P vs log ρ .

In spite of the uncertainty as to the controlling parameter behind the conductivity behaviour, the present author's results show a virtually linear relationship in the $\log_{10}\sigma$ vs $1000/T^{\circ}K$ plot. This suggests, as it did for the chalcogenide glasses, that electrical conduction in sulphur is a process controlled by an energy gap. In the case of sulphur, it is reasonable to postulate an intrinsic type semiconduction (79,82), electrons and holes being present in equal numbers in the melt. The conductivity may thus be described by

$$\sigma = \sigma_0 \exp\left(-\frac{\Delta E}{2kT}\right).$$

In the present case, the slope of the $\log_{10}\sigma$ vs 1000 $(T^{\circ}K)^{-1}$ graph, Figure 25, gives a value for ΔE of around 3.1 eV. Values of ΔE found by other workers or calculated by the present author from their results are given in Table 11, and are all fairly similar at around 3.0 eV, except for the higher temperature results of Vezzoli (80) and those of Steunenberg et al. (86). The data presented here can thus be seen to have extended that obtained by other workers, and to have confirmed that the approximately linear behaviour they detected near 400°C continues up to 900°C with about the same ΔE. (The actual values of conductivity reported differ sharply, though, as noted earlier). Whether such behaviour persists to much higher temperatures is not certain. The critical point lies not far away, at 1040°C, and marked changes in conductivity behaviour can probably be expected if this temperature is approached, caused perhaps by the falling liquid density. This region could not be studied in the present work as the increasing convective heat transfer made the Perspex lid of the pressure vessel dangerously hot, and it was felt that the vessel could not be operated safely at the critical pressure, just over 200 atm (87). In addition, there were indications that gold electrodes might not be immune to attack if the temperature were raised above 900°C. Electrodes used repeatedly at high temperatures appeared to show signs of grain relief, although no gold was found in the sulphur from such a conductivity run down to the limits of detection of the X-ray fluorescence technique used (50 p.p.m.). It is thus possible that the grain relief was due to recrystallisation beneath a polished surface rather than to etching by the sulphur.

Table 11. Values of ΔE for liquid sulphur at high temperature

(Calculated using intrinsic semiconductor equations)

Source	ΔE (eV)	Temperature range
Present work	3.1	400 - 900°C
Watanabe and Tamaki (79)	2.83	300 - 500°C
Vezzoli (80)	2.65	200 - 350°C
"	4.76	350 - 420°C
Steunenberg et al. (86)	1.62	325 - 425°C

It is instructive to compare the results of the present work on sulphur with those given in the literature for a closely analogous material, selenium (77, 79, 80). By analogy with the reasoning presented above for sulphur, the conductivity behaviour of selenium should be related to its liquid structure. However, unlike sulphur, liquid selenium consists of a mixture of chains and rings just above the melting point, and as the temperature is raised the rings break open and form chains, while the longer chains break up to form shorter ones. This is different to the case of sulphur, where no chains are present until a transition temperature is attained. It is thus unlikely that the conductivity/temperature behaviour of the two liquids will be similar at low temperatures. This is borne out by the work of Watanabe and Tamaki (79). However, once the structures of both liquids are entirely composed of chains, then some similarity in behaviour can be expected. This can be confirmed by examining the work of Watanabe and Tamaki over the range 250 → 400°C, where they found both selenium and sulphur to have linear $\log \sigma / \frac{1000}{T^{\circ}K}$ plots. The present work shows that this is true for sulphur even up to 900°C, and that of Baker (77) shows that the linearity for selenium persists up to about 1000°C. In this linear region, a value of ΔE can be calculated for selenium in the same way as it was for sulphur. From the slopes of published graphs, for selenium, this would appear to range from 2.1 to 2.4 eV over the linear portions of the plot, compared to about 3.0 eV for sulphur over the same temperature range, and the actual values of σ tend to be lower by a factor of about 10^3 x in the case of sulphur. This greater ease of conduction in selenium will probably turn out to be related to a shorter chain length at any given temperature compared to sulphur. At present, however, the magnetic

susceptibility (123) and the viscosity (124) give chain lengths for selenium which disagree. The former indicates that the selenium chains are twice the length of the sulphur ones, whereas the viscosity suggests they are only one tenth of the length. Until this is resolved, the hypothesis that differing chain lengths are responsible for the differing conductivities of the two materials will remain unproven.

Before leaving the discussion of the data obtained by the author on liquid sulphur, it is worth considering whether the pressure used to prevent volatilisation of the sulphur was sufficient to affect the polymerisation reactions, and thus possibly the conductivity values obtained. The effect of pressure on the various transformations in sulphur has been investigated by Vezzoli, Dachille and Roy (125), and considered theoretically by Eisenberg (126). Unfortunately, these two sources disagree as to the effect of pressure on the polymerisation transition temperature. Vezzoli et al. believe it rises to a maximum with increasing pressure and then begins to fall, whereas Eisenberg calculated it would fall continuously as the pressure was raised. In spite of this, both authors show very little change (only a few degrees) in this temperature with pressures up to the maximum used here (100 atmospheres), indicating that the results presented can be considered not to have been significantly affected by the pressures used.

5.3. The Si-Te Phase Diagram

As shown in Figure 21, the present results combine well with those of Bailey (92). The phase diagram shows a single compound Si_2Te_3, which

undergoes a peritectic decomposition at 880–890°C. The boundary produced by this decomposition was not always found by the present author, but would appear to extend to at least the point $Si_{80}Te_{20}$, indicating that any solid solubility at the high-Si end of the diagram will be less than this. It has been found empirically by Hume - Rothery (127) that primary solid solubility is severely limited if the difference in atomic radii exceeds 15%. In the case of silicon (1.173 Å) and tellurium (1.37 Å) this ratio is almost exactly 15%, so that the situation is not clear cut, but on both this basis and that of the experimental data presented here, it is likely that solid solubility is much less than the upper limit of 20% set by the thermal arrests.

No reactions were detected which could be attributed to the other compounds which were once thought to exist in this system, such as SiTe and $SiTe_2$ (89,90). Bailey (92) and Brebrich (93) have shown fairly conclusively that these do not exist in the solid, although SiTe seems to be present in the vapour phase (93). The present work is consistent with the existence of only one compound in this system, at Si_2Te_3, and serves to increase confidence that this interpretation of the system is correct. Additionally, the author was able to duplicate Bailey's vapour phase growth experiment to manufacture the compound.

It is at first sight curious that the present results do not show an arrest corresponding to the upper line of the eutectic which Bailey shows between Te and Si_2Te_3, nor was any arrest found when heating and cooling material of exactly the compound composition. Si_2Te_3 is very difficult to crystallise, however, (92) and it is probable that no

arrests are obtained unless a suitable nucleant is present. Between Si_2Te_3 and the eutectic point, the compound is trying to form directly from the liquid as the first phase to solidify, and has thus no suitable nuclei on which to form. Between Si_2Te_3 and Si, however, the liquid first deposits silicon, which can then nucleate the Si_2Te_3.

Although no detailed investigations were carried out close to the compound composition, no evidence was found to contradict Bailey's assertion that Si_2Te_3 is incongruently melting. Ploog et al. (94) disagree with this, stating that it is a congruently melting compound. However, as they merely state this conclusion, and present no experimental evidence, this notion, which would also result in a very unusual phase diagram, with a small peak at the compound composition, must be discounted for the time being.

The type of behaviour shown in Fig. 21, with both peritectic and eutectic reactions, is not uncommon. The compound in such a system is often called an "intermediate phase", and in some systems, has a range of composition. In this system, however, Bailey's results suggest that the compound composition is fixed, as his analyses of the compound extracted from several different melts produced very similar results.

The details of the construction of the phase diagram near the peritectic composition are somewhat tentative. In the present work, only one melting point measurement was attempted at the Si_2Te_3 composition as it was at the high-silicon end of the phase diagram that data were lacking completely. The liquidus representing the solidification

of silicon from the liquid alloy cannot meet the horizontal line representing the peritectic reaction exactly at the peritectic composition for thermodynamic reasons, but Bailey's data suggest that these points are relatively close together, and that the liquidus rises steeply from the intersection, reaching about 1200°C near the compound composition. With his experimental techniques, Bailey could not reach higher temperatures and was thus unable to investigate high silicon alloys, but the data he was able to obtain near the peritectic point are consistent with those of the present author. Bailey's construction near the peritectic composition meets the thermodynamic requirement mentioned above, and has been preserved in the construction of Fig. 21, which combines the data from Bailey's investigations with those of the present author.

Turning next to that part of the diagram which had not been investigated previously, namely the high-silicon end, the thermal arrest data indicate a high, almost horizontal liquidus running out from pure silicon to about 60-70% Si, before curving steeply down towards the peritectic point. A liquidus of approximately this shape, indicating a positive departure from ideality, would be expected in a system which contains a peritectic reaction. However, the almost horizontal nature of the present liquidus suggests that the departure is considerable in the part of the Si-Te diagram between 0.7 and 0.9 atom fraction of silicon, and that conditions may be approaching those for a miscibility gap over this range.

If such a miscibility gap did exist, it would be extremely difficult

to locate experimentally for two main reasons. Firstly, the temperature of the upper boundaries of the miscibility gap may be very high over much of the composition range which it covers, and thus beyond the working range of the apparatus used here. The platinum-wound resistance furnace was operating at its upper limit determining the melting point of the higher silicon alloys at around 1400°C. It is possible that totally different experimental techniques would be needed to locate the upper phase boundary of any miscibility gap. The second reason why the present apparatus would be unlikely to find the boundaries of the miscibility gap is that the energy changes involved in the mixing and unmixing of the liquids would be quite small, resulting in small thermal arrests. It is unlikely that such arrests could be detected using apparatus of the type employed here for liquidus determination.

Thus it is unlikely that any direct experimental evidence of a miscibility gap would be obtained in the present set of thermal arrest determinations, and indeed, no arrests were seen which could be attributed to the mixing or unmixing of liquids. In the absence of such experimental evidence, it is necessary to resort to some of the theoretical or empirical tests which have been developed.

The first of these tests, and the simplest, is attributed by Kleppa (128) to Axon. It was observed that some form of liquid immiscibility was likely if the atomic radii differed by more than 30%. Although this is analogous to Hume-Rothery's rule concerning solid solubility, referred to earlier, it is less reliable, particularly if there is a

large difference in the melting points of the two constituents. This is unfortunately the case for Si and Te, so any indications from this test must be treated with caution. Thus, although the difference in atomic radii is only about 15%, (as discussed earlier), and the liquids should thus be miscible, this should not be taken as a particularly firm indication.

A second guideline given by Kleppa, and one which is slightly more reliable, involves the use of "solubility parameters" which characterize the pure components, and are designated δ. The criterion for miscibility is that

$$2RT \geqslant \tfrac{1}{2}(V_A + V_B)\ (\delta_A - \delta_B)^2$$

To the accuracy of the approximations used in deriving this criterion, the molar volumes of most metals (V_A & V_B) are around 10 c.c. If this is also assumed to be the case for Si and Te, the δ values must differ by less than 20 $cal^{\frac{1}{2}}cm^{-3/2}$ at 1000°K and by less than 28 $cal^{\frac{1}{2}}cm^{-3/2}$ at 2000°K for the liquids to mix. For Si and Te, Kleppa gives σ values of 88 and 31 $cal^{\frac{1}{2}}cm^{-3/2}$ respectively. In this case then, the indications are strongly in favour of liquid immiscibility.

The third test which can be applied involves the use of the α-function. This function, defined as:

$$\alpha_A = \frac{\ln \gamma_A}{(1 - N_A)^2} \qquad - 5.3.1.$$

(where γ_A is the activity coefficient and N the atom fraction) was originally devised to facilitate the graphical integration of the Gibbs-Duhem equation and thus allow the thermodynamic properties of one component of a system to be found when the properties of the other component were known. The use of this function to assess the likelihood of immiscibility relies on the fact that the liquid will separate if in doing so, it lowers the free energy of the system.

The free energy/composition curves of hypothetical systems showing complete liquid miscibility and a miscibility gap are shown in Fig. 29 together with the corresponding activity vs. composition curves. In the case of complete miscibility, the free energy curve is continuously curving and always concave up. Thus the lowest free energy state the system can reach is that of the single mixed liquid. In the miscibility gap case, the curvature of the free energy graph reverses and there is a concave down portion. Anywhere between the two minima, the system can lower its free energy by separating into two liquids. The corresponding activity/composition graph is horizontal over the miscibility gap region. Between these two situations there must be a limiting case, in which the liquid is on the verge of separating (called imminent unmixing), and in which the free energy curve has a short portion of constant slope, as shown in Fig. 29(c). The corresponding activity curve has a point of inflection in the mathematical sense that its slope is momentarily zero. Darken and Gurry (127) show that a similar point of inflection occurs on the corresponding liquidus as well.

From these curves, the limiting case can be expressed as the state

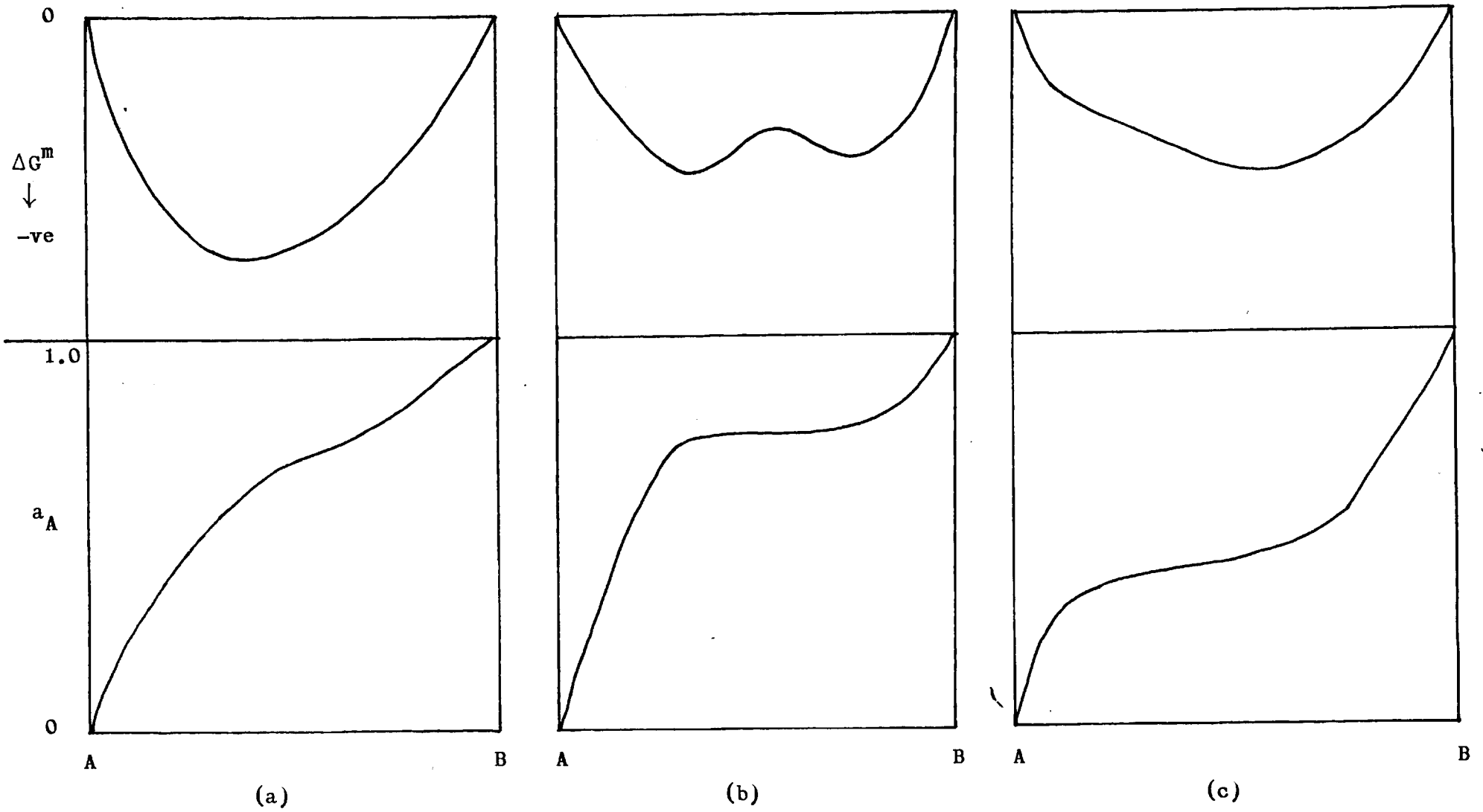

Fig. 29. Three hypothetical systems showing (a) complete miscibility, (b) some immiscibility and (c) imminent unmixing.

in which the second and third derivatives of ΔG^m, the free energy of mixing, are both zero, but to make use of this definition, it would be necessary to know ΔG^m as a function of composition. Such data are rarely available. However, in the case of a regular solution, in which the α-functions for both components are equal and constant, and can thus be replaced by the single constant α, the activity coefficient γ, and the atom fraction N are related by:

$$\ln \gamma_A = \alpha N_B^2 \text{ and } \ln \gamma_B = \alpha N_A^2 \qquad - 5.3.2.$$

Now, the free energy of mixing of any solution is given by

$$\Delta G^m = RT\ (N_A \ln a_A + N_B \ln a_B) \qquad - 5.3.3.$$

(where a is the activity)

and can also be considered as divided into two components, the ideal part ($\Delta G^{m,id.}$) and the difference between this and the real value, known as the excess, $\Delta G^{m,xs}$, thus:

$$\Delta G^m = \Delta G^{m,id} + \Delta G^{m,xs}. \qquad - 5.3.4.$$

By the definition of an ideal solution,

$$\Delta H^{m,id} = 0$$

and

$$\Delta S^{m,id} = -R\ (N_A \ln N_A + N_B \ln N_B) \qquad -5.3.5.$$

Thus, since $\Delta G = \Delta H - T\Delta S$,

$$\Delta G^{m,id} = RT\ (N_A \ln N_A + N_B \ln N_B) \qquad -5.3.6.$$

Substituting 5.3.6 and 5.3.3 into 5.3.4,

$RT\ (N_A \ln a_A + N_B \ln a_B) = RT\ (N_A \ln N_A + N_B \ln N_B) + \Delta G^{m,xs}$.

rearranging, and using the fact that $\gamma_A = \frac{a_A}{N_A}$,

we find:

$$\Delta G^{m,xs} = RT\ (N_A \ln \gamma_A + N_B \ln \gamma_B)$$

but, from - 5.3.2. $\ln \gamma_A = \alpha N_B^2$ etc.

so,

$$\Delta G^{m,xs} = RT\ (N_A \alpha N_B^2 + N_B \alpha N_A^2)$$
$$= RT\, \alpha N_A N_B.$$

Thus, for a regular solution, the free energy of mixing is given by:

$$\Delta G^m = RT\ (N_A \ln N_A + N_B \ln N_B + \alpha N_A N_B).$$

This equation can be repeatedly differentiated with respect to N_B to give

$$\frac{d\Delta G^m}{dN_B} = RT\ (\ln \frac{N_B}{N_A} + \alpha(N_A - N_B)\ )$$

$$\frac{d^2(\Delta G^m)}{dN_B^2} = RT\ (\frac{1}{N_A} + \frac{1}{N_B} - 2\alpha)$$

and

$$\frac{d^3(\Delta G^m)}{dN_B^3} = RT\ (\frac{1}{N_A^2} - \frac{1}{N_B^2})$$

The latter two equations give the derivatives of ΔG^m which become zero in the limiting case for liquid miscibility. Setting the third derivative equal to zero shows that $N_A = N_B$, which can only happen at $N_A = N_B = 0.5$. Substituting this in the previous equation with the second derivative set to zero shows that $\alpha = 2$. When $\alpha < 2$ the liquids will mix, and when $\alpha > 2$ there will be a miscibility gap. Although the derivation of this limit involves a number of assumptions, the most important of which is that the solution is regular, the limit derived will apply at least approximately to solutions exhibiting strong positive departures from ideality. This test can only be used away from the ends of the phase diagram as α_A can exceed 2 near $N_A = 1$ even in systems which show virtually ideal mixing e.g. in the Cd-Cu system (129), $\alpha Cd \to 3$ as $NCd \to 1$, but this system is close to ideal.

The signs of imminent unmixing are thus an inflection in the liquidus and in the activity/composition graph and, away from the ends of the diagram, a value of $\alpha \geqslant 2$. Figure 21 shows that the first of these features is present in the Si-Te system over the range $N_{Si} = 0.9$-0.7. To find out whether the second two features are also present, it is necessary to know the activity of silicon as a function of composition over the range in question. Once a_{Si} and N_{Si} are known, γ_{Si} and thus α_{Si} can be readily calculated. In theory, the ΔG^m vs. N and a vs. N graphs in Fig. 29 are only valid at one temperature, but in the present case, the activity can only be found by examining the depression of the freezing point of silicon by tellurium additions, which does involve working over a small temperature range. However, provided

this range is not too great, the fact that the activity/composition data generated are not isothermal will not be significant.

The depression of the freezing point can be used to find the activity using the Van t'Hoff relationship:

$$\ln a_{Si} = \frac{-\Delta H^f_{Si}}{R} \left[\frac{1}{T} - \frac{1}{T_f}\right] \qquad - 5.3.7.$$

in which a_{Si} is the activity of silicon in an alloy of melting point T^oK, T_f is the melting point of pure Si (1410°C) and ΔH^f_{Si} its heat of fusion (11 kcal/mole). R is the gas constant.

The values of a_{Si} obtained from this equation, and the resulting values of γ_{Si} and α_{Si}, are given in Table 12. The activity/composition relationship is plotted in Fig. 30, and shows that the second of the features of imminent unmixing is present, as the activity curve has an inflection in the range $N_{Si} = 0.9$–0.7. Inspection of Table 12 shows that the third feature is also present, as α_{Si} exceeds 2 as far across the diagram as $N_{Si} \simeq 0.6$. Strictly speaking, these α values are consistent with a miscibility gap, at least near the middle of the diagram, however, the number of assumptions which were required to find the limiting value of α and to obtain the values of a_{Si} is such that it would be unwise to draw a hard and fast conclusion from the results. All that it is probably safe to conclude in the present case is that the values of α obtained suggest that the alloys are at least in a state of imminent unmixing over the range near $N_{Si} = 0.7$ and may very well show a miscibility gap.

Table 12. Values of the activity (a), the activity coefficient (γ) and the α-function for silicon.

Melting Point of alloy °C	Atom fraction N_{Si}	Activity a_{Si}	Activity coefficient γ_{Si}	α-function α_{Si}
1380	0.90	0.942	1.049	4.795
1380	0.80	0.942	1.177	4.085
1370	0.70	0.923	1.318	3.073
1360	0.62	0.904	1.458	2.612
1350	0.59	0.870	1.462	2.316
1340	0.57	0.850	1.478	2.168
1330	0.56	0.835	1.490	2.060
1320	0.54	0.825	1.522	2.003
1310	0.52	0.805	1.533	1.894
1300	0.51	0.790	1.543	1.821
1280	0.49	0.762	1.549	1.696
1260	0.48	0.730	1.515	1.548
1240	0.47	0.700	1.474	1.408
1220	0.467	0.665	1.424	1.244
1200	0.460	0.623	1.354	1.039
1180	0.452	0.595	1.316	0.914
1160	0.450	0.570	1.267	0.783
1140	0.442	0.542	1.226	0.654
1120	0.440	0.510	1.159	0.471
1100	0.435	0.473	1.087	0.261

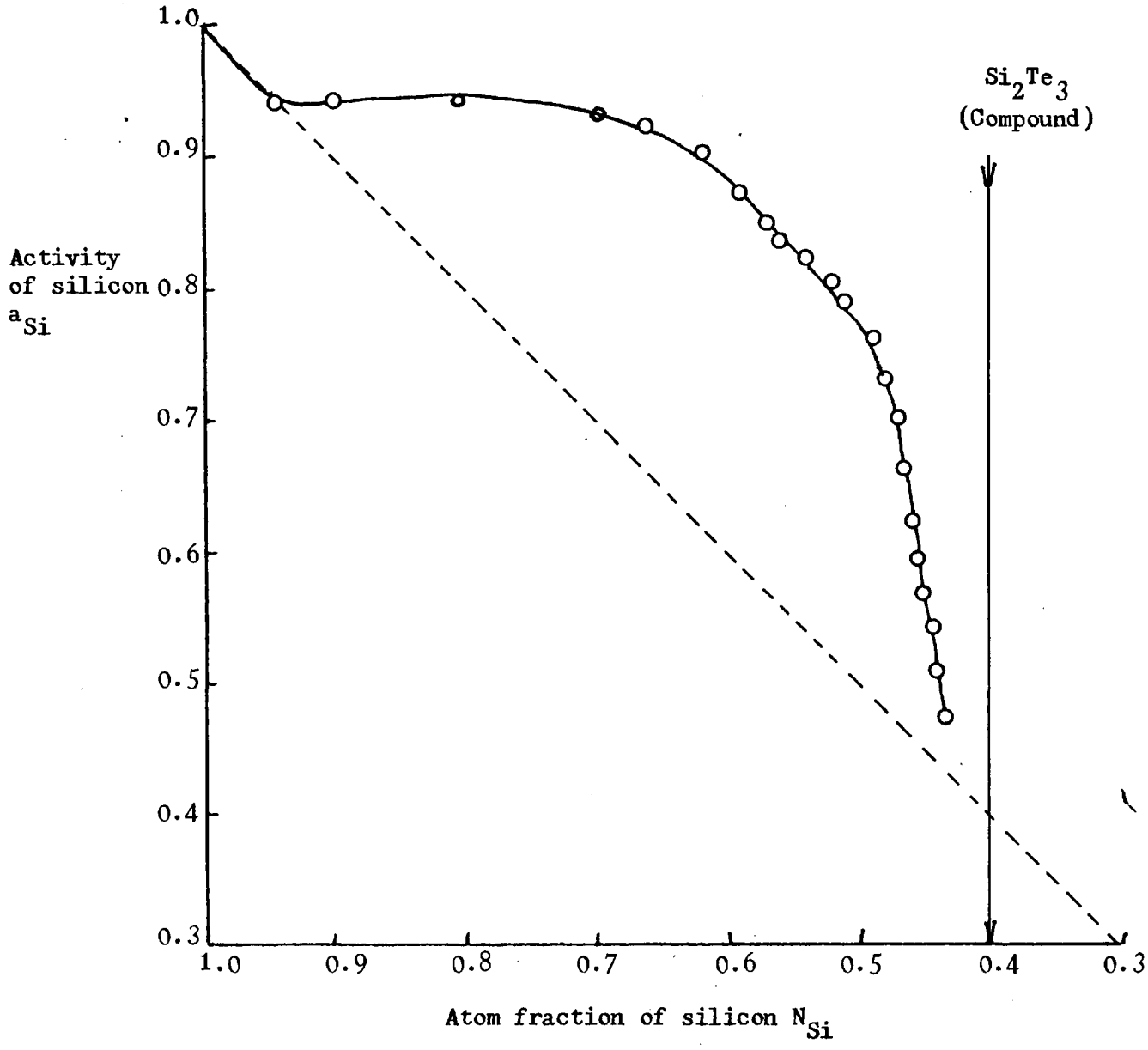

Fig. 30. Activity of Si vs atom fraction of Si for the Si-Te system. Activities calculated using equation 5:3:7.

o – calculated values.

– – – – – ideal behaviour.

——— – calculated behaviour.

Thus, to summarise the discussion of the liquid miscibility of the alloys at the high-silicon end of the Si-Te phase diagram, the simple tests given by Kleppa disagree as to the existence of a miscibility gap, but that the liquidus and activity curves and the α-function indicate that the liquid is at least in a state of imminent unmixing, and that a miscibility gap may actually be present.

The activity data of Fig. 30 show a strong positive deviation from ideality in the imminent unmixing range, as would be expected since this indicates that Si-Si bonds and Te-Te bonds are stronger than Si-Te bonds. Further across the diagram, at $N_{Si} = 0.4$, the compound Si_2Te_3 is formed, indicating that Si-Te bonds are strongest, and suggesting a negative deviation from ideality. Although the data in Fig. 30 become less reliable as N_{Si} decreases, they do suggest that this negative deviation will in fact occur, as the a_{Si}/N_{Si} graph is falling rapidly towards the ideal line as the compound composition is approached. It is unusual for a system to show both positive and negative deviations from ideality, but not unknown. Darken and Gurry cite Zn-Sb, Cd-Bi and Cd-Sb as examples, and more recent work by Predel et al.(130) shows three systems involving selenium (Se-Tl, Se-Bi, Se-Sb) in which the activity curve crosses the ideal line, going from a positive to a negative deviation from ideality.

In these latter three systems, the deviations are sufficiently large to produce compounds and miscibility gaps in the same systems. The activity curves given for these cases are not dissimilar to that shown in Fig. 30 for Si-Te. Thus, the behaviour postulated here for Si-Te, with a compound and the possibility of a miscibility gap, though unusual, is not without precedent.

5.4. Crystallisation of $S_{15}Ge_{43}As_{23}Te_{19}$ and Segregation in $S_{15}Ge_{43}As_{27}Te_{25}$.

As shown in the results section, attempts to produce a glass of the composition $S_{15}\ Ge_{43}\ As_{23}\ Te_{19}$ using the radio-frequency induction furnace were unsuccessful, and the resulting material showed an extensive network of GeTe dendrites, with a smaller number of crystals of composition $Ge_2\ As$, in a matrix approximating to $S_{30}\ Ge_{42}\ As_{11}\ Te_{16}$.

The failure of this composition to vitrify clearly shows the effect of cooling rate on glass formation, as Douglas and Maghrabi (116) report compositions near $S_{15}\ Ge_{43}\ As_{23}\ Te_{19}$ as lying within the glass forming region of this system, see Figure 30. Their technique differed from the author's radio-frequency furnace technique in that they quenched direct from the melt into ice and water, transferring the ampoule to liquid nitrogen after 10 seconds. Although they do not quote the cooling rate produced by this method, it must be several hundred degrees per minute at the very least. This contrasts with the cooling rate of about $10^{\circ}C$ per minute in the r.f. furnace, which would only be sufficient to avoid crystallisation at compositions where the glass was relatively stable. This suggests that, although this composition can be produced as a glass by rapid cooling, the likelihood that it will give long service in an electronic device is not particularly high, as crystallisation will set in.

The phases produced by the crystallisation of $S_{15}\ Ge_{43}\ As_{23}\ Te_{19}$ are also of interest, as they will probably be formed when switches of

Fig. 31. Pseudo-ternary section at 15% sulphur in the Ge-As-Te-S system, after Douglas and Maghrabi (116).

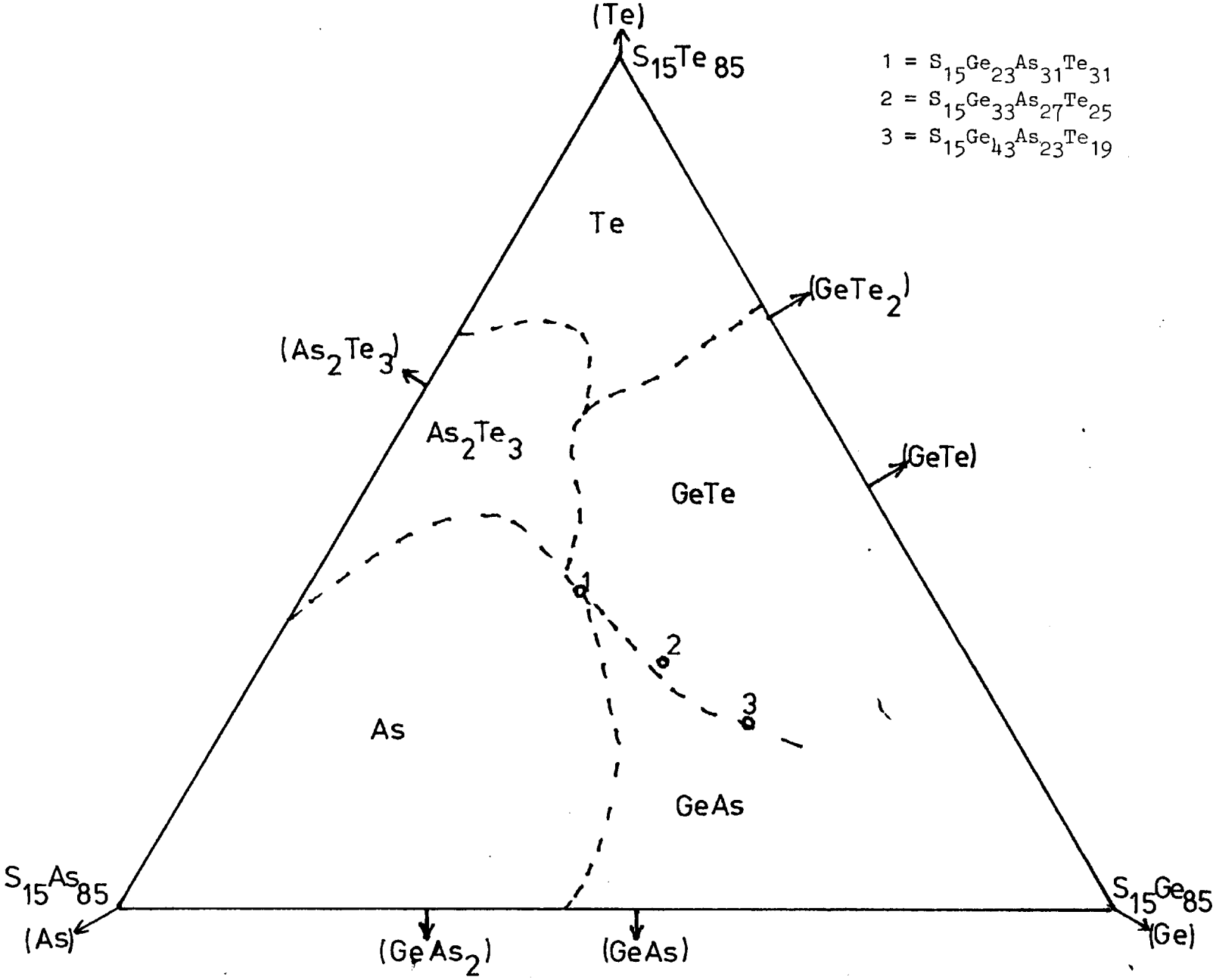

similar compositions fail. GeTe is a relatively well-known compound, and the occurrence of GeTe dendrites is not perhaps surprising. The larger crystals appeared completely homogenous and the electron probe microanalysis was very definite in indicating Ge_2As, so it is unlikely that the crystals consisted of a mixture (say of GeAs + Ge) with overall composition Ge_2As. Ge_2As has not, however, been reported in previous investigations of this system. Maghrabi and Douglas found both GeAs and $GeAs_2$, as shown in Figure 30, but not Ge_2As, althought it is possible that their investigation did not reach a sufficiently high Ge content to cause the compound to form. However, it seems the finding of Ge_2As must be taken as valid, and, as Te and GeTe have been found in failed switches of similar materials (131), it is possible that future investigations may show Ge_2As as well. The apparent enrichment of the matrix in sulphur when compared to the original starting material must be attributed to the fact that the bulk glass was being depleted in the other elements as it precipitated GeTe and Ge_2As. Nevertheless, this does not seem to fully account for the unusual matrix composition, so it is possible that some inhomogeneity was present in this sample of glass, possibly occurring in preparation for the crystallisation of other phases which might have appeared had the cooling rate been slower. However, as the attempt to make this particular glass was only a sideline of the main research, it was not pursued further.

In the investigation of failed devices referred to above (131), Allinson et al. found signs of segregation of Te to the positive electrode. The attempt to duplicate this segregation on a macro-scale is considered a partial success, as the analysis results suggested that a small amount of segregation of Te had occurred. This is in spite of the much lower

current densities and much shorter time for which the current was passed in the simulation compared to the case of a thin film device. Allinson et al. examined devices which had seen 90% duty cycle, and contained traces of a conducting channel at most 1 μm wide. The size and shape of this channel are not precisely known, but it may be reasonable to assume that the current is passing through a 1 μm x 1 μm area. In this case, the on-state current of 500 μA gives a current density of 5×10^8 A/m^2. The macroscopic simulation, on the other hand, involved passing a current which averaged about 5 A through a capillary 2.0 mm in diameter, giving a current density of about 1.5×10^6 A/m^2. In addition, the fact that the high-pressure furnace used in the simulation was required for the more important conductivity measurement part of the project meant that the high-current experiment was limited to 24 hours duration. In view of these limitations, the agreement between macro- and micro-scale experiments is encouraging, and suggests that a more marked effect might be obtained if greater current densities and/or longer times could be used in the simulation.

CONCLUSIONS

From the experimental work reported here, the following conclusions may be drawn.

(1) The conductivity/temperature behaviour of the four new switching chalcogenide glasses investigated (S_{15} Ge_{23} As_{31} Te_{31}, S_{15} Ge_{33} As_{27} Te_{25} and their selenium-bearing analogues) is similar to that shown in the literature for other well-known chalcogenides

such as STAG (Si_{12} Te_{48} As_{30} Ge_{10}).

(2) The $\log_{10}\sigma$ vs $1000/T^{o}K$ behaviour of all the four new materials consists of a linear portion from room temperature up to the glass transition temperature, at which point there is a gradual increase in the slope. Above $500^{o}C$, the slopes begin to decrease again, giving temperature independent behaviour at temperatures over $1100^{o}C$.

(3) The linear low-temperature portions of the $\log_{10}\sigma$ vs $1000/T^{o}K$ graphs may be interpreted using the equation $\sigma = \sigma_0 \exp\left(\frac{-\Delta E}{kT}\right)$, and give values of the mobility gap ΔE between 0.77 and 0.64 eV for the sulphur and selenium bearing glasses, and 0.52 eV for STAG.

(4) The form of the conductivity/temperature plots is consistent with the thermal theory of switching, and suggests that the conducting channel would contain material at a temperature in excess of $1000^{o}C$, as proposed in computer simulations of the switching process. Apart from this, the present results do not support or contradict either theory of switching.

(5) The differences in composition amongst the four glasses, and between them and STAG, have little effect on the conductivity/temperature behaviour, and any differences which do exist decrease as the temperature rises. The differences detected cannot be explained on any simple notion of the structure of the amorphous state (e.g. by comparison with the network former/network modifier

classification of the components of a conventional glass). This is attributable to the nature of semiconduction in the chalcogenide materials, being controlled by a "mobility gap" whose nature renders it relatively insensitive to composition.

(6) It was not possible to produce a uniform amorphous material of composition S_{15} Ge_{43} As_{23} Te_{19} at the cooling rate associated with the radio frequency furnace technique described in section 3.3.1. (about 10°C per minute). Dendrites of GeTe and rectangular crystals of Ge_2As were formed. It is probable that if a switch could be made of this material, making it glassy by increasing the cooling rate, the device would fail by formation of GeTe and/or Ge_2As in the conducting channel, and it is also possible that such compounds may be responsible for the failure of devices of the two more stable compositions described in conclusion (1).

(7) An attempt to duplicate on a large scale the segregation of Te reported by Allinson et al. (129) in devices using S_{15} Ge_{33} As_{27} Te_{25} gave encouraging results, but only a very tentative enrichment of Te at the positive electrode was detected.

(8) The linear behaviour of the electrical conductivity of sulphur, (plotted as $\log_{10}\sigma$ vs 1000 $(T°K)^{-1}$) which had been known to exist up to about 500°C, was found to persist to 900°C with little change in slope. No direct relationship was found between conductivity and the most likely controlling parameter, chain length, P, although over the linear portion of the data obtained, the equation

log (resistivity) = 2.0 log P appeared to apply. There was also a general similarity of trends between the conductivity data and viscosity data obtained from the literature.

(9) The Si-Te phase diagram was confirmed as being essentially as determined by Bailey, with a single incongruently melting compound Si_2Te_3. Between Si_2Te_3 the liquidus was found to rise steeply to a plateau, indicating a strong positive deviation from ideality at the high-Si end of the diagram. This departure is such as to suggest that the system is close to a miscibility-gap situation in this region.

(10) The method given by Bailey for the manufacture of Si_2Te_3 was duplicated, and was found to be effective.

During the course of this project, as in the case of all research, a number of areas were identified where knowledge is at present lacking, and which further experimentation might be able to clarify. Chief among these were:

(1) The lack of any systematic knowledge of the effect of composition on any of the properties of the chalcogenide glasses, except perhaps on Tg.

(2) The lack of data on most chalcogenides, apart from their electrical conductivity, above relatively modest temperatures.

(3) The crucial experiments to differentiate the thermal and space-charge theories of switching have not been carried out, chiefly due to the extreme experimental difficulties involved.

(4) Data on the properties of sulphur seem to be lacking between about 500^{o}C and the critical point, 1040^{o}C, apart from the conductivity data presented here.

REFERENCES

(1) AMAGAT, E.H. Ann. chim. et phys. 1893, 29, 6, p.68.

(2) BRIDGEMAN, P.W. Book: "The Physics of High Pressure", pub. Bell & Sons, London 1949.

(3) COMINGS, E.W. Book: "High-Pressure Technology", pub. McGraw-Hill, 1956.

(4) ANON. Book: "Perspex Acrylic Materials". pub. I.C.I.

(5) SCHUTZ - SELLACK, M. Ann. Phys. Chem., 1870, 139, p.182.

(6) FRERICHS, R., Jnl. Opt. Soc. America, 1953, 43, p.1153.

(7) FRASER, W.A., Jnl. Opt. Soc. America, 1953, 43, p.823.

(8) GLAZE, F.W. et al., Jnl. Res. Nat. Bureau of Stds., 1957, 59, p.83.

(9) GORYUNOVA, N.A. and KOLOMIETS, B.T., Zh. Tech. Fiz. 1955, 25, p.984.

(10) KOLOMIETS, B.T., Phys. Stat. Solidi 1964, 7, p.359.

(11) GORYUNOVA, N.A. et al. Sov. Phys.-Tech.-Phys. 1958, 3, p.912.

(12) OVSHINSKY, S.R., Jnl. Non-Crystalline Solids. 1970, 2, p.9.

(13) OVSHINSKY, S.R. U.S. Patent No. 3, 052,830 (1962).

(14) OVSHINSKY, S.R. Phys. Rev. Letters. 1968 (Nov), 21, 20, p.1450.

(15) SHENG, W.W. et al. I.E.E.E. Trans. (electron devices), 1972, 19, 2, p.288.

(16) SUNTOLA,T. Acta. Polytech. Scand. Phys. Ind. Nucleonics, 1971, No. 82, p.41.

(17) SCHUÖCKER, D. et al., J. Appl. Phys. 1972, 43, 6, p.2647.

(18) SCHLOVSKII, B.I. et al. Zh. Eksp. Teor. Fiz. 1972, 62, 3, p.1156.

(19) Van ROESBROEK, W. Phys. Rev. Lett. 1972, 28, 17, p.1120.

(20) HAMAKAWA, Y. Oyo Butsuri, 1972, 41, 2, p.117.

(21) EMIN, D. et al. Phys. Rev. Lett. 1972, 28, 13, p.813.

(22) PRYOR, R.W. and HENISCH, H.K. J. Non-Cryst. Sol. 1972, 7, 2, p.181.

(23) GRIGORIVICI, R. Thin Solid Films, 1972, 9, 1, p.1.

(24) SHOUSHA, A.H. J. Appl. Phys. 1971, 42, 12, p.5131.

(25) THORNBURG, D.D. Phys. Rev. Lett. 1971, 27, 18, p.1208.

(26) PINTO, R. and RAMANATHAN K.V. Appl. Phys. Lett. 1971, 19, 7, p.221.

(27) HENISCH, H.K., PRYOR, R.W. Solid State Electronics, 1971; 14,9, p.765.

(28) MOTT, N.F. Phil. Mag. 1971, 24, 190, p.911.

(29) BUNTON, G.V. et al. J. Non-cryst. Sol. 1971, 6, 3, p.251.

(30) MOTT, N.F. Disc. Faraday Soc. 1970, 50, p.7.

(31) JOHNSON, R.T. et al. Sol. State Commun., 1971, 9, 16, p.1397.

(32) MACMILLAN, P., NESUADKA, P. J. Phys. D. 1971, 4, 9, p.1401.

(33) SCHUÖCKER, D. Appl. Phys. Lett. 1971, 19, 1, p.7.

(34) PINTO, R. Thin Solid Films, 1971, 7, 6, p.391.

(35) ARMITAGE, D. et al. Canad. J. Phys. 1971, 49, 12, p.1662.

(36) OVSHINSKY, S.R. et al. Met. Trans. 1971, 2, 3, p.641.

(37) ALLGAIER, R.S. J. Vac. Sci. & Technol. 1971, 8, 1, p.113.

(38) JONSCHER, A.K. ibid. p.135.

(39) INGLIS, G.B., WILLIAMS, F. J. Non-cryst. Sol. 1971, 5, 4, p.313.

(40) FORLANI, F., MINNAJA, N. Thin Solid Films, 1970, 6, 4, p.R43.

(41) ARMITAGE, D. et al. Canad. J. Phys. 1970; 48, 22, p.2870.

(42) OVSHINSKY, S.R. and BOER, K.W. J.Appl. Phys. 1970, 41, 6, p.2675.

(43) CHEN, HO-SON and WANG, TAI TZER. Phys. Status Solidi. A. 1970, 2, 1, p.79.

(44) WARREN, A.C. J. Non-cryst. Sol. 1970; 4, 1, p.613.

(45) STOCKER, H.J. J. Non-cryst. Sol. 1970; 2,1, p.371.

(46) STOCKER, H.J. Appl. Phys. Lett. 1969, 15, 2, p.55.

(47) MOTT, N.F. Contemp. Phys. 1969, 10, 2, p.125.

(48) WALSH, P.J. et al. Phys. Rev. 1969, 178, 3, p.1274.

(49) BOER, K.W. Phys. Stat. Solidi (A), 1971, 4, p.571.

(50) MALE, J.C. and Warren, A.C. New Scientist, 1970, 47, p.128.

(51) STOCKER, H.J. et al. J. Non-cryst. Sol. 1970, 4, p.523.

(52) HENISCH, H.K. et al. ibid. p.538.

(53) EUSNER, R.R. et al. J. Amer. Ceram. Soc. 1972, 55, 1, p.43.

(54) KIKUCHI, M. et al. Sol.State Commun. 1970, 8, 17, p.1333.

(55) ADLER, D. Scientific American, 1977, 236, 5, p.36.

(56) COHEN, M.H. J. Non-cryst. Sol. 1970, 4, p.391.

(57) ADLER, D. Book: "Amorphous Semiconductors", pub. by Butterworths as a C.R.C. Monograph.

(58) MOTT, N.F. Nature, 1975, 257, September, p.15.

(59) SAVAGE, J.A. and NIELSEN, S. Infrared Physics. 1965, 5, 4, p.195.

(60) U.S. Patent No. 3,343,972.

(61) SAVAGE, J.A. and NIELSEN, S. Phys. Chem. Glasses. 1966, 7, 2, p.56.

(62) SHAW, R.F. et al. Appl. Phys. Lett. 1972, 20, 7, p.241.

(63) OVSHINSKY, S.R. Science Jnl. 1969, 5A, 2, p.73.

(64) HENISCH, H.K. and VENDURA, G.J. Appl. Phys. Lett. 1971, 19, 9, p. 363.

(65) JOHNSON, R.E. and HAISTY, R.W. U.S. Patent No. 3,611,060.

(66) DEIS, D.W. et al. J. Non-cryst. Sol. 1970, 2, 1, p.141.

(67) ADLER, D. Scientific American. 1977, 236, 5, p.36.

(68) EDMOND, J.T., MALE, J.C. and CHESTER, P.F. J. Scientific Instruments. 1968, Ser. 2, Vol. 1. p.373.

(69) MALE, J.C. Electronics Letters, 1970, 7, 4, p.91.

(70) WEBB, L.M. and BAKER, E.H. J. Chem. Soc. (Dalton Transactions) 1972, p.769.

(71) BAKER, E.H. and WEBB, L.M. J. Mat. Sci. 1974, 9, p.1128.

(72) MALE, J.C. Electronics Lett. 1970, 6, 4, p.91.

(73) SIE, C.H. J. Non-cryst. Sol. 1970, 4, 1, p.548.

(74) EPSTEIN, A.S., FRITZSCHE, H., LARK-HOROWITZ, K. Phys. Rev. 1957, 107, p.412.

(75) TIÉCHE, Y., ZAREBA, A. Phys. de Kondensierte Materie. 1963, 1, p. 402.

(76) PERRON, J.C. Adv. Phys. 1967, 16, p.657.

(77) BAKER, E.H. J. Chem. Soc. A. 1968, p.1089.

(78) IOFFE, A.F., REGEL, A.R. In "Progress in Semiconductors", pub. Heywood, London, 1960.

(79) WATANABE, O., and TAMAKI, S. Electrochimica Acta, 1968, 13, p.11.

(80) VEZZOLI, G.C. J. Amer. Ceram. Soc. 1972, 55, 2, p.65.

(81) WIGAND, A. Verhandlungen der Deutschen Physikalischen Gesellschaft II, 1908, 10, p.495.

(82) FEHER, F. and LUTZ, H.D. Zeitschrift fur anorganische und allgemeine. Chemie, 1964, 333, p.216.

(83) MONCKMANN, J. Proc. Royal Soc. 1888, 46, p.136.

(84) BLACK, D.H. Proc. Cambridge Philosophical Soc. 1924, 22, p.393.

(85) FOUSSEREAU, M.G. Comptes Rendus, 1883, 97, p.996.

(86) STEUENENBERG, R.K. et al. Adv. Chem. Series 110, 1972, p.190.

(87) BAKER, E.H. Trans. Inst. Min. Metall. 80 C, 1971, p.93.

(88) SMITHELLS, J. "Metals Reference Book", pub. Butterworths.

(89) WEISS, A. and WEISS, A. Zeischer. Anorg.und Allgem. Chemie 1953, 274, p.124.

(90) SMIROUS, K. et al. Czech. J. Phys. 1957, 7, p. 120.

(91) VENNICK, J. and CALLAERTS, R. Comptes Rendus 1965, 260, p.496.

(92) BAILEY, L. J. Phys. Chem. Solids. 1966, 27, p.1593.

(93) BREBRICH, R.F. J. Chem. Phys. 1968, 49, 6, p.2584.

(94) PLOOG, K. et al. Mat. Res. Bulletin, 1976, 11, p.1147.

(95) BAKER, E.H. Trans. Inst. of Min. & Met. C. 1974, 83, p.237.

(96) MACHOL, R.E. and WESTRUM, E.F. J. Amer. Chem. Soc. 1958, 80, p. 2950.

(97) RAU, H. J. Chem. Thermodyn. 1973, 5, 6, p.833.

(98) GREEN, M., GEE, W., LEVY, A.; J. Phys. D. 1972, 5, 7, p.L55.

(99) GREEN, M. et al. Surface Science 1970, 23, 2, p.409.

(100) International Critical Tables. pub. McGraw-Hill.

(101) TALUKDAR, M.I. and BAKER, E.H. Solid State Commun. 1969, 7, 2, p.309.

(102) SAVAGE, J.A. private communication.

(103) BAKER, E.H., DAVEY, T.G. J. Mat. Sci. 1978, 13, p.1951.

(104) MOTT, N.F. J. Non-cryst. Sol. 1978, 28, p.147.

(105) ANDERSON, P.W. Phys. Rev. 1958, 109, p.1492.

(106) MOTT, N.F. and DAVIS, E.A. Book: "Electronic Processes in Non-crystalline Materials", pub. Oxford University Press, 1974.

(107) MALE, J.C. Brit. Jnl. Appl. Phys. 1967, 18, p.1543.

(108) ADLER, D. et al. J. Non-cryst. Sol. 1970, 4, 1, p.330.

(109) OWEN, A.E. J. Non-cryst. Sol. 1977, 25, p.372 (Proceedings of "Glass 1977").

(110) EDMOND, J.T. Brit. J. Appl. Phys. 1966, 17, p.979.

(111) ECKENBACH, S.W. et al. J. Non-cryst. Sol. 1971, 5, p.264.

(112) SEAGER, C.H. et al. Phys. Rev. B. 1973, 8, 10, p.4746.

(113) HAISTY, R.W. and KREBS, H. J. Non-cryst. Sol. 1969, 1, p.427.

(114) GIRIDHAR, A. et al. ibid. 1980, 37, p.165.

(115) BAKER, E.H. Private communication.

(116) DOUGLAS, R.W., MAGHRABI, C. Research Report RV-26, Dept. of Ceramics, Glasses and Polymers, Univ. of Sheffield.

(117) PANUS, V., BORISOVA, Z.V. Vestn. Leningrad. Univ. Fiz. Khim. 1971, 2, p.125.

(118) MALE, J.C. New Scientist, 1974, 62, p.892.

(119) MACKNIGHT, W.J., TOBOLSKY, A.V. Ch. 5 of "Elemental Sulphur - Chemistry and Physics". pub. Interscience, New York.

(120) POULIS, J.A., MASSEN, C.H. ibid. Ch. 6.

(121) BAKER, E.H. "Physical Chemistry of Process Metallurgy - the Richardson Conference". Inst. Min and Metall. 1974, p.11.

(122) VEZZOLI, G.C. et al. Applied Optics. 1976, 15, 2, p.327.

(123) MASSEN, C.H. et al. Trans. Faraday Soc. 1964, 60, p.317.

(124) EISENBERG, A., TOBOLSKY, A.V. J. Polymer Sci. 1960, 46, p.19.

(125) VEZZOLI, G.C. et al. ibid. part A1, 1969, 7, p.1557.

(126) EISENBERG, A. J. Chem. Phys. 1963, 39, 7, p.1852.

(127) DARKEN, L.S., GURRY, R.W. Book: "Physical Chemistry of Metals", pub. McGraw-Hill.

(128) KLEPPA, O.J. "Thermodynamics and properties of liquid solutions", p. 56, In: "Liquid Metals and Solidification", A.S.M. Conference, Cleveland, Ohio, 1958.

(129) BAKER, E.H. Trans. Inst. Min. and Met. C., 1977, 86, p.23.

(130) PREDEL, B. et al. Zeitschr. Metallkunde. 1977, 70, p.109.

(131) ALLINSON, D.L. et al. National Physical Laboratory Div. of Inorganic and Metallic Structure. Annual Report R.P. 32-3, October, 1974.